Nagra
Nationale
Genossenschaft
für die Lagerung
radioaktiver Abfälle

Cédra
Société coopérative
nationale
pour l'entreposage
de déchets radioactifs

Cisra
Società cooperativa
nazionale
per l'immagazzinamento
di scorie radioattive

TECHNICAL REPORT 87-14 E

GRIMSEL TEST SITE

GEOLOGY

H.R. Keusen
J. Ganguin
P. Schuler
M. Buletti

GEOTEST, Zollikofen / Bern

FEBRUARY, 1989

GRIMSEL TEST SITE / SWITZERLAND
A JOINT RESEARCH PROGRAM BY

- NAGRA – National Cooperative for the Storage of Radioactive Waste, Baden, Switzerland
- BGR – Federal Institute for Geoscience and Natural Resources, Hannover, Federal Republic of Germany
- GSF – Research Centre for Environmental Sciences, Munich, Federal Republic of Germany

Parkstrasse 23 5401 Baden / Schweiz Telephon 056 / 20 55 11

Nagra
Nationale
Genossenschaft
für die Lagerung
radioaktiver Abfälle

Cédra
Société coopérative
nationale
pour l'entreposage
de déchets radioactifs

Cisra
Società cooperativa
nazionale
per l'immagazzinamento
di scorie radioattive

TECHNICAL REPORT 87-14 E

GRIMSEL TEST SITE

GEOLOGY

H.R. Keusen
J. Ganguin
P. Schuler
M. Buletti

GEOTEST, Zollikofen / Bern

FEBRUARY, 1989

GRIMSEL TEST SITE / SWITZERLAND
A JOINT RESEARCH PROGRAM BY

- NAGRA – National Cooperative for the Storage of Radioactive Waste, Baden, Switzerland
- BGR – Federal Institute for Geoscience and Natural Resources, Hannover, Federal Republic of Germany
- GSF – Research Centre for Environmental Sciences, Munich, Federal Republic of Germany

Parkstrasse 23 5401 Baden / Schweiz Telephon 056 / 20 55 11

FOREWORD

Concepts which foresee the disposal of radioactive waste in geological formations lay great weight on acquiring knowledge of the proposed host rock and the surrounding rock strata. For this reason, Nagra has, since May 1984, been operating the Grimsel Test Site which is situated at a depth of 450 m in the crystalline formation of the Aar Massif. The general objectives of the research being carried out in this system of test tunnels include, in particular

- the build-up of know-how in planning, performing and interpreting underground experiments in different scientific fields and

- the aquisition of practical experience in developing, testing and applying test equipment and measuring techniques.

The Test Site (GTS) is operated by Nagra. On the basis of a German-Swiss cooperation agreement, the various experiments are carried out by Nagra, the Federal Institute for Geoscience and Natural Resources (BGR) and the Research Centre for Environmental Sciences (GSF); the latter two bodies are supported in this venture by the German Federal Ministry for Research and Technology (BMFT).

NTB 85-47 gives an overview of the GTS and a review of the status of the investigation programme as at August 1985.

VORWORT

Bei Konzepten, die die Endlagerung radioaktiver Abfälle in geologischen Formationen vorsehen, ist die Kenntnis des Wirtgesteins und der angrenzenden Gesteinsschichten von grundlegender Bedeutung. Die Nagra betreibt deshalb seit Mai 1984 das Felslabor Grimsel in 450 m Tiefe im Kristallin des Aarmassivs. Die generelle Zielsetzung für die Arbeiten in diesem System von Versuchsstollen umfasst insbesondere

- den Aufbau von Know-how in der Planung, Ausführung und Interpretation von Untergrundversuchen in verschiedenen Experimentierbereichen und

- den Erwerb praktischer Erfahrung in der Entwicklung, Erprobung und dem Einsatz von Testapparaturen und Messverfahren.

Das Felslabor (FLG) wird durch die Nagra betrieben. Die verschiedenen Untersuchungen werden aufgrund eines deutsch-schweizerischen Zusammenarbeitsvertrages durch die Nagra, die Bundesanstalt für Geowissenschaften und Rohstoffe (BGR) und die Gesellschaft für Strahlen- und Umweltforschung (GSF) durchgeführt, beide gefördert vom Deutschen Bundesministerium für Forschung und Technologie (BMFT).

Eine Uebersicht des FLG und die Zusammenfassungen der Untersuchungsprogramme sind mit Status August 1985 im NTB 85-47 enthalten.

AVANT-PROPOS

La connaissance de la roche d'accueil et des couches rocheuses avoisinantes est d'importance fondamentale pour l'élaboration de concepts prévoyant le stockage de déchets radioactifs dans des formations géologiques. C'est pour cela que la Cédra exploite depuis mai 1984 le laboratoire souterrain du Grimsel à 450 m de profondeur dans le cristallin du massif de l'Aar. Les objectifs généraux des travaux menés dans ce complexe de galeries d'essais comprennent notamment:

- la constitution d'un savoir-faire dans la préparation, l'exécution et l'interprétation d'essais souterrains dans divers domaines et

- l'acquisition d'expérience pratique dans le développement, la mise à l'épreuve et l'engagement d'appareillages d'essais et de techniques de mesure.

Le laboratoire souterrain est exploité par la Cédra. Les différentes recherches sont réalisées dans le cadre d'un accord de collaboration germano-suisse par la Cédra, la "Bundesanstalt für Geowissenschaften und Rohstoffe" (BGR) et la "Gesellschaft für Strahlen- und Umweltforschung" (GSF), ces deux dernières instances étant soutenues par le Ministère allemand pour la recherche et la technologie (BMFT).

Un aperçu du laboratoire souterrain et un résumé des programmes de recherches apparaissent dans le rapport NTB 85-47 d'août 1985.

Le présent rapport a été élaboré dans le cadre de la collaboration entre les trois partenaires. Les auteurs ont présenté leurs vues et conclusions personnelles. Celles-ci ne doivent pas forcément correspondre à celles de la Cédra, de la BGR et de la GSF.

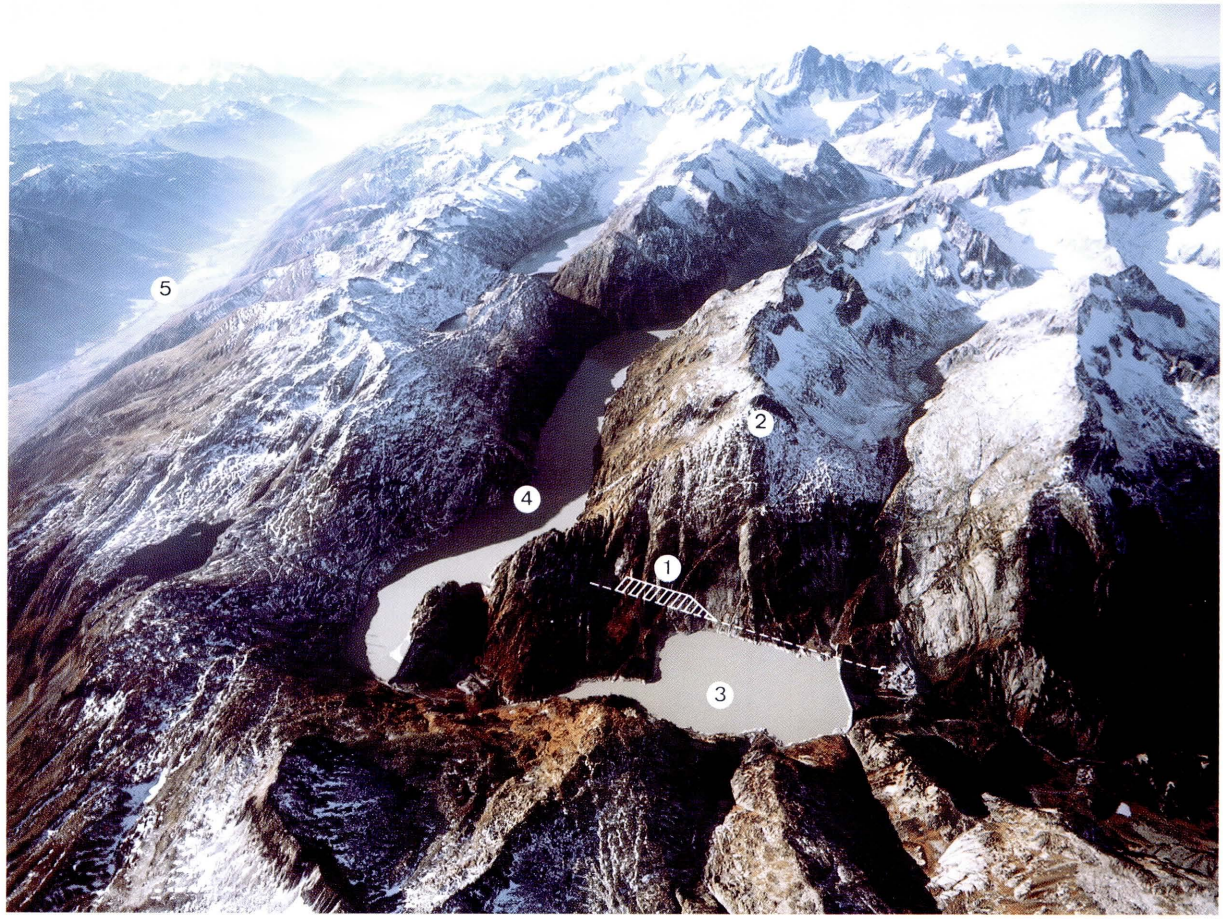

GRIMSEL-GEBIET

Blick nach Westen

1 Felslabor
2 Juchlistock
3 Räterichsbodensee
4 Grimselsee
5 Rhonetal

GRIMSEL AREA

View looking West

1 Test Site
2 Juchlistock
3 Lake Raeterichsboden
4 Lake Grimsel
5 Rhone Valley

FLG FELSLABOR GRIMSEL
GTS *GRIMSEL TEST SITE*

Situation

0 100 m

- Zugangsstollen/*Access tunnel*
- Fräsvortrieb/*by tunnel boring machine*
- Sprengvortrieb/*excavated by blasting*
- Zentraler Aaregranit ZAGR / *Central Aaregranite CAGR*
- Biotitreicher ZAGR / *CAGR with high content of biotite*
- Grimsel-Granodiorit / *Grimsel-Granodiorite*
- Scherzone/*Shear zone*
- Lamprophyr/*Lamprophyre*
- Wasserzutritt/*Water inflow*
- SB Sondierbohrung/*Exploratory borehole*
- US US Bohrung/*US borehole*

ZB	Zentraler Bereich/*Central facilities*
AU	Auflockerung/*Excavation effects*
BK	Bohrlochkranz/*Fracture system flow*
EM	El.magn. HF-Messungen/*-measurements*
FRI	Kluftzone/*Fracture zone investigation*
GS	Gebirgsspannungen/*Rock stresses*
HPA	Hydr. Parameter/*Hydr. parameters*
MI	Migration/*Migration*
MOD	Hydrodyn. Modellierung/*H. modeling*
NM	Neigungsmesser/*Tiltmeters*
UR	Untertageradar/*Underground radar*
US	Seismik/*Underground seismic testing*
VE	Ventilationstest/*Ventilation test*
WT	Wärmeversuch/*Heat test*

A — A Schnitt/*Section*

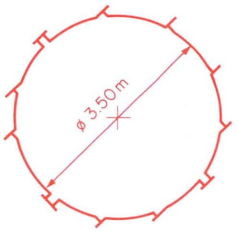

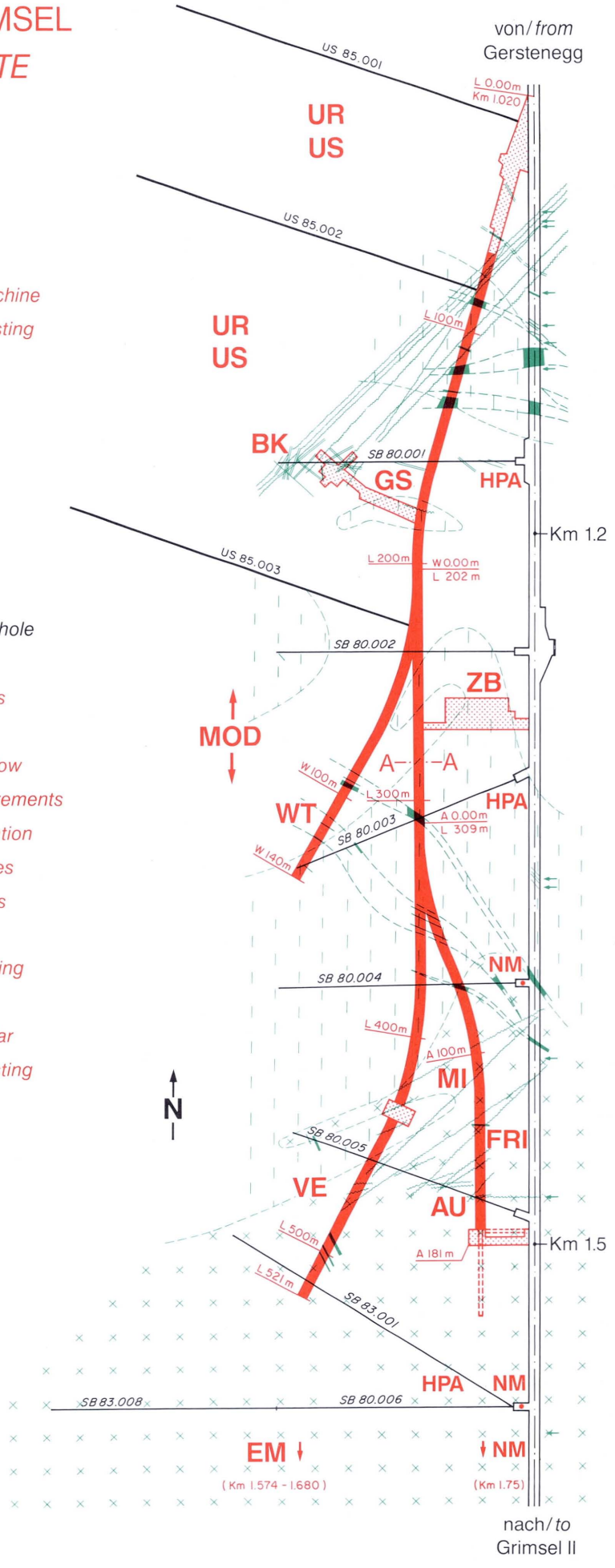

6/88

ABSTRACT

This report discusses the results of geological and petrographic investigations which were carried out in the Juchlistock and Grimsel Test Site (GTS) area between 1980 and 1987. The investigations basically consisted of:

- geological surface mapping of the Juchlistock;
- geological mapping of around 840 m of tunnel;
- logging of around 1476 m of cored boreholes;
- statistical evaluation and interpretation of around 3500 structural data points (underground);
- hydrogeological investigations such as measurement of the discharge of formation water into tunnels and boreholes.

Geology

The GTS is located in the southern part of the Central Aar Massif, around 400 m below the surface of the Juchlistock. The rocks in this area are almost exclusively granitic, the northern part of the GTS being located in Central Aare granite and the southern part in Grimsel granodiorite. These rocks are intruded by sets of lamprophyres and, to a lesser extent, by aplites. The Variscan age of solidification of the granites is approximately 290-300 Ma and that of the aplites around 250 Ma.

The whole Aar Massif was subjected to strong alpine deformation and metamorphism. The dominant textural overprinting of the rocks occurred contemporaneously with the development of the greenschist facies metamorphism some 20-25 Ma ago. The P-T conditions during the metamorphism were 400-450°C for temperature and around 3kb for pressure, corresponding to a depth of 10 km. The deformation affected all the rocks but overprinted them to varying degrees, so that both ductile and brittle structures occurred. The former

include schistosities, shear zones and mylonites and the latter cross- and shear fractures. Metamorphic alterations accompanied and, to some extent, promoted the ductile deformation, e.g. the alteration of potassium feldspar to micaceous minerals.

In addition to these structures, tension joints were formed during a later phase of the alpine textural overprinting, mainly along significant mechanical discontinuities such as granite/lamprophyre contacts. The minimum age of these tension joints is 15 Ma. The formation of these features was accompanied by strong hydrothermal activity. Some areas of rock were leached, leading to a marked increase in porosity (to a max. of 18 Vol-%). This hydrothermal fluid circulation also sealed most of the brittle structures.

The alpine orogeny was followed by the uplift of the Aar Massif, which is still occurring to some extent today. During this uplift phase, the most significant zones of weakness were reactivated, the result being the formation of the majority of the open fractures which today represent potential water flow-paths.

Structural geology

For the purposes of statistical evaluation, the brittle structure data points were divided into categories depending on the mineral coatings on the fracture surfaces. The data come from the tunnel sections and from 12 boreholes. Three discontinuity systems with a ductile origin and preferred mineral orientation could be recognised:

- the NE-SW-striking main schistosity S_2 which dips steeply to the SE and
- the steep shear surfaces conjugate to S_2, i.e. S_1 (often subparallel to S_2) and S_3 (E-W strike).

Since S_1 can barely be distinguished from S_2 on the basis of azimuth and angle of dip alone, these two systems were treated together (S_1 + S_2).

Six brittle structure systems are also covered (generally described by K, except for the nomenclature S_4 and S_5 originating from STECK, 1968a). These are:

- S_4/K_4, K_2/L (L = lamprophyre direction), K_1, K_3, S_5 and
- a sub-horizontal tension joint system ZK.

These systems generally form conjugate pairs to S_2. S_4/K_4 and K_2/L were treated as one system since, in most cases, there is no clear distinction due to extensive overlapping of the orientations.

The GTS was sub-divided into areas corresponding either to a borehole or a tunnel section. There are marked differences in the frequency distribution of the systems and deviations in direction and changes in the angle of dip (10 to 20°) are common. In general, the most widely-spread systems contain the highest percentage of open fractures; these dominate mainly in S_1+S_2. However, since individual areas are characterised by different discontinuity populations, systems such as S_3, K_2/L and S_5 can also be rich in open fractures.

The surface mapping programme allowed the data acquired underground to be extended spatially, although fewer systems were recognised at the surface. Besides the main schistosity S_2, only S_1, S_3, K_2/L and K_3 were identified.

Surface-, tunnel- and borehole measurements are based on the same one-dimensional data acquisition process (logging of drill-cores, measurements in tunnel sections and along profiles). Analyses of data acquired underground allow comparative studies of discontinuity locations and frequency distributions to be performed, while surface mapping completes the picture by providing data on

the extent of the systems and spacing of the discontinuities. Surface observations also give an indication of movement directions.

On a small scale, the Juchlistock-GTS area appears to be very complex; extensive unfractured areas are either non-existent or very rare. The large-scale picture is much simpler since fewer discontinuity systems (basically only S_1+S_2, S_3 and K_2/L) can be recognised.

Water circulation

The GTS was purposely located outwith the sphere of influence of the large, water-bearing disturbed zones which can be identified in the main access tunnel to the Oberhasli power plant (KWO). It therefore lies in a relatively dry area of rock. Disturbed zones with marked water discharge were encountered only in the north (fracture system flow test zone) and in the south (excavation effects zone).

The water present in the rock circulates mainly in the discontinuities, in this case in the systems S_1+S_2 and along lamprophyre contacts. These systems extend over considerable distances and often penetrate right to the surface.

In the case of water discharge into the main access tunnel, climatic factors such as snow-melt and changes in water-level in the lakes affect discharge down to a depth of around 250 m. In the GTS area with an overburden of more than 400 m, such external influences are no longer recognisable.

In general, water discharge into the GTS is low. The amounts are

- 0 - 12 ml/min•m' in the borehole
- 0.1 - 3 ml/min per open discontinuity in the borehole.

There is a marked local increase in water discharge in strongly fractured areas (BK, US, MI).

ZUSAMMENFASSUNG

Im vorliegenden Bericht werden die Ergebnisse von geologischen und petrographischen Untersuchungen, die seit 1980 bis 1987 im Gebiet des Juchlistocks und des Felslabors Grimsel (FLG) durchgeführt wurden, kommentiert. Sie beinhalten im wesentlichen:

- die geologische Oberflächenkartierung des Juchlistocks;
- die geologische Aufnahme von ca. 840 m Stollen;
- die geologische Aufnahme von ca. 1476 m Kernbohrungen;
- die statistische Auswertung und Interpretation von ca. 3500 Strukturdaten (untertage);
- hydrogeologische Untersuchungen, wie Messungen von Bergwasserschüttungen in Stollen und Bohrungen.

Geologie

Das FLG befindet sich im südlichen Teil des Zentralen Aar-Massivs und liegt durchschnittlich in 400 m Tiefe unter dem Juchlistock. Es sind fast ausschliesslich granitische Gesteine aufgeschlossen. Der nördliche Teil des FLG wird von Zentralem Aaregranit aufgebaut, der südliche von Grimsel-Granodiorit. Diese Gesteine werden von in Scharen auftretenden Lamprophyren, sowie von wenigen Apliten durchschlagen. Das variszische Erstarrungsalter der Granite liegt bei ungefähr 290-300 MJ, dasjenige der Aplite bei ca. 250 MJ.

Das ganze Aar-Massiv wurde alpidisch stark deformiert und metamorphisiert. Die Hauptgefügeprägung der Gesteine fand gleichzeitig mit der grünschieferfaziellen Metamorphose vor etwa 20-25 MJ statt. Die bei der Metamorphose erreichten P-T Bedingungen liegen bei 400-450°C für die Temperatur, sowie etwa 3 kb für den Druck, was einer Versenkung von ungefähr 10 km entspricht. Die Deformation erfasste sämtliche Gesteine, überprägte diese jedoch unterschiedlich, wobei sowohl duktile als auch spröde Strukturen entstanden. Zu den ersteren

gehören Schieferung(en), Scherzonen und Mylonite, zu den letzteren Quer- und Scherbrüche. Metamorphe Umwandlungen begleiteten und begünstigten teilweise die duktile Deformation, wie z.B. die Verglimmerung von Kalifeldspat.

Nebst diesen Strukturen sind in einer Spätphase der alpidischen Gefügeprägung Zerrklüfte - bevorzugt entlang grösserer, mechanischer Diskontinuitäten wie Granit/Lamprophyr-Kontakte - entstanden. Das Mindestalter dieser Zerrklüfte beträgt 15 MJ. Die Zerrkluftbildung wurde von einer starken hydrothermalen Tätigkeit begleitet. Einige Gesteinsbereiche wurden stark ausgelaugt, so dass die Porosität deutlich stieg (bis max. 18 Vol-%). Als Folge dieser hydrothermalen Fluidzirkulation wurden auch die meisten Sprödstrukturen versiegelt.

Der alpidischen Orogenese folgte die Hebung des Aar-Massivs, die z.T. noch heute andauert. Während dieser Hebung wurden die wichtigsten Gefügeflächen spröd reaktiviert. Als Folge entstanden die meisten offenen Klüfte, die heute potentielle Wasserzirkulationswege darstellen.

Strukturgeologie

Für die statistische Auswertung der Sprödstrukturdaten erfolgte eine Ausscheidung in Kategorien, je nach Mineralbelag auf den Fugenflächen. Die Daten stammen aus den Stollenabschnitten sowie aus 12 Bohrungen. Drei duktil entstandene Trennflächensysteme mit bevorzugter Mineraleinregelung konnten erkannt werden:

- die steil SE fallende, NE-SW streichende Hauptschieferung S_2 und
- die steilen, in bezug auf S_2 konjugierten Scherflächen S_1 (oft subparallel zu S_2) und S_3 (E-W streichend).

Da S_1 allein aufgrund von Fallazimut und Fallwinkel nur bedingt von S_2 unterscheidbar ist, wurden diese beiden Trennflächensysteme zusammengefasst behandelt (S_1+S_2).

Sicher belegt sind zusätzlich sechs Sprödstruktursysteme (allgemein mit K beschrieben, ausser den von STECK 1968a stammenden Bezeichnungen S_4 und S_5). Es handelt sich um:

- S_4/K_4, K_2/L (L=Lamprophyrrichtung), K_1, K_3, S_5, sowie
- ein subhorizontales Zerrkluftsystem ZK.

Allgemein bilden diese Systeme konjugierte Paare zu S_2. S_4/K_4 sowie K_2/L wurden jeweils zu einem System zusammengefasst, da in den meisten Fällen wegen zu grosser Überschneidungen der Orientierungen, oft keine klare Unterscheidung möglich ist.

Das FLG wurde in Bereiche unterteilt, welche jeweils entweder einer Bohrung oder einem Stollenabschnitt entsprechen. Es treten deutliche Unterschiede in der Häufigkeitsverteilung der jeweiligen Systeme auf. Richtungsschwankungen und Änderungen im Fallwinkel von 10 bis 20° sind häufig. Im allgemeinen besitzen die verbreitesten Fugensysteme auch den höchsten prozentualen Anteil an offenen Klüften; diese dominieren vor allem in S_1+S_2. Da aber verschiedene Trennflächenpopulationen die einzelnen Bereiche kennzeichnen, können auch Systeme wie S_3, K_2/L und S_5 reich an offenen Klüften sein.

Mit den Oberflächenaufnahmen konnten die untertage gewonnen Daten räumlich erweitert werden, obwohl hier weniger Systeme erkannt wurden. Nebst der Hauptschieferung S_2 wurden nur S_1, S_3, K_2/L und K_3 gefunden.

Oberflächen-, Stollen- und Bohrungsaufnahmen basieren auf der gleichen, eindimensionalen Datenerfassung (Aufnahme an Bohrkernen, Stollenabschnitten, bzw. entlang von Profilen). Die Untertageauswertungen ermöglichen Vergleiche bezüglich Trennflächenlagen und Häufigkeitsverteilungen. Oberflächenauswertungen ergänzen die Charakteristiken der Systeme mit der Erstreckung und den Trennflächenabständen. Zusätzlich liefern die Oberflächenbeobachtungen Hinweise auf Bewegungsrichtungen.

Kleinräumig gesehen, zeichnet sich das Juchlistock-FLG Gebiet durch eine grosse Komplexität aus, denn grössere ungeklüftete Bereiche fehlen oder sind nur spärlich vorhanden. Grossräumig erscheint das Bild einfacher, da weniger Trennflächensysteme erkennbar sind und das Gesamtbild im wesentlichen nur von S_1+S_2, S_3 und K_2/L geprägt wird.

Wasserzirkulation

Das FLG wurde bewusst ausserhalb der grösseren und stärker wasserführenden Störzonen angelegt, welche im Hauptzugangsstollen der Kraftwerke Oberhasli (KWO) kartiert werden konnten. Es liegt deshalb in einem relativ trockenen Gebirgsbereich. Nur im Norden (BK-Bereich) und im Süden (AU-Bereich) wurden stärker schüttende Störzonen angefahren.

Das im Gebirge vorhandene Wasser zirkuliert vorwiegend auf Trennflächen und hier in erster Linie in den Systemen S_1/S_2 und entlang von Lamprophyrkontakten. Diese Systeme weisen grosse Erstreckungen auf und durchschlagen das Gebirge häufig bis zur Oberfläche.

Bei den Wasseraustritten im Hauptzugangsstollen wirken sich bis zu einer Überdeckung von 250 m die klimatischen Einflüsse (Schneeschmelze, Seespiegelschwankungen) auf die Schüttung aus. Im Bereich des FLG mit einer Überdeckung von mehr als 400 m, sind solche äusseren Einflüsse nicht erkennbar.

Allgemein sind die Bergwasserschüttungen im FLG gering. Sie betragen

- 0 - 12 ml/min·m′ im Bohrloch,
- 0.1 - 3 ml/min pro offene Trennfläche im Bohrloch.

In stark zerklüfteten Bereichen bei BK, US und MI werden lokal stark erhöhte Wasserschüttungen beobachtet.

RESUME

Les résultats des études géologiques et pétrographiques entreprises entre 1980 et 1987 dans la région du Juchlistock ainsi que dans le laboratoire souterrain du Grimsel (LSG) sont répertoriés et commentés dans le présent rapport. Ces investigations comprennent:

- la cartographie géologique du Juchlistock;
- le relevé géologique d'environ 840 m de galeries;
- le relevé géologique d'environ 1476 m de forages carottés;
- le dépouillement statistique et l'interprétation d'environ 3500 données structurales souterraines;
- la mesure du débit des pointements d'eau souterraine dans les galeries et les forages.

Géologie

Le LSG se trouve dans la moitié méridionale de la partie centrale du massif de l'Aar, à une profondeur moyenne de 400 m sous le Juchlistock, où n'affleurent pratiquement que des roches granitiques. C'est ainsi que la moitié nord du LSG est comprise dans le granit central de l'Aar, alors que la moitié sud est taillée dans la granodiorite du Grimsel. Des filons intrusifs de lamprophyre, rassemblés en faisceaux, ainsi que quelques filons d'aplites peu fréquents entrecoupent ces roches granitiques. L'âge de consolidation varisque des granits est de l'ordre de 290-300 Ma, alors que celui des aplites voisine 250 Ma.

L'ensemble du massif de l'Aar a été affecté par une déformation et un métamorphisme alpins importants. Le développement de la fabrique dominante des roches est contemporain de l'empreinte métamorphique de faciès "schistes verts", dont l'âge oscille entre 20 et 25 Ma. Les conditions de température et de pression atteintes pendant le métamorphisme sont de l'ordre de 400 à 450 °C et 3 kb, ce qui cor-

respond à un enfouissement d'environ 10 km. La déformation a affecté toutes les roches, avec une intensité toutefois variable, conditionnant ainsi le développement de structures aussi bien ductiles que cassantes. La première catégorie comprend une on plusieurs schistosités, des zones de cisaillement et des mylonites, alors que la seconde regroupe des fractures de cisaillement et de tension. Les transformations métamorphiques ont acompagné et parfois favorisé la déformation ductile, notamment dans le cas du remplacement du feldspath potassique par le mica blanc.

En plus de ces structures, des fentes de tension se sont formées pendant une phase tardive de la structuration alpine, de préférence le long de discontinuités mécaniques majeures telles les contacts entre granits et lamprophyres. La formation de ces fentes alpines, dont l'âge est de l'ordre de 15 Ma, a été accompagnée par une importante activité hydrothermale. En effet, aux abords de ces fentes, la roche a été intensément lessivée, augmentant ainsi de manière substantielle la porosité (jusqu'à un maximum de 18 %-vol.). En conséquence de cette activité hydrothermale, les fractures ont été en grande partie scellées.

Succédant à l'orogénèse alpine, le soulèvement du massif de l'Aar, se poursuit encore en partie à l'heure actuelle. Les structures planaires les plus importantes ont été réactivées de manière cassante pendant ce soulèvement. C'est ainsi que se sont formées la plupart des fractures "ouvertes", constituant à l'heure actuelle des voies potentielles de circulation d'eau souterraine.

Géologie structurale

Le dépouillement statistique des données structurales (structures cassantes uniquement) a nécessité une discrimination basée sur la nature des minéraux scellant les fractures. Les données proviennent de tronçons de galeries du LSG ainsi que de 12 forages. Trois systèmes structuraux ductiles avec orientation préférentielle des miné-

raux ont pu être distingués:

- la schistosité principale S_2, très redressée, d'orientation NE-SW et plongeant vers le SE;
- les plans de cisaillement S_1 et S_3, également redressés, conjugués par rapport à S_2 et d'orientation subparallèle à S_2 (S_1) ou E-W (S_3).

Comme S_1 ne peut être que difficilement séparé de S_2 en ne tenant compte que de l'azimut et de l'angle du pendage, les deux systèmes ont été regroupés en un ensemble (S_1+S_2).
En plus de ces structures ductiles, l'existence de six systèmes de fractures est bien documentée (ces structures sont décrites à l'aide préfixe K, hormis S_4, S_5 et S_6 qui ont été repris de STECK 1968a). Il s'agit des systèmes suivants:

- S_4/K_4, K_2/L (L = orientation de lamprophyres), K_1, K_3;
- ZK (fentes subhorizontales)

L'existence des systèmes S_5 et S_6 peut être soupçonnée, mais le peu de données structurales les étayant grève leur identification.
En général, ces systèmes forment des couples de structures conjuguées par rapport à S2. S4/K4 et K2/L ont été regroupés en un système du fait que dans la plupart des cas, des recoupements d'orientation hypothèquent toute discrimination.

Le LSG a été divisé en secteurs correspondant soit à un forage, soit à un tronçon de galerie. La distribution et l'abondance des systèmes structuraux varie sensiblement d'un secteur à l'autre; de plus, des changements d'orientation de 10 à 20° sont fréquents. En règle générale, la part des fractures ouvertes est nettement supérieure dans les systèmes structuraux quantitativement dominants comme S_1+S_2. Toutefois, comme les populations de fractures diffèrent d'un secteur à l'autre, les diaclases ouvertes peuvent également abonder dans les systèmes S_3, K_2/L et S_5.

Les observations faites à la surface permettent d'élargir le spectre des données obtenues sous terre, bien que seule une partie des systèmes ait été reconnue. En effet, en dehors de la schistosité principale S_2, seuls S_1, S_3, K_2/L et K_3 ont pu être mis en évidence. L'obtention des données structurales en surface le long de profils, dans les galeries ou sur les carottes procède de la même manière unidimensionelle. Le dépouillement des données souterraines permet une comparaison avec les distributions spatiale et quantitative des structures en surface. Les données de surface complètent d'ailleurs la caractérisation des différents systèmes, par l'estimation de l'extension latérale des structures ainsi que par les indices de mouvements le long des fractures.

A l'échelle de l'affleurement, le secteur Juchlistock-LSG se traduit par une grande complexité du fait du manque ou de la rareté de zones sans développement de structures planaires. A l'échelle régionale toutefois, une image plus simple se dégage en raison de la dominance des systèmes S_1+S_2, S_3 et K_2/L.

Circulation d'eau souterraine

Le site du LSG a été sciemment choisi en se basant sur le relevé géologique de la galerie d'accès à la centrale des "Kraftwerke Oberhasli" (KWO), là où font défaut les importantes zones déformées aquifères. C'est ainsi que le LSG se trouve dans une secteur rocheux plutôt sec, car des zones déformées où circule de l'eau souterraine, n'ont été rencontrées qu'au Nord (secteur BK) ou au Sud (secteur AU) du LSG.

L'eau rencontrée dans le massif rocheux se cantonne aux structures planaires, en premier lieux dans les fractures des systèmes S_1+S_2 et le long des contacts granits/lamprophyres. Ces structures possèdent une extension latérale très importante et se poursuivent jusqu'à la surface ou communiquent avec des structures en surface.

Les pointements d'eau dans la galerie d'accès sont influencés par des facteurs climatiques (fonte des neiges, variation du niveau des retenues d'eau) jusqu'à une profondeur de 250 m sous terre. Dans le secteur du LSG, où le recouvrement rocheux atteint 400 m, de telles influences ne peuvent être mises en évidence.

En règle générale, les débits d'eau souterraine sont faibles, puisqu'ils n'atteignent que:

- 0-12 ml/min·m' dans les forages;
- 0.1-3 ml/min par fracture ouverte dans les forages.

Des débits plus importants peuvent être localement observés dans les zones fortement fracturées des secteurs BK, US et MI.

TABLE OF CONTENTS

LIST OF APPENDICES

LIST OF FIGURES

LIST OF TABLES

1 INTRODUCTION

1.1 The Grimsel Test Site (GTS)

In 1979, Nagra decided to construct an underground laboratory in the crystalline basement of Switzerland, the aim being to complete the scientific research being carried out in the Stripa Rock Laboratory (central Sweden) in which NAGRA also takes an active part.

Strictly speaking, it would have been appropriate to construct a crystalline rock laboratory in the basement of Northern Switzerland since this formation is being considered as a potential host rock for high-level radioactive waste. However, since exposures of crystalline rock were lacking in this region, a laboratory would have to have been located at a considerable depth and identification of a suitable site would have involved extensive reconnaissance programmes.

The Juchlistock area offered a readily available location with geological conditions which were generally easy to survey. Geological surface mapping and investigations carried out in the tunnels belonging to the Oberhasli power plant confirmed the suitability of the granitic rock as a site for an underground laboratory. The location also has the advantage of already being accessible via a power plant tunnel which is suitable for road vehicles.

1980 saw the beginning of the first investigation campaign directed at closer characterisation of the area selected for the Test Site. The actual construction phase followed three years later with excavation of the laboratory tunnel using a full-face tunnelling machine (Figure 1).

The geological, hydrogeological, geophysical and geochemical experiments which have been carried out at the Test Site have four basic objectives:

- Assessing the qualitative and quantitative applicability of foreign research results to the specific geological conditions at potential repository sites in Switzerland.
- Carrying out specific experiments which are relevant to the particular aspects of the NAGRA repository concept.
- The build-up of know-how at all levels (planning, performance and interpretation) of underground investigations in different experimental fields.
- Acquisition of practical experience in development, testing and application of suitable measurement techniques and associated instrumentation.

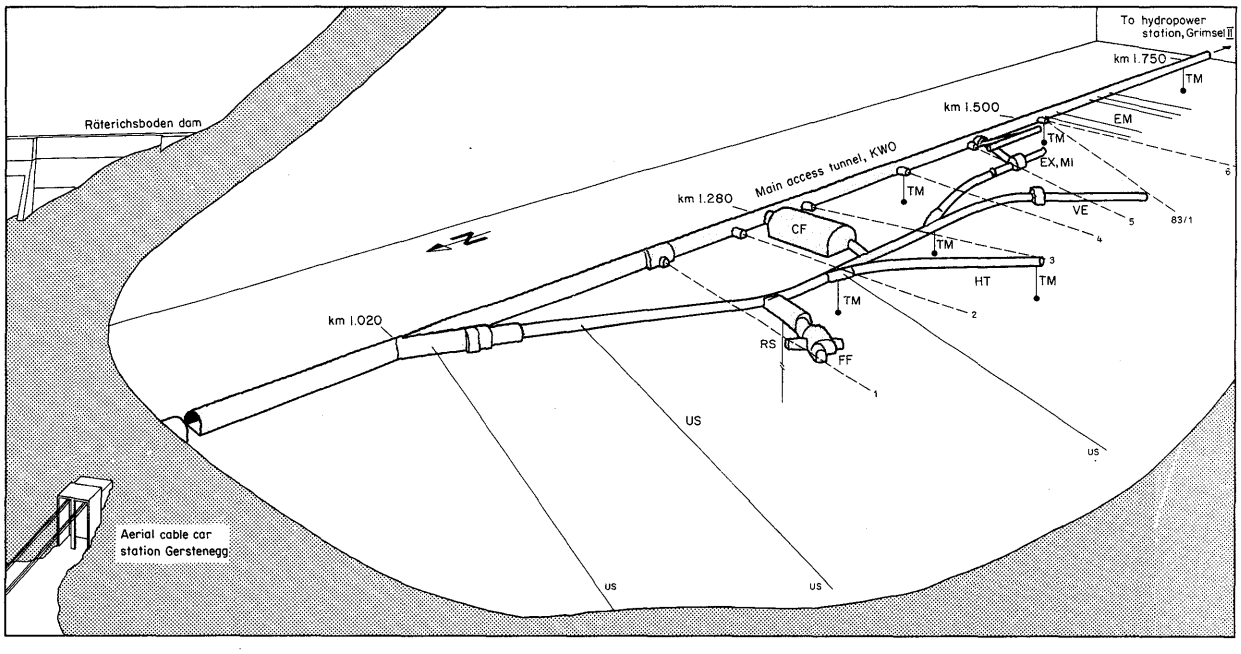

Figure 1: Perspective view of the Grimsel Test Site

1.2 Scope and objectives of this report

GEOTEST, a Swiss geological consulting group, has been responsible for performing and evaluating the geological and petrographic investigations at the GTS, the results of which are presented in this report. GEOTEST also acted as geological consultants for different experiments at the GTS.

The aim of the report can be defined as follows:

- documentation of the geological and petrographic conditions present in the Juchlistock;
- description of the structural properties of the granitic rocks at the GTS.

The documentation should provide a basis for:

- geological interpretation of hydrogeological experiments already carried out or presently being performed at the GTS;
- hydrogeological modelling of the Juchlistock;
- planning of new experiments.

The investigations carried out at the GTS also give useful information on methods and techniques which could be applied in geological characterisation of potential host rock formations.

Since geology is a common link between numerous other fields of earth science such as hydraulics, hydrochemistry, geophysics and rock mechanics, it is difficult (but also not necessarily relevant) to draw a clear distinction between the different disciplines. For this reason, data from different technical fields will be presented here in so far as they appear to be relevant to the **overall** geological understanding of the Grimsel area. The results from individual test projects at the GTS are not presented here.

Reference should also be made at this point to the **raw data report** (KEUSEN and SCHULER, 1987) prepared by GEOTEST. This report contains detailed documentation on all the geological investigations (particularly all drilling and tunnel profiles), as well as an index of all experiments carried out at the GTS up to July 1987.

1.3 Investigations carried out

Table 1 gives an overview of all the investigations carried out on behalf of NAGRA at the GTS for the purpose of rock characterisation. Detailed information on performance and evaluation of the individual tests can be found in the Tables of the raw data report (KEUSEN and SCHULER 1987).

Aim of investigation	Recording actual condition of rock				Checking effects of tunnel construction	
Aspects / Field / Investigation method	Petrography/ Mineralogy	Tectonics/ Jointing	Hydrogeology	Technical Properties	Rock formation	Flow-paths
Geology						
Surface mapping	X	X	X			
Tunnel mapping KWO facilities, GTS	X	X	X			
Core logging	X	X	X			
Geophysics						
Electrical and electromagnetic investigations in tunnels and boreholes		X	X			
Radiometry	X					
Seismics/acoustics, surface, tunnels, boreholes		X		X	X	
Borehole TV and SABIS		X				
Rock temperature measurements				X	X	
Mineralogy/ Geochemistry						
Tunnel mapping with UV light	X		X			
Microscopy	X					
Chemical analysis	X		X			
Rock mechanics						
Measurements and experiments in boreholes and tunnel				X	X	
Laboratory experiments				X		
Drillability of rock				X		
Rock hydraulics						
Water-flow and temperature measurements			X			X
Pressure measurements in boreholes			X			X
Injection tests in boreholes and tunnel			X			X
Flow-through experiments			X			
Hydro-chemistry						
General chemical and physical parameters in surface- and groundwaters			X			X
Trace elements in groundwater			X			
Isotopes in surface and groundwaters			X			X

Table 1: Overview of investigations at the GTS in geology, hydrogeology, rock mechanics and geophysics.

2 REGIONAL GEOLOGY

2.1 Introduction

The Aar Massif is a crystalline massif some 120 km long and 20-25 km wide which extends SW-NE and, despite imbrication, is largely autochthonous (Appendix 1; HÜGI 1956, LABHART 1977). From a tectonic point of view, it belongs to the Helvetic belt and represents the pre-Triassic basement of the lower Helvetic nappes which were partly sheared off and transported northwards. The latter consist mainly of the Doldenhorn and Gellihorn nappes in the W, the Infrahelvetic complex in the E (MILNES and PFIFFNER 1977, 1980) and the sediments of the Autochthonous which occur mainly at the NW margin of the Massif. Towards the W, NW, N and E, the Aar Massif dips below the autochthonous and parautochthonous sediments of the Helvetic belt, while to the SE it borders with the Gotthard Massif along the Urseren zone (or "syncline"). Towards the east (Upper Rhine valley) the Aar and Gotthard Massifs are additionally separated by the Tavetsch Massif.

The Aar Massif can be seen as the equivalent of the Aiguilles Rouges and Mont Blanc Massifs which are located to the West. All these external crystalline massifs are typical structural elements of the Western and Central Alps. They crop out where earlier, forward-directed overthrusting and folding phases are superposed by a late backfolding (STECK 1984). The SW-NE-striking backfolding at the SE margin of the Aar Massif (Glishorn anticline; STECK et al. 1979, STECK 1984) and the later E-W axial culmination (Gastern-Aletsch flexure; STECK 1968a, 1984) have resulted in a dome-basin interference pattern which explains the form of the Aar Massif (STECK 1984).

The crystalline basement of Northern Switzerland, which was not affected by the alpine deformation, represents the northern con-

tinuation of the Aar Massif. Both are similar in that they consist of a pre-granitic basement (polymetamorphic gneiss- and migmatite-complex with Carboniferous volcanoclastites and sediments) intruded by Variscan granitoids (Appendix 1).

The Variscan orogeny was followed by a Permian peneplanation, during the course of which locally thick continental sediments were deposited in graben (Verrucano). During the Triassic, the sea covered the area, although some areas of the Aar Massif were not flooded until the Jurassic (e.g. the Windgällen). The process of sedimentation continued - depending on palaeogeographic location and with interruptions of varying length - from the Triassic into the early Tertiary. The most recent sediments deposited at the northern edge of the Aar Massif, i.e. the fish fauna of the Engi slates, are Early Oligocene (~35 Ma).

In the Late Oligocene and the Miocene (~25-10 Ma), the alpine orogeny affected the whole Aar Massif which was subjected to reverse faulting, folding and imbrication, with contemporaneous overprinting by a greenschist facies metamorphism. There was no homogeneous tectonometamorphic overprinting of the Massif, but rather development of deformation and metamorphism gradients increasing from N to S.

A more detailed presentation of the geology of the Aar Massif would be outwith the confines of this report. Reference should be made in this respect to the guide-book "Aarmassiv und Gotthardmassiv" by LABHART (1977). The chapter in this report entitled "Regional Geology" is therefore restricted to a detailed description of the geological conditions in the Grimsel cross-section set against a background of general information on the whole Aar Massif area.

2.2 Geology and tectonic evolution of the Aar Massif in the Grimsel cross-section

2.2.1 Structure

Based on recent work (ABRECHT and SCHALTEGGER 1988, SCHENKER and ABRECHT 1987), the classic subdivision of the Central Aar Massif into the Gastern-Innertkirchen-Lauterbrunnen granite zone, the northern "schist envelope" ("Altkristallin"), Aare granites and the southern "schist envelope" ("Altkristallin"; HÜGI 1956, 1967) can be refined along the Oberhasli from N to S as follows (Table 2, Figure 2, Appendix 2).

Migmatitic Innertkirchen-Lauterbrunnen Crystalline Complex	
Variscan Basement/ "Altkristallin" and Volcanoclastites	- Erstfelden gneiss zone (polymetamorphic gneiss/migmatite complex) - Guttannen unit (polymetamorphic gneiss/migmatite complex) - Trift formation (Carboniferous volcanoclastites) - Ofenhorn-Stampfhorn unit (polymetamorphic gneiss/migmatite complex) - Diechter glacier formation (Carboniferous volcanoclastites)
Aare granites	- Mittagfluh granite - Central Aare granite - Grimsel-granodiorite

Table 2: Regional structure of the Aar Massif along the Oberhasli (ABRECHT and SCHALTEGGER 1988; see Figure 2).

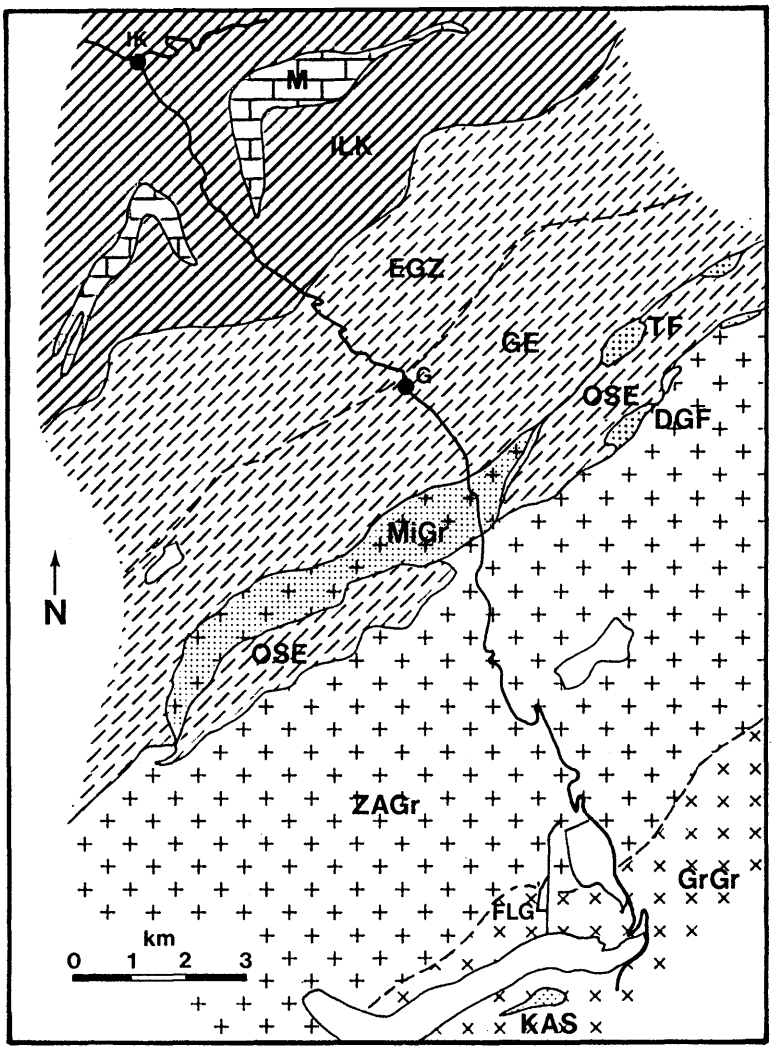

Figure 2: Tectonic sketch map of the Oberhasli, slightly simplified and completed according to ABRECHT and SCHALTEGGER (1988).

Abbreviations:

DGF	Diechter glacier unit
EGZ	Erstfelden gneiss zone
GE	Guttannen unit
GrGr	Grimsel-granodiorite
ILK	Innertkirchen-Lauterbrunnen Crystalline complex
KAS	Kessiturm aplite stock
FLG	Grimsel Test Site
G	Guttannen
M	Mesozoic
MiGr	Mittagfluh granite
OSE	Ofenhorn-Stampfhorn unit
TF	Trift formation
ZAGr	Central Aare granite
IK	Innertkirchen

Further to the south, from the summit of the Grimsel Pass, there follow the gneiss-schist interzone with partly imbricated volcanoclastites, the Southern Aare granite and the Southern "gneiss envelope" (HÜGI 1956, 1967, STALDER 1964, LABHART 1977).

The units which form the pre-granitic Variscan basement north of the Aare granite are separated from one another by Variscan mylonite zones which were partly reactivated by the alpine deformation (KAMMER 1985, cited in ABRECHT and SCHALTEGGER 1988).

2.2.2 Age of the geological units

The Innertkirchen-Lauterbrunnen migmatite complex consists mainly of a paragneiss series which was affected by selective anatexis. The predominantly sedimentary origin of this gneiss series is clearly evidenced by the extensively block-bearing (biotite-gneisses, amphibolites, marbles) pinite granites; these were previously cordierite granites and show gradual transitions to migmatites (HÜGI 1956, 1967, LABHART 1977). The age of migmatisation has not been determined geochronologically but HÜGI (1967) and STECK (1968a) assume that the migmatic granite formation took place during the Variscan, although it is older than the intrusion of the Aare granites in the wider sense.

The Erstfelden gneiss zone and the Guttannen- and Ofenhorn-Stampfhorn-units (Figure 2; summarised in Appendix 2 as "Altkristallin") consist basically of a polymetamorphic paragneiss series (biotite gneisses, amphibolites, calc-silicate rocks), migmatites and small, pre-Aare-granite acid and intermediate to basic intrusive stocks, aplites and pegmatites (LABHART 1977, SCHENKER and ABRECHT 1987, ABRECHT and SCHALTEGGER 1988). A pre-migmatitic, amphibolite facies metamorphism affected all these units but its traces have been obscured to a greater or lesser extent by the alpine green-

schist facies overprinting. The fact that the migmatisation also affected amphibolite facies gneisses and amphibolites indicates a possible pre-Variscan (HUEGI 1956, 1967) or Caledonian age (LABHART 1977, SCHENKER and ABRECHT 1987, ABRECHT and SCHALTEGGER 1988) for this metamorphism.

In the coarse detrital sequences of the Carboniferous Diechter glacier unit (indicated as volcanoclastites in Appendix 2), there are gravels consisting of re-worked basement rocks, including migmatites. This erosion of the mesometamorphic crystalline basement can be used to postulate a Caledonian age for the migmatisation (SCHENKER and ABRECHT 1987).

Geochronological dating of biotites (Rb-Sr) in these basement gneisses give values between 297 and 315 Ma (WÜTHRICH 1965; age with up-to-date decay constants re-calculated by ABRECHT and SCHALTEGGER 1988). However, these are cooling ages (T at 300°C) which could possibly be explained by a temperature rise during the Variscan. In this case, they would not correspond to the period of cooling following migmatisation.

In contrast to the basement gneisses, the Carboniferous volcanoclastic sequences were affected neither by an amphibolite facies metamorphism nor by migmatisation. This again indicates the high probability that these events have a Caledonian age. The Carboniferous units consist of volcanic rocks (mainly rhyolites), pyroclastites (ignimbrites, tuffs) and epiclastites with conglomeratic to argillaceous sediments which are intruded locally by small post-Aare-granitic diorite stocks (SCHENKER and ABRECHT 1987). During the Variscan orogeny, the Central Aare granite intruded into the Diechter glacier unit and caused a contact metamorphism (including growth of andalusite; SCHENKER and ABRECHT 1987). Similarly to the whole Aar Massif, the volcanoclastic units were subjected to alpine greenschist facies overprinting.

The (late) Variscan intrusion of the Aare granites (in the wider sense) to a shallow crustal level is clearly evidenced by the

intrusive contact and the contact metamorphism in the Diechter glacier unit. Different granite bodies can be distinguished in the Grimsel cross-section, e.g. Mittagfluh granite (MiGr), Central Aare granite (ZAGr) and Grimsel-granodiorite (GrGr), although many of the contacts between these different intrusive rock bodies were largely obscured by the alpine events. In the W of the Aar Massif, the intrusive contacts within the Central Aare granite are an indication of multi-phase emplacement of the granite plutons (STECK et al. 1979). The order of the intrusions is as follows: GrGr -> ZAGr -> MiGr. While geological evidence indicates that the MiGr must be younger than the ZAGr, the age relationships between the ZAGr and GrGr in the field are generally unclear. This is mainly because there is a mutual lithological assimilation of these two granites along contacts (STALDER 1964). An indication of the sequence GrGr -> ZAGr is given by the inclusion of hornblende-bearing granodiorite in the ZAGr near the end of the Unteraar glacier (STALDER 1964).

The Kessiturm aplite stock west of the Grimsel Pass which intruded into the GrGr shows clear intrusive contacts (STALDER 1964; Figure 2). Both the MiGr and the Kessiturm aplite stock, as well as the numerous aplite dykes, belong to the same magmatic cycle as the ZAGr and should be seen as products of a continuing magmatic differentiation (SCHALTEGGER 1987). In contrast to this, the late intrusions of lamprophyre dykes belong to another magmatic event, despite close spatial links with the granites.

The history of the development of the basement gneisses is still incomplete due to the lack of geochronological measurements. On the other hand, the picture of the development of the Aare granites (in the wider sense) is fairly clear.

Dating of ZAGr has given values of 281 ± 11 Ma (Rb-Sr total rock, isochron with 4 samples; WÜTHRICH 1965; age with up-to-date decay constants re-calculated by FREY et al. 1976) and, recently, also 286 Ma (ABRECHT and SCHALTEGGER 1988).

In the Grimsel cross-section, SCHALTEGGER (1987) obtained an average age of 280 ± 12 Ma (all ZAGr samples), the samples with $^{87}Rb/^{86}Sr < 10$ giving an age of 297 ± 15 Ma. In the Reuss valley cross-section, the average age of all granite samples is 291 ± 4 Ma (SCHALTEGGER 1987). All these data are interpreted as ages of solidification and confirm the Variscan, Upper Carboniferous age of the ZAGr.

The total rock age of the GrGr could not be determined using the Rb-Sr method (SCHALTEGGER 1987). The age of intrusion assumed for the GrGr (270-300 Ma) is based primarily on an age determined for zircons using the U-Pb method (PASTEELS 1964, cited by LABHART 1977). Ages of 264 ± 5 Ma (Rb-Sr, total rock) for the Kessiturm aplite stock and 250 ± 5 Ma (Rb-Sr, total rock) for different aplite dykes confirm that these rocks originated as a result of progressive magmatic differentiation (SCHALTEGGER 1987). Dating of MiGr has given an astonishingly young age of 230 ± 8 Ma (Rb-Sr, total rock; SCHALTEGGER 1987). An even younger age of 208 ± 26 Ma was found for an aplitic granite stock which was melted out from the overlying granitic gneisses by the magma of the ZAGr and penetrated into the Ofenhorn-Stampfhorn unit (ABRECHT and SCHALTEGGER 1988). The last two ages are interpreted as an indication of a Triassic or Jurassic hydrothermal overprinting which has obscured the true age of solidification of the rocks (ABRECHT and SCHALTEGGER 1988).

2.2.3 Deformation

A popular hypothesis claims that the intrusion of the Aare granites (in the wider sense) occurred along Variscan, NE-SW orientated fault zones and fractures (STECK 1968a, STECK et al. 1979, SCHENKER and ABRECHT 1987). In both the polymetamorphic gneiss series and the volcanoclastic units, there are relatively widespread traces of deformation of pre-alpine structures which are still clearly recognisable as such. On the other hand, it is not clear to what extent the granites were subjected to a Variscan magma-tectonic structural overprinting since the alpine deformation has obscured older structural elements to the point where they are unrecognisable. However, it appears quite probable that dykes such as aplites and lamprophyres intruded into (at least) late-magmatic structurally weak zones. On the other hand, areas of granite which remained unaffected by the alpine overprinting show no traces of older deformation phenomena. The granites were generally present as isotropic bodies before being subjected to alpine deformation (CHOUKROUNE and GAPAIS 1983).

Although the dominant SW-NE-striking structural trend in the Variscan basement was established as early as the Palaeozoic (STECK 1968a, LABHART 1977), all the structural elements in the granites have an alpine age (STECK 1968a). This can be deduced mainly from the fact that all observed structures are linked more or less strongly with the main schistosity (STECK 1968a, 1984, STECK et al. 1979, CHOUKROUNE and GAPAIS 1983). In addition, the NE-SW-striking, steeply-dipping main schistosity of the granites corresponds to that of the Mesozoic and Tertiary sediments of the Autochthonous and Parautochthonous (STECK 1968a, LABHART 1977, MILNES and PFIFFNER 1977).
As a result of the continuous alpine deformation, the structural elements shown in Figure 3 and Table 3 were formed in the different rock bodies (STECK 1968a, 1984, STECK et al. 1979).

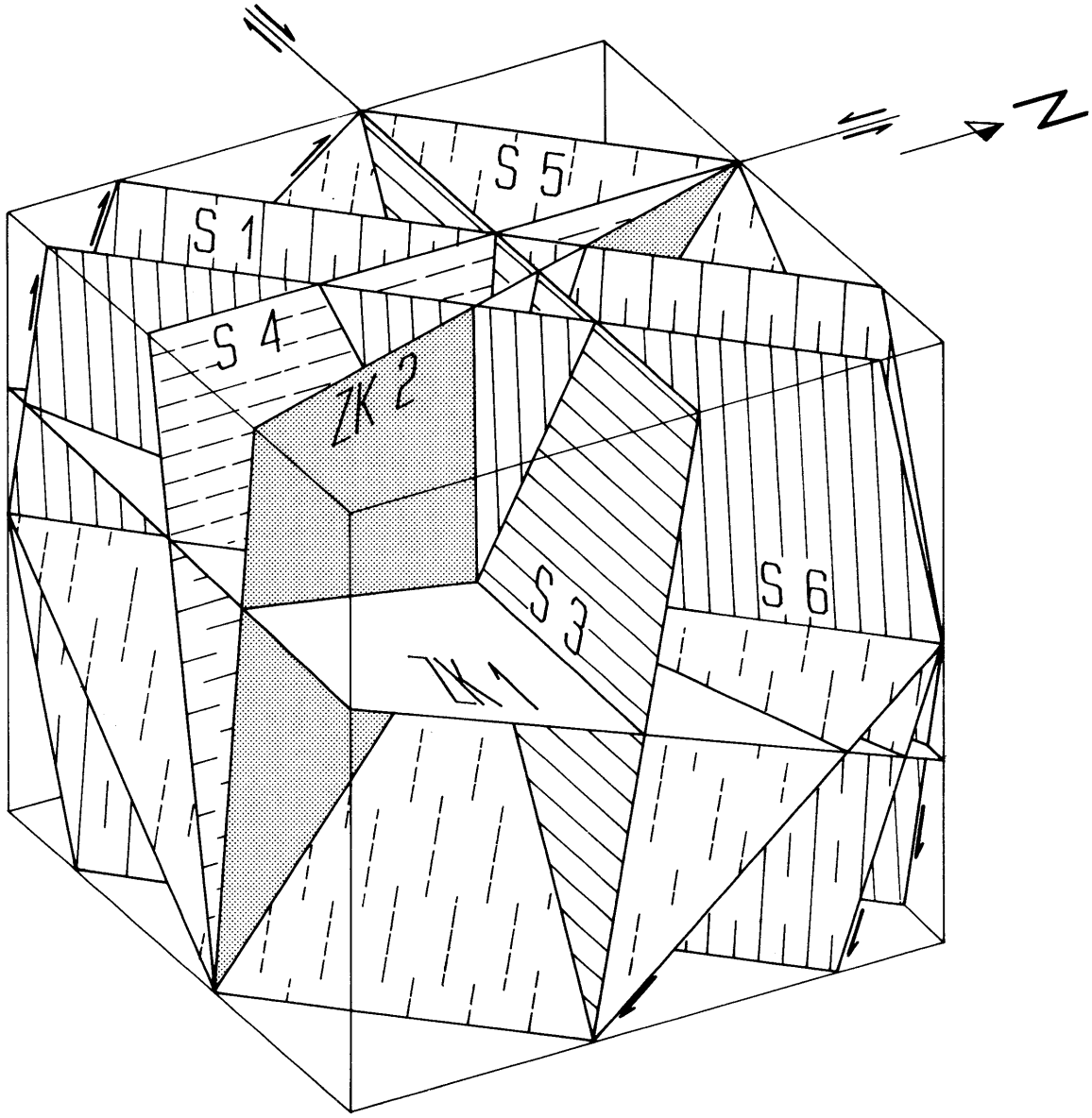

Figure 3: Alpine structures according to STECK (1968a). The locally occurring crenulation schistosity S_2 which dips steeply to the NW is not shown in the Figure.

Apart from the tension joints which correspond to a late phase of the alpine structural overprinting, all these structures are syn-metamorphic and developed more or less simultaneously. This was a result of the increasing flattening of the Aar Massif which began with the formation of the main schistosity (STECK 1968a, 1984, STECK et al. 1979).

S_1 ($=S_2$)	NE-SW-striking, steeply SE-dipping partly inverted main schistosity characterised by a strong mineral orientation (biotite, muscovite, chlorite) and the formation of a steep lineation L_1 (= X1) more or less parallel to the dip
S_2 ($=S_2{}^C=S_4$)	second schistosity, steeply NW-dipping, appearing as crenulation in strongly deformed areas (mylonites, biotite schists) and linked with a NE-SW-striking small-scale folding (B_2)
S_3 ($=S_3{}^C=S_{2.1}$)	E-W-striking dextral faults
S_4 ($=S_4{}^C=S_{2.2}$)	N-S-striking sinistral faults
S_5 ($=S_5{}^C=S_{2.3}$)	horizontal to SE-dipping reverse faults
S_6 ($=S_6{}^C=S_{2.4}$)	reverse faults dipping steeply to the NW
ZK_1	sub-horizontal, open tension joints ± perpendicular to L_1
ZK_2	steep, NW-striking filled tension joints ± parallel to L_1 and perpendicular to B_2

Table 3: Alpine structures in the Aar Massif according to STECK (1968a). The terms in brackets come from STECK et al. (1979) and STECK (1984). c, 2.1, 2.2, 2.3 and 2.4 are conjugate shear surfaces.

The orthogonal shear surfaces S_3 and S_4 and the conjugate surfaces S_5 and S_6 are directly linked with a lateral and vertical elongation of the Massif which resulted from its flattening (STECK 1984, STECK et al. 1979). For this reason, the overall picture of deformation is influenced not only by the flattening but also by movements along shear surfaces and shear zones (CHOUKROUNE and GAPAIS 1983).

A somewhat simpler, but nevertheless similar, range of structures in the Grimsel area is described in the work by CHOUKROUNE and GAPAIS (1983). Detailed observations point clearly towards a continuous deformation process rather than one divided into different phases. This can be deduced from the more or less simultaneous formation of schistosity and conjugate shear surfaces. While the schistosity is the result of a continuous penetrative deformation mechanism, the conjugate shear surfaces represent a non-penetrative, non-continuous deformation mechanism.

Because of the rise in the ductility of the rocks with increasing metamorphic grade, the deformation phenomena within the Aar Massif increase from NW to SE (VOLL 1976). Additional local deformation gradients are widespread and are responsible for the heterogeneity of the structural overprinting. There are therefore both gradual transitions from isotropic granite to schistose orthogneiss as well as abrupt changes to areas with strong deformation which are, for example, typical of shear zones (CHOUKROUNE and GAPAIS 1983).

2.2.4 Metamorphism

The deformation and metamorphic overprinting of the Aar Massif occurred simultaneously. Similarly to the deformation, the greenschist facies metamorphism formed a gradient increasing from NW to SE. The estimated P-T conditions increase from ~300°C/2kb in the N to ~450°C/3kb in the southern Aar Massif (FREY et al. 1976, 1980). Although the formation of tension joints corresponds to a late phase of the structural overprinting (STECK 1968, STECK et al. 1979), it nevertheless occurred under conditions which are characteristic of the greenschist facies metamorphism (POTY et al. 1974).

Deformation and metamorphism are closely linked with one another. On the one hand, mineralogical alterations promote deformation (e.g. alteration of feldspars to micas) and, on the other hand, deformation allows fluid to penetrate and/or circulate in the rock. Such an aqueous phase can again alter the mechanical properties and the chemical composition of the rocks (MARQUER et al. 1985). The general reduction in grain size with increasing deformation is the product of combined ductile (recrystallisation of quartz and biotite) and brittle processes (cataclasis of feldspars; VOLL 1976, CHOUKROUNE and GAPAIS 1983).

DEMPSTER (1986) suggests a maximum age of 25 Ma (Rb-Sr on muscovite) for the contemporaneous metamorphism and deformation of the Aar Massif. Cooling to 300°C was reached at around 14-16 Ma (Rb-Sr and K-Ar on biotite and muscovite; DEMPSTER 1986). This age could correspond to the backfolding and compression of the southern margin of the Aar Massif (DEMPSTER 1986). This led to the late uplift and erosion of the Massif, the first Molasse gravels originating from the Helvetic realm appearing in the Helvetian (~15 Ma) (SCHAER and JEANRICHARD 1974).

The uplift of the Aar Massif is still continuing today and is concentrated along young, sub-recent to recent fracture systems (STECK 1968b, LABHART 1977). The uplift rate shows local variations, the average rate being 0.5-1 mm/a (GUBLER 1976). The uplift is also responsible for the reactivation of alpine structural elements (STECK 1968a, 1968b). This has a significant influence on water flow in the granites since it can lead to the formation of new flow-paths.

The development of the Aar Massif in the Grimsel cross-section is given in Table 4.

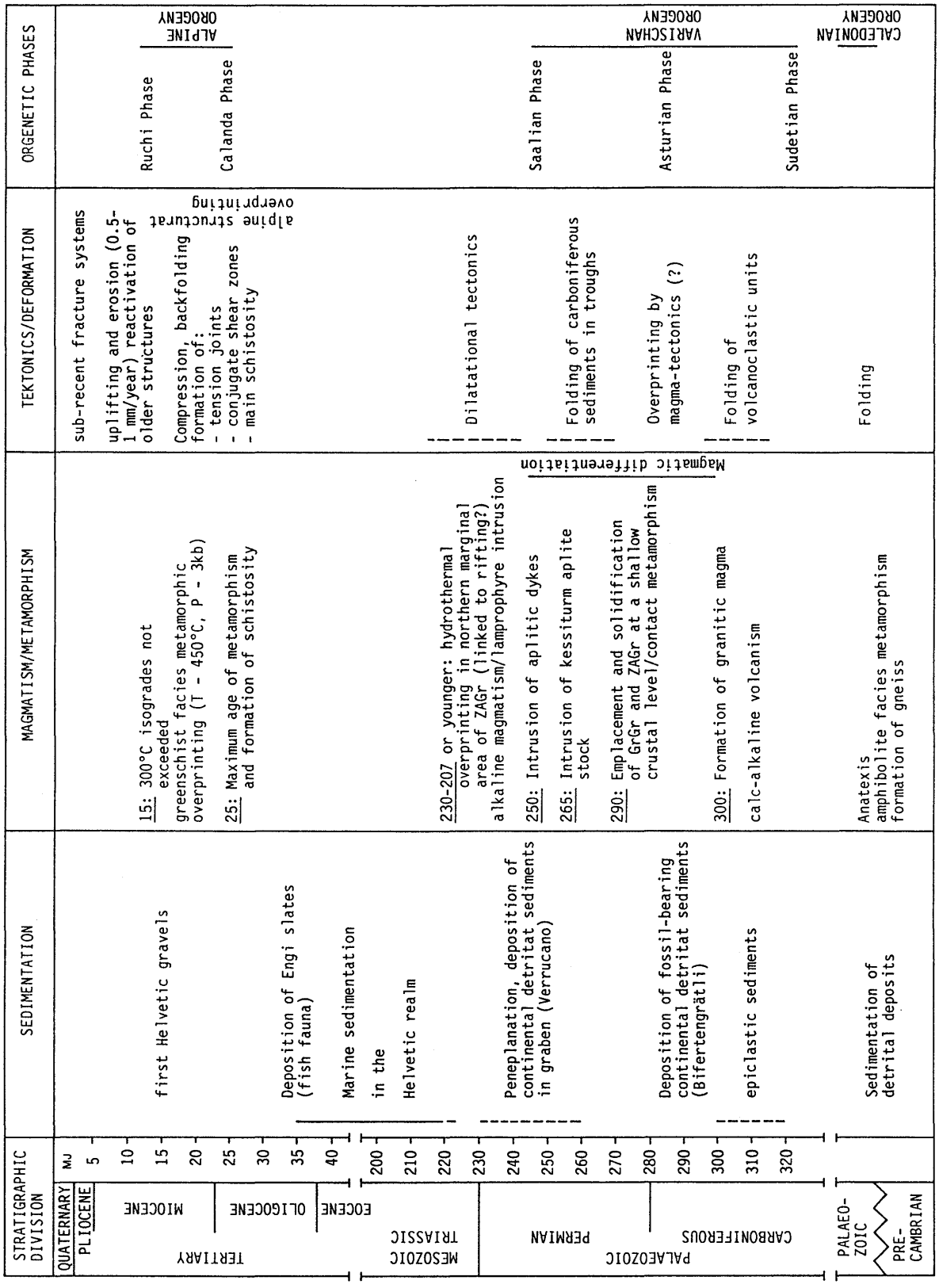

Table 4: Development of the Aar Massif in the Grimsel cross-section.

3 GEOLOGY OF THE GTS

3.1 Petrography

3.1.1 Description of the rocks occurring at the GTS

Two categories of rock with an exclusively magmatic origin can be distinguished at the GTS:

a) Granitic rocks: these are represented by the Central Aare granite (ZAGr) and the Grimsel granodiorite (GrGr) which together make up over 95% of the rock volume. There are several varieties of ZAGr and GrGr which are a result of variations in the modal frequency of the mineral components. For example, an increased biotite content can give the ZAGr the appearance of a GrGr. Particularly in contact zones, it may be difficult to distinguish the two types of granite from one another since these zones are characterised by a mutual assimilation of the individual mineralogical compositions of the granites (STALDER 1964).

Figure 4: Lamprophyres at the GTS

A Two lamprophyre dykes intrude into the Central Aare granite (AU zone, A50). The boudinage of the granite is a result of the differing rheological behaviour of the lamprophyre (ductile) and the Aare granite (more brittle).

B Formation of tension joints at granite/lamprophyre contact, i.e. along mechanical discontinuities (tunnel branch AU/VE zone). These tension joints are surrounded by a light leaching halo.

C Thin section of a lamprophyre of the widelyfound kersantite variety. The matrix which consists of plagioclase, biotite, epidote, potassium feldspar, sphene and ore shows a clearly recognisable magmatic (ophitic) texture (DS SB5/88.8, picture detail 2.8 x 2.0 mm).

A

B

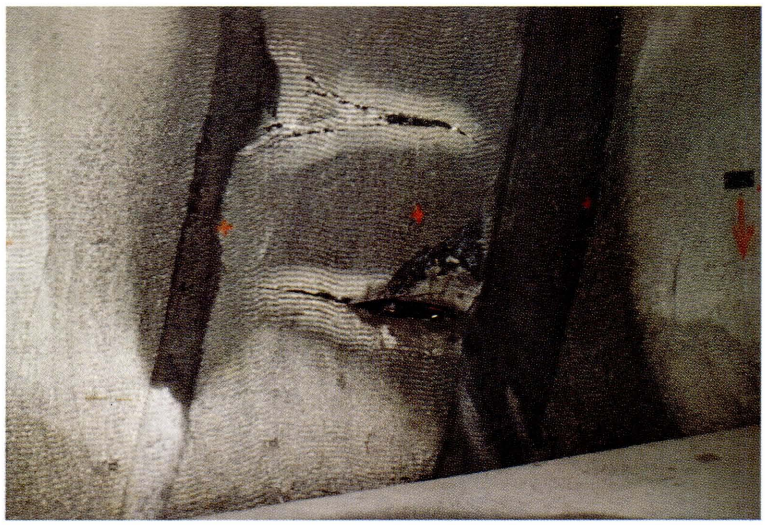

C

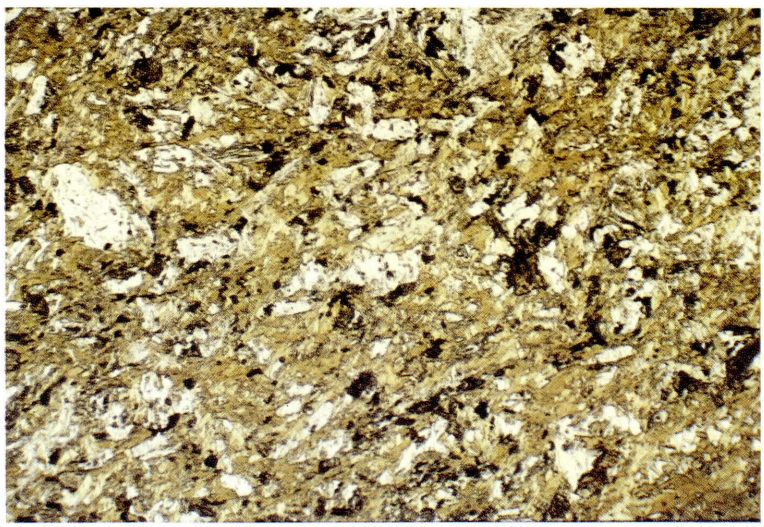

Figure 4: Lamprophyres at the GTS

b) Dyke rocks: dm- to m-thick dykes which penetrate the granite. These are either light aplites (no aplite stocks were encountered) or, more often, dark lamprophyres (Figure 4A-4C) which occur in sets in certain areas.

The different rocks are characterised in Appendix 4 according to their occurrence and mineral composition. The information originates mainly from the detailed NAGRA internal report on the petrography of the GTS (STALDER 1981).

All rock types were affected by an alpine tectono-metamorphic overprinting of varying strength which is expressed most clearly as a schistosity of the rocks. The deformation is also made clear by the flattened form of the cm- to dm-thick dark basic inclusions which occur frequently in the granites.

The following phenomena, mostly representing structurally weak zones, also occurred:

- In dm- to m-thick strongly deformed zones (shear zones)along which considerable movement occurred, mylonites and biotite schists with a clear parallel texture were formed.

- The rock was subjected to both ductile and brittle deformation, the latter tending to produce planar mechanical discontinuities (joints, shear surfaces, fractures). These brittle structures belong to several discontinuity systems and generally have a monomineralic infill (e.g. quartz-, epidote- and chlorite- bearing joints).

- Tectonic deformation processes led locally to formation of cavities of differing size in the rock body. The associated hydrothermal activity contributed to the alteration of the mechanical properties of the rock. Tension joints formed preferentially at the contacts between granite and lamprophyre dykes due to the marked rheological contrast between these two rock types (Figure 4B). The lamprophyres represented preferen-

tial water flow-paths, which also promoted the formation of tension joints. The tension joints are more or less all partly or completely infilled, often with well-formed quartz crystals.

3.1.2 Petrology of the rocks

All the rocks at the GTS were formed during the Variscan but were subjected to varying degrees of alpine tectonic and metamorphic overprinting (Figures 5A and 5B). The textures and mineral compositions of most rocks have been altered as a result of the alpine orogeny.

The petrographic development of the granitic rocks can be divided into five stages which are summarised in Table 5.

3.1.2.1 The magmatic stage

The emplacement and solidification of the Aare granites began in the Late Carboniferous with the intrusion of the GrGr, which was followed shortly after by that of the ZAGr (dated at approximately 290 Ma) (SCHALTEGGER 1987). Genetically speaking, both granites are a mixture of granitic products of crustal anatexis and a dioritic magma originating perhaps partly from the mantle (SCHALTEGGER 1987, SCHENKER and ABRECHT 1987). The numerous basic inclusions in the granites could represent the mantle component (STECK et al. 1979, SCHALTEGGER 1987). The basic blocks of the Mont-Blanc granite (comparable with the ZAGr) which clearly originate from a dioritic magma (BUSSY 1987) support this theory. The aplite dykes are residual melts produced by the differentiation of the granitic magma. Their intrusion into the already solid granite was dated at 250 Ma (SCHALTEGGER 1987).

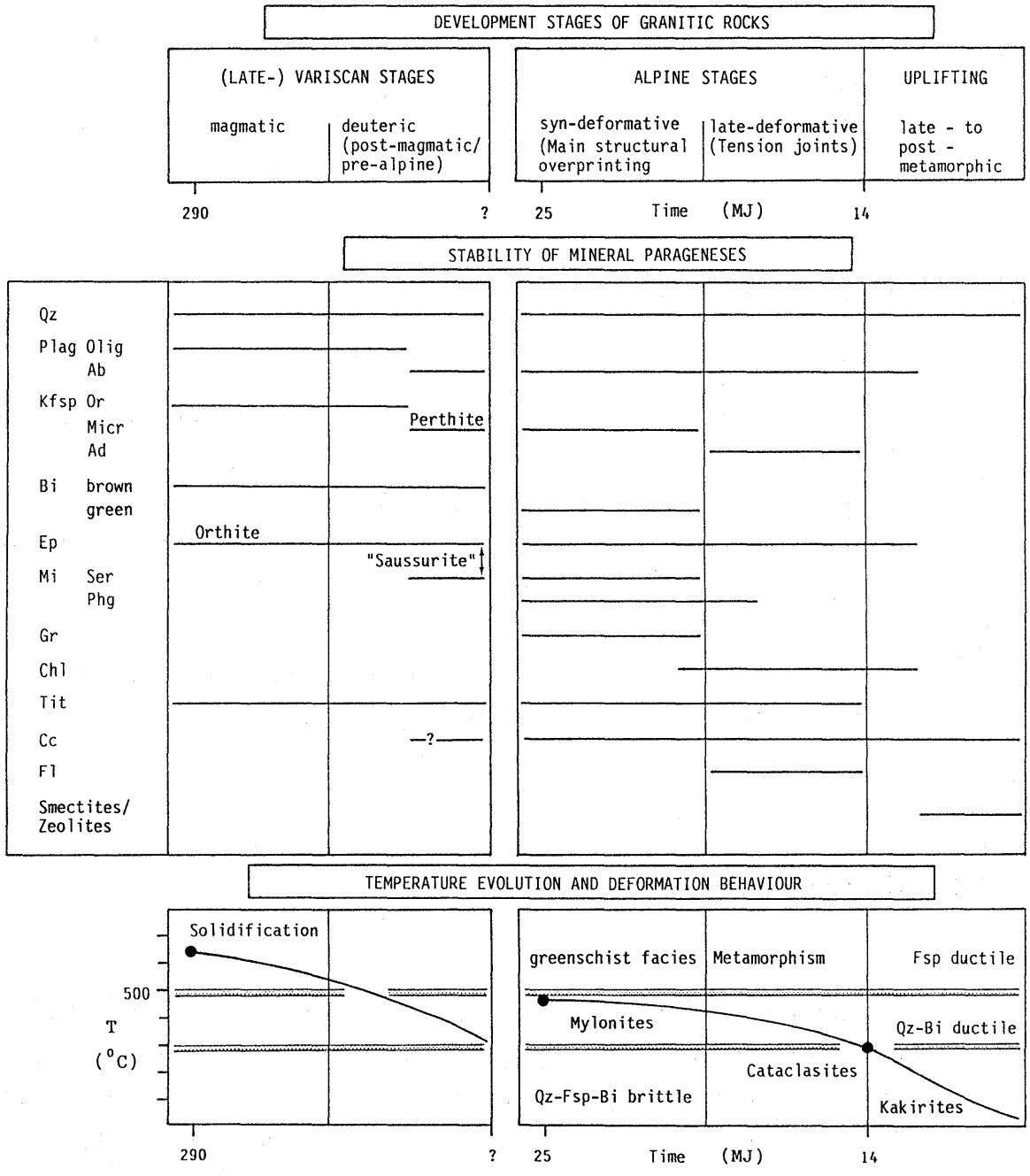

Table 5: Petrographic development of the granitic rocks (ZAGr, GrGr, aplites) of the Grimsel area

Abbreviations:

Ab	Albite	Fl	Fluorite	Or	Orthoclase
Ad	Adularia	Gr	Garnet	Phg	Phengite
Bi	Biotite	Mi	K-white Mica	Plag	Plagioclase
Cc	Calcite	Kfsp	K-Feldspar	Qz	Quartz
Chl	Chlorite	Micr	Microcline	Ser	Sericite
Ep	Epidote	Olig	Oligoclase	Tit	Titanite

The lamprophyres definitely do not originate from the granitic magma, but show a certain similarity to the the dioritic stocks in the volcanoclastic units (SCHENKER and ABRECHT 1987). Their intrusion age is unknown but it must be post-granitic since the lamprophyre dykes penetrate the granites.

The magmatic texture of the granites (Figure 5A) is coarse-grained, massive and isogranular to slightly porphyritic (phenocrysts of feldspar). The aplites are fine-grained to dense and, despite metamorphic overprinting, the lamprophyres show a clearly recognisable magmatic (ophitic) texture (Figure 4C, page 21).

The ZAGr, GrGr and the aplites have the same mineralogical composition and differ only with respect to the modal frequency of potassium feldspar, plagioclase, quartz and biotite (Appendix 4). Although now present pseudomorphically as microcline, the magmatic potassium feldspar crystallised as orthoclase with locally recognisable Karlsbad twinning. The saussuritised plagioclase, present today as albite, crystallised as oligoclase.

The lamprophyres occur in two varieties:

a) Kersantite, which is by far the more frequent type, contains mainly biotite and plagioclase (Figure 4C, page 21) while

b) Spessartite contains amphibole in addition to biotite and plagioclase.

3.1.2.2 The deuteric stage

This stage comprises all post-magmatic, pre-alpine events. It is characterised by the saussuritisation of the oligoclase (formation of a fine dusting of sericite and epidote, Figure 6A) which is altered to albite. The perthitic exsolution (formation of albite lamellae) of the potassium feldspar can be ascribed to the same stage, as can the structural change of potassium feldspar to microcline. Since they are both static processes, neither of these changes had any real effect on the magmatic texture of the rock.

Figure 5: Thin section photographs of GTS rocks

A Slightly deformed Grimsel granodiorite with a still clearly recognisable mainly magmatic texture consisting of plagioclase, potassium feldspar, biotite and quartz. Larger quartz grains with undulatory extinction are extensively replaced by a mosaic of dynamically re-crystallised grains (DS SB5/55.01 + polarizer, picture detail 31.8 x 22.0 mm).

B Well developed main schistosity in an augen gneiss formed by the strong penetrative deformation of a Grimsel granodiorite. Plagioclase- and potassium feldspar porphyroclasts and lenticular quartz grain aggregrates with syn-/post-kinematic mosaic texture are surrounded by newly-grown white mica coatings. In addition to this phengite formation, the potassium feldspar suffered also a strong albitisation as a result of deformation (DS SB6/62.83 + polarizer, picture detail 31.8 x 22 mm).

C Ductile deformation behaviour of quartz in Central Aare granite. Subgrain-formation took place in larger deformed magmatic quartz crystals which are replaced at the edges by recrystallised metamorphic quartz grains (granoblastic quartz mortar). (BGR thin section DBS 21/19 from BOGS 84041A, depth around 118m, + polarizer, picture detail around 1.4 x 1 mm).

D Brittle deformation behaviour of feldspar in Central Aare granite. The fragmented magmatic potassium feldspar is healed along fracture surfaces by recrystallised quartz and newly-formed polysynthetically twinned albite. In contrast to the metamorphic albite, the plagioclase (which has a similar deformation behaviour to potassium feldspar) is slightly saussuritised. (BGR thin section DBS 21/18 from BOGS 84041A, depth around 118 m, + polarizer, picture detail around 5.6 x 4 mm).

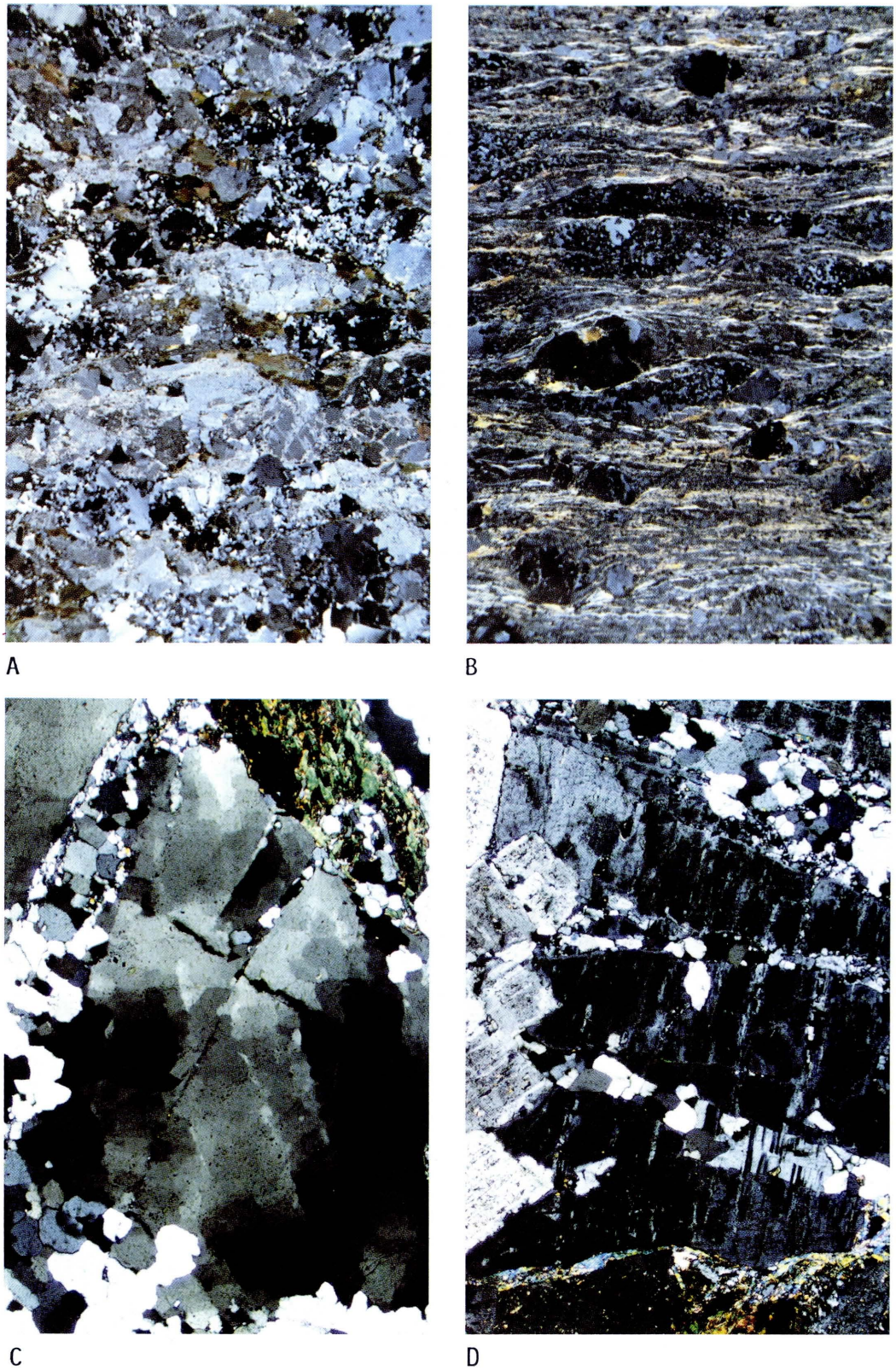

Figure 5: Thin section photographs of GTS rocks

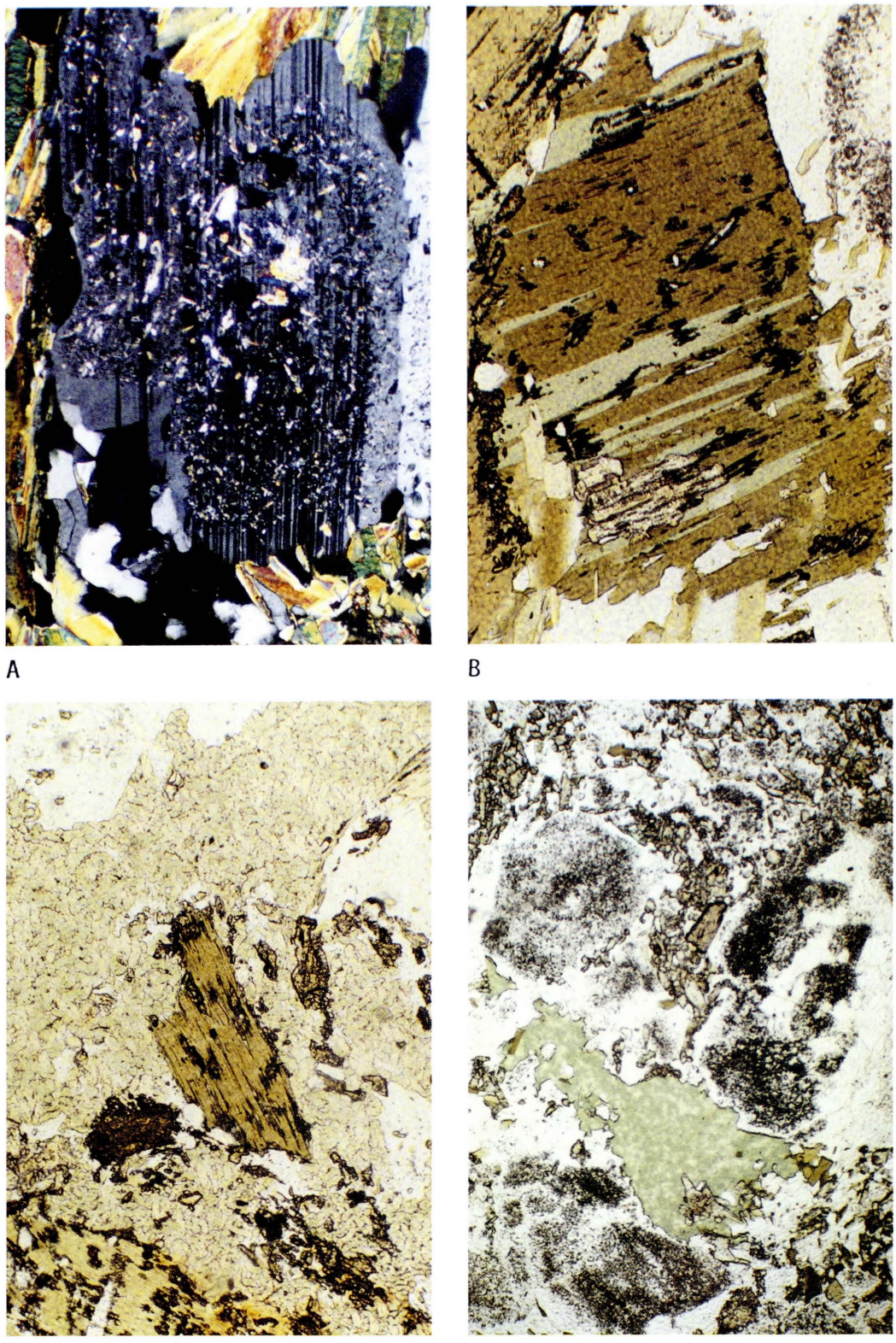

A B

C D

Figure 6: Thin section photographs of GTS rocks

The age of the mineral alterations, which can possibly be ascribed to several different events, is unknown. It is possible that the hydrothermal alteration in the Mittagfluh granite, dated at around 230 Ma, also affected the granites of the investigation area (ABRECHT and SCHALTEGGER 1988). There is no geochemical evidence for this but the saussuritisation of the plagioclases could be explained by this or by similar events.

Figure 6: Thin section images of GTS rocks

A Metamorphic neoformations in magmatic plagioclase of a Grimsel granodiorite. The clouding ("saussuritisation") is produced by the alteration of the anorthite component into epidote, while sericite replaces the potassium feldspar component. The relict plagioclase is homoaxially overgrown by a metamorphic albite seam. (DS SB5/51.96, + polarizer, picture detail 2.8 x 2.0 mm).

B Alteration of biotite to chlorite in the Grimsel granodiorite. The chlorite replaces the biotite homoaxially (and pseudomorphically) parallel to the (001)-plane. There is also some epidote growth. (DS SB5/34.14 picture detail 1.1 x 0.8 mm).

C Replacement of biotite by hydrothermal chlorite and epidote in Grimsel granodiorite. The chlorite aggregates consist of vermicular crystals and differ significantly from the normal chloritisation of biotite (Figure 6B); they show a strong nucleation during the alteration process. (DS SB6/80.4, picture detail 1.1 x 0.8 mm).

D Hydrothermally altered Grimsel granodiorite. The plagioclases are strongly clouded and partly altered to epidote, while chlorite aggregates completely replace the biotite (DS SB6/88.1, picture detail 2.8 x 2.0 mm).

3.1.2.3 The syn-deformative stage

The alpine structural overprinting which characterises the rocks at the GTS was accompanied by a syn-kinematic greenschist facies metamorphism. Neomineralisations and mineral recrystallisations thus seal both ductile and brittle alpine structures. The main structural overprinting occurred during the flattening and compression of the Aar Massif. In addition to the main schistosity (NE-SW), several systems of shear surfaces to shear zones were also formed (STECK 1968a, CHOUKROUNE and GAPAIS 1983). A good knowledge of the rock mineralogy is of great importance for interpreting the different structures since the mineral associations found on the discontinuity surfaces can provide information on the relative age of the structure. A typical example of a mineral sequence arising through replacement is the growth of chlorite at the expense of biotite grown or recrystallised during the alpine metamorphism. In the syn-deformative stage, biotite has already been homoaxially overgrown by chlorite (Figure 6B). This replacement is completed only in the late-deformative stage by the segregation of hydrothermally formed ("sand")-chlorite (Figures 6C and 6D).

Although the deformation phenomena appear to be both selective and heterogeneous, areas of granite which were not affected by the alpine deformation are in fact very rare. Such areas can be found most often in the ZAGr and, to a lesser extent, in the GrGr since the latter contains more biotite and the schistosity caused by preferred mica orientation is therefore more clear in this case.

Within the Aar Massif, the deformation- and metamorphism-gradients increase from N to S. Estimates of temperatures and pressures reached during the alpine metamorphism are 300-350°C and 2 kb for the northern Aar Massif and 400-450°C and 3 kb for the central to southern Massif area (FREY et al. 1980, HOERNES and FRIEDRICHSEN 1980, RICHTER and HOERNES 1988). The Juchlistock lies immediately to the south of the microcline/sanidine isograd, for which a

temperature of around 450°C was estimated (BERNOTAT and BAMBAUER 1982). Using fluid inclusions in tension joint quartzes, POTY et al. (1974) have derived a mean temperature of 430°C and a pressure of 2.8 kb. Although STALDER (1964) tends to consider the pressures derived from the fluid inclusions as hydrostatic, POTY et al. (1974) consider them to be lithostatic, particularly in view of an estimate of the overburden of the Aar Massif at the time of the metamorphism of around 10 km (~2.8 kb). Since the tension joints were formed during a late phase of the alpine structural overprinting, the temperatures and pressures derived are minimum values for the syn-deformative stage (STECK 1968a).

The age of the alpine metamorphism was determined by DEMPSTER (1986). The maximum age is 25 Ma (Rb-Sr on muscovite/phengite) while the drop below the 300°C isotherms at around 14 Ma (Rb-Sr on biotite) represents a minimum age. The increase in the metamorphism from N to S is expressed by a gradual rejuvenation of the biotite ages in a southerly direction (WÜTHRICH 1965, DEMPSTER 1986). In the Juchlistock area, all the biotites have an alpine age, which can be explained by the formation of metamorphic olive-green biotite at the expense of brown magmatic biotite.

The four rock types occurring at the GTS can be divided petrographically into two lithological groups (STECK et al. 1979):

a) granitic rocks (ZAGr, GrGr, aplites / "quartz-feldspar series") with typical metamorphic mineral association Qz-Micr-Ab-Bi(green)-Phg ± garnet (Figure 7);

b) intermediate to basic rocks (lamprophyres, basic blocks) with the metamorphic mineral association Ab-Ep-Chl-Bi(green)-Phg or Ab-Ep-Act ± Micr, Qz (Figure 7).

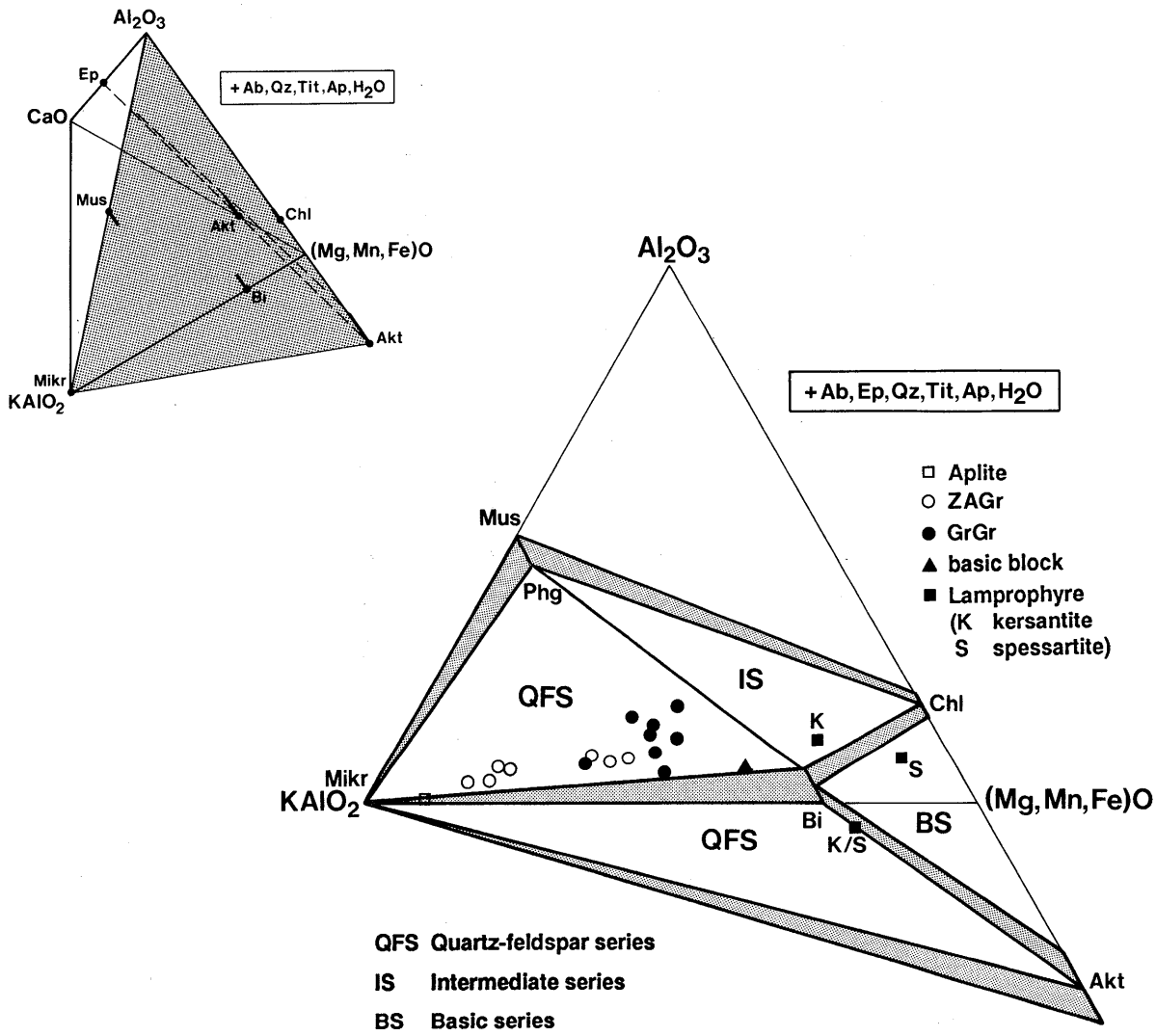

Figure 7: Schematic representation of the metamorphic mineral associations as observed in the rocks exposed in the Grimsel area. The parageneses are projected from albite (Ab), epidote (Ep), quartz (Qz), sphene (Tit), apatite (Ap) and H_2O (further abbreviations: actinolite (Act), biotite (Bi), chlorite (Chl), microcline (Micr), muscovite (Mus), phengite (Phg)). The linking lines correspond to a greenschist facies topology. Except for microcline, the variation of the mineral chemistry is shown schematically as the result of the coupled exchange 2Al for MgSi (reversed in phengite). The projected rock analyses come from STALDER (1964, 1981, Appendix 5), where the whole Fe was calculated as FeO.

The different rocks were deformed heterogeneously, i.e. unaffected areas with a largely massive structure alternate with strongly deformed zones with parallel texture. As a direct result of this deformation gradient, the intensity of metamorphic recrystallisation and neoformation also varies. The more fine-grained the rock type, the easier it is to deform, i.e. an equilibrium regarding grain size is set up through deformation and metamorphism. In general, the grain size decreases with increasing deformation. This phenomenon is a product of combined brittle or ductile processes, depending on the mineral type. The originally coarse magmatic texture is gradually obscured by the deformation since the plasticity of the crystalline basement clearly increases above 300°C as a result of the ductile behaviour of quartz and biotite (Figure 5C, page 27) (VOLL 1976). On the other hand, the feldspars behaved in a brittle manner during the whole structural overprinting (Figure 5D, page 27). In rocks which have been deformed to protomylonites (HEITZMANN 1985), the feldspars form clasts which lie in an usually recrystallised quartz-mica matrix with preferred mineral orientation (schistosity) (Figure 5B, page 27). This phenomenon is illustrated most clearly by the local deformation of GrGr to augen gneisses.

Mineralogical alterations are coupled with the deformation, the most important of these being the replacement of potassium feldspar by phengite (Figure 5B, page 27). In areas of extensive deformation, e.g. shear zones, alteration of potassium feldspar to mica has increased the rock ductivity. This shows the complementary behaviour of the deformation and metamorphism with respect to one another. The metamorphic alterations are not isochemical since, as the deformation proceeds, the Na_2O-, CaO- and MgO-contents increase while the K_2O-content decreases (alteration of potassium feldspar to mica). The K_2O values only increase again in mylonitic zones, while the Na_2O- and CaO-contents decrease (replacement of epidote and albite; MARQUER et al. 1985). Figure 8 shows the chemical development of non-deformed granite to mylonite.

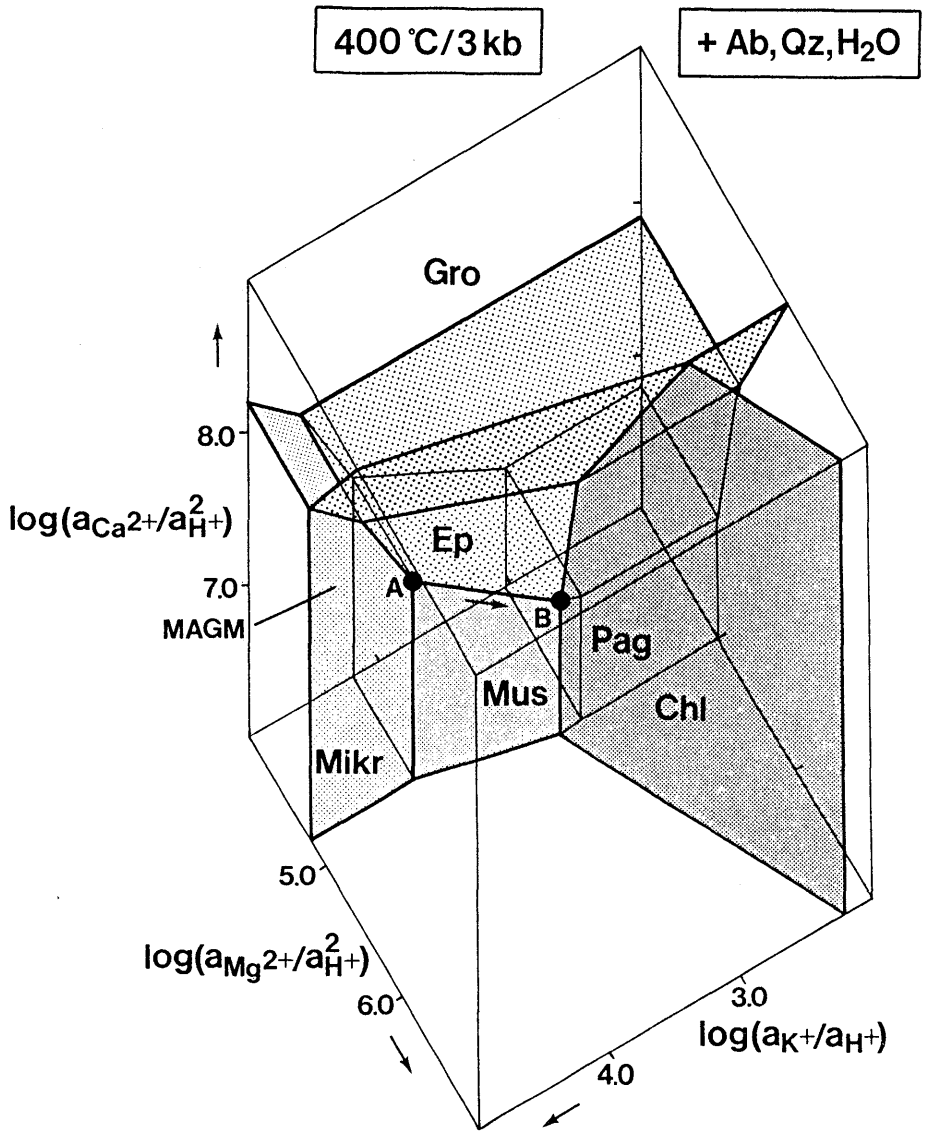

Figure 8: Simplified three-dimensional activity diagram in the ideal system Na_2O-K_2O-CaO-MgO-Al_2O_3-SiO_2-H_2O according to BOWERS et al. (1984). The diagram shows the stable topology at 400°C and 3 kb, with the phases biotite (Bi), chlorite (Chl), epidote (Ep), grossularite (Gro), potassium feldspar (Kfsp), muscovite (Mus) and paragonite (Pag) in the presence of albite (Ab), quartz (Qz) and H_2O. As a result of the increasing alpine deformation, the stable mineral association of the granites develops from Kfsp-Bi (MAGM, purely magmatic) to Kfsp-Bi-Mus-Ep (Point A). In strongly deformed zones, Kfsp can disappear completely and, in extreme cases, Bi-Mus-Ep-Chl can even form (Point B). This tectonometamorphic process is indicated with an arrow.

3.1.2.4 The late-deformative stage

The traces of this stage can be seen in the form of tension joints and leached granite zones (Figure 4B, page 21). The alpine structural overprinting ended with the formation of tension joints (STECK 1968a). The associated hydrothermal activity was responsible for leaching the areas of rock immediately bordering tension joints (mostly quartz and biotite were dissolved out). The dissolved material was then deposited in the tension joints in the form of idiomorphic crystals (quartz, chlorite, adularia, calcite, fluorite etc.). Characteristic minerals for the tension joint stage are adularia and fine-grained hydrothermal chlorite. These replaced the biotite which gradually disappeared during the tension joint stage. STALDER (1964) has described two mineral associations in the tension joints of the Grimsel area:

a) the most frequent paragenesis (location group 4a) with **quartz, chlorite, adularia, calcite and fluorite** as the most important minerals and

b) the rarer paragenesis (location group 4c) with mainly **quartz, muscovite, calcite, chlorite and ankerite** (Fe-rich dolomite) as the main minerals.

Only the mineral association of the location group 4a was found at the GTS. As can be seen from Figure 9, the paragenesis 4c can form instead of 4a with a slight increase in the chemical potential (μ) of CO_2 in the fluid. This was confirmed by POTY et al. (1974) who investigated fluid inclusions in quartz of both groups. They determined that the fluid is primarily an aqueous salt solution and that, as expected, the CO_2-contents in paragenesis 4c are higher. The average composition of the fluid inclusions is given in Table 6.

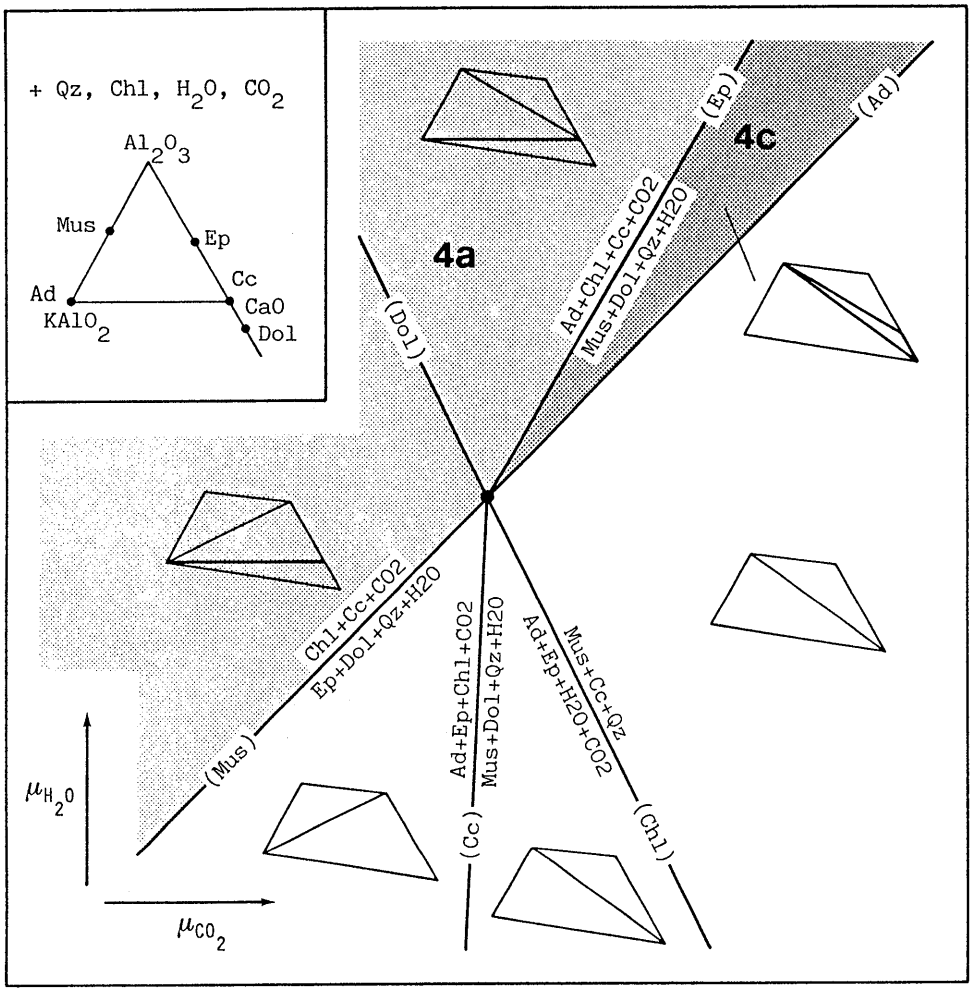

Ad	Mus	Ep	Chl	Dol	Cc	Qz	H2O	CO2	Reaktion
		+ 2	- 3	+15	-19	+ 3	+11	-11	(Ad ,Mus)
- 1	+ 1		- 1	+ 5	- 5	+ 3	+ 3	- 5	(Ep)
- 3	+ 3	- 2			+ 4	+ 6	- 2	- 4	(Chl,Dol)
-19	+19	-10	- 4	+20		+42	+ 2	-40	(Cc)

Figure 9: Qualitative μCO_2-μH_2O diagram in the pure system K_2O-CaO-MgO-Al_2O_3-SiO_2-H_2O-CO_2 in the presence of quartz (Qz), H_2O and CO_2. The figure shows the stability ranges of the two mineral associations found in the tension joints: paragenesis 4a with quartz, adularia (Ad), chlorite (Chl) and calcite (Cc); paragenesis 4c with quartz, muscovite (Mus), chlorite, dolomite (Dol) and calcite. The triangles show the stable parageneses in the presence of quartz, chlorite, H_2O and CO_2. The rarer paragenesis 4c occurs rather than the more frequent 4a only if μCO_2 is increased. The mineral in brackets indicates the phase which is missing in the reaction.

Alterations in the texture of the rocks occur only in chemically altered areas where, as a result of leaching, the porosity (up to 18 Vol-%; STALDER 1981) is generally much higher. The element migrations which had occurred in the syn-deformative stage reached their peak in the tension joint stage (see section 3.2).

	H_2O	CO_2	NaCl	
Paragenesis 4a	87	1.5	11.5	(wt-%)
Paragenesis 4c	82	9	9	(wt-%)

Table 6: Average composition of the fluid inclusions in quartz of the location groups 4a and 4c (POTY et al. 1974).

3.1.2.5 Uplift

The drop below the 300°C isotherms as a result of the uplift caused the rock to react in a brittle manner to tectonic stresses. Post-crystalline movements were not expressed by the formation of new structures but tended rather to reactivate existing structures, particularly the main schistosity (STECK 1968a, b). Thus, for example, mylonites produced by ductile processes were cataclastically overprinted. With the decrease in temperature, the rock lost its cohesion in tectonically stressed zones and kakirites were formed, some with fault gouges (STALDER 1981, MEYER 1988). In addition to "grounded" quartz, feldspar, muscovite and chlorite, the fault gouges also contain illite and smectites (montmorillonite was identified inter alia; STALDER 1981).

More or less all the open joints were produced during this stage since no mineral fillings (or very few) were deposited at this time.

3.1.2.6 Summary

The mineralogical composition of the rocks exerted an influence on the deformation. Fine-grained, mica-rich rocks such as lamprophyre formed preferential weak zones along which deformation was channelled. Granitic rocks reacted in a more brittle manner and tension joints therefore tended to be formed at the contacts between granite and lamprophyre due to the strong rheological contrast between the two rock types. Besides the lamprophyres, strongly deformed zones (mylonites, shear zones) formed preferential pathways for fluid circulation. This led to element migrations which were most important in the leached areas around the tension joints. The resulting increase in the porosity caused by this process again led to formation of preferential pathways for water circulation. Despite differing tectonometamorphic stresses within the granites, the rock mechanical properties did not alter significantly (STALDER 1981; Table 7).

3.2 Geochemistry

3.2.1 Chemical characterisation of the rocks

One of the most important results of the chemical analyses is the finding that ZAGr and GrGr differ only slightly from one another (STALDER 1981; Appendix 5, Figures 10 and 11). This confirms the observation made in the field to the effect that there is a mutual assimilation of ZAGr and GrGr at contact zones (STALDER 1964). Such a transition zone exists in the Juchlistock and in the GTS. It can be seen from the QAP- and R1-R2 diagrams (Figures 10 and 11) that the GrGr does not actually have a granodioritic composition

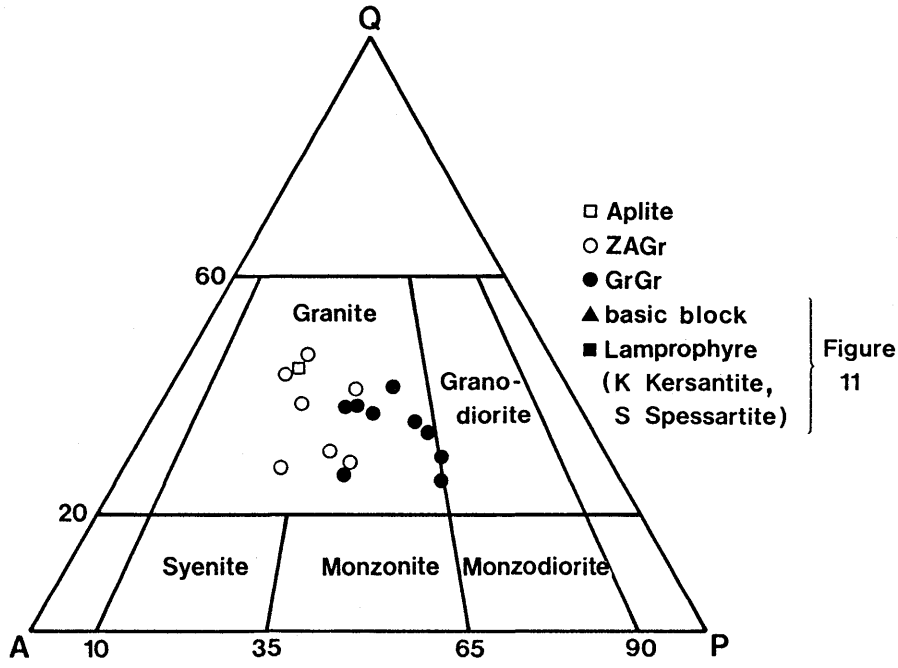

Figure 10: QAP-triangle (Quartz-Alkalifeldspar-Plagioclase) according to STRECKEISEN (1976)

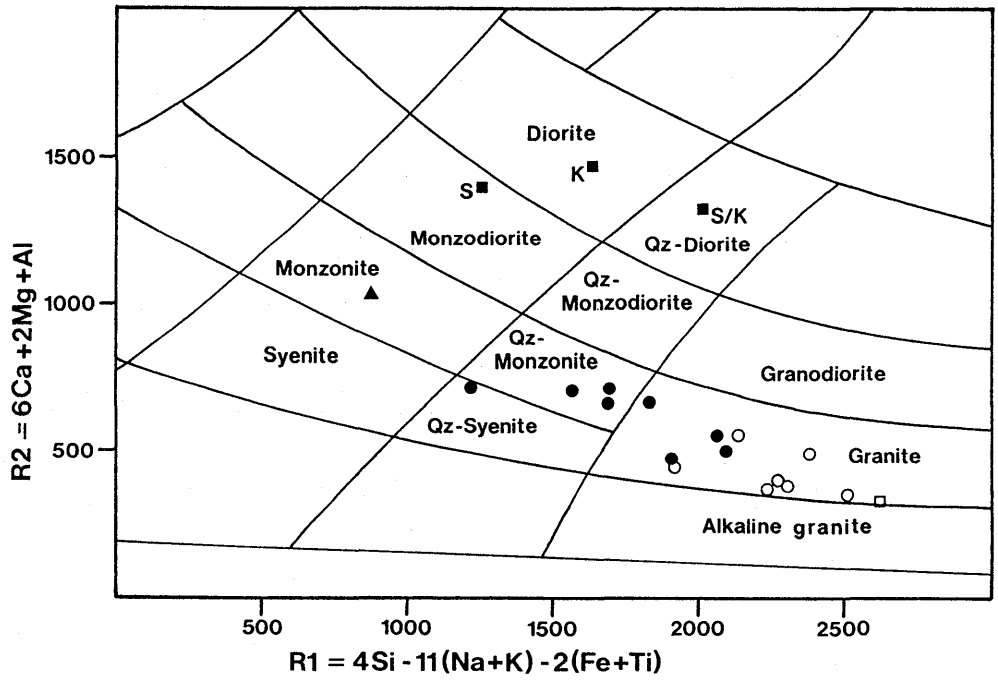

Figure 11: R1-R2 diagram (in milli-cations) according to DE LA ROCHE et al. (1980), completed by STRECKEISEN (1981). The distribution of the analysed values for aplite, ZAGr, GrGr and basic inclusions indicates a common magmatic development sequence for these rocks. The lamprophyres are clearly not part of this; they belong to a different magmatic series.

but rather that of a granite. The distribution of the different rock analyses in the R1-R2 diagram shows a magmatic trend which probably begins with the basic inclusions and ends with the aplites. The same diagram also shows that the lamprophyres belong to a different magmatic development.

3.2.2 Chemical alterations

Mineralogical and chemical alterations increase with increasing deformation. The most important alteration is that of potassium feldspar to mica, which is coupled with a decrease in the K_2O-content (Figure 5B, page 27). In preferential deformation pathways (mylonites, shear zones), this alteration can occur completely. Locally, even chlorite occurs and its formation is linked with an enrichment of the MgO-content (MARQUER et al. 1985).

The most important chemical alterations affect the rock surrounding the tension joints (Figure 6D, page 28). STALDER (1964, 1981) has shown that mainly quartz, biotite and phengite are leached out of the rock. These minerals can then re-precipitate out of the hydrothermal solution but generally not in the proportion in which they were initially dissolved. This process results in an increase in the porosity of the rock affected.

Besides the leaching around the tension joints, the granite or granodiorite can be altered locally by albitization or epidotization. Comparisons between unaltered and chemically altered rock are generally based on the assumption that either the volume or the Al-content of the rock remains constant. This is not necessarily always the case, particularly not with hydrothermal events such as tension joint formation, although MARQUER et al. (1985) were able to show there was no significant volume increase or decrease in the Grimsel area during the main alpine deformation.

The occurrence of chlorite and epidote as joint or cleft fillings shows that at least some of the aluminium was mobilised. GRESENS (1967) has suggested a diagram in which the variation of the main element contents between a chemically altered and an unaltered rock can be represented as a function of a volume factor (Figure 12A-D). The lines in the diagram for each oxide component are calculated using the following equation:

$$\Delta_n = f_v \, (\varrho_{uv}/\varrho_v) \, C_n^{uv} - C_n^{v}$$

Δ_n : Increase resp. decrease of the element in weight-% (grams oxide/100g rock)

f_v : Volume factor

ϱ : Specific weight of unaltered (ua) and altered (a) rock

C_n : Content of the element (oxide) in weight-% in unaltered (ua) and altered (a) rock

In the case of alteration of GrGr by epidotization (Figure 12A and 12B; analyses from STALDER 1981; Appendix 5), it can be seen that the variation lines for SiO_2 and Al_2O_3 intersect at around $f_v = 1$. This means that the volume can be expected to remain constant when estimating the element migrations. In this case, there is virtually no increase in the porosity of the altered GrGr. Ca and Fe are introduced into the rock, while K and Mg and, to a lesser extent, Ti, Na and H_2O (the latter corresponding more or less to the loss of ignition GV) are removed. SiO_2 and Al_2O_3 contents remain more or less constant. These chemical alterations confirm the microscopic observations that mainly biotite (+ sagenite) and, to a lesser extent, potassium feldspar and albite are replaced by epidote. The numerous discontinuities filled with epidote could be linked with this alteration to epidote which is promoted by a similar introduction of Ca.

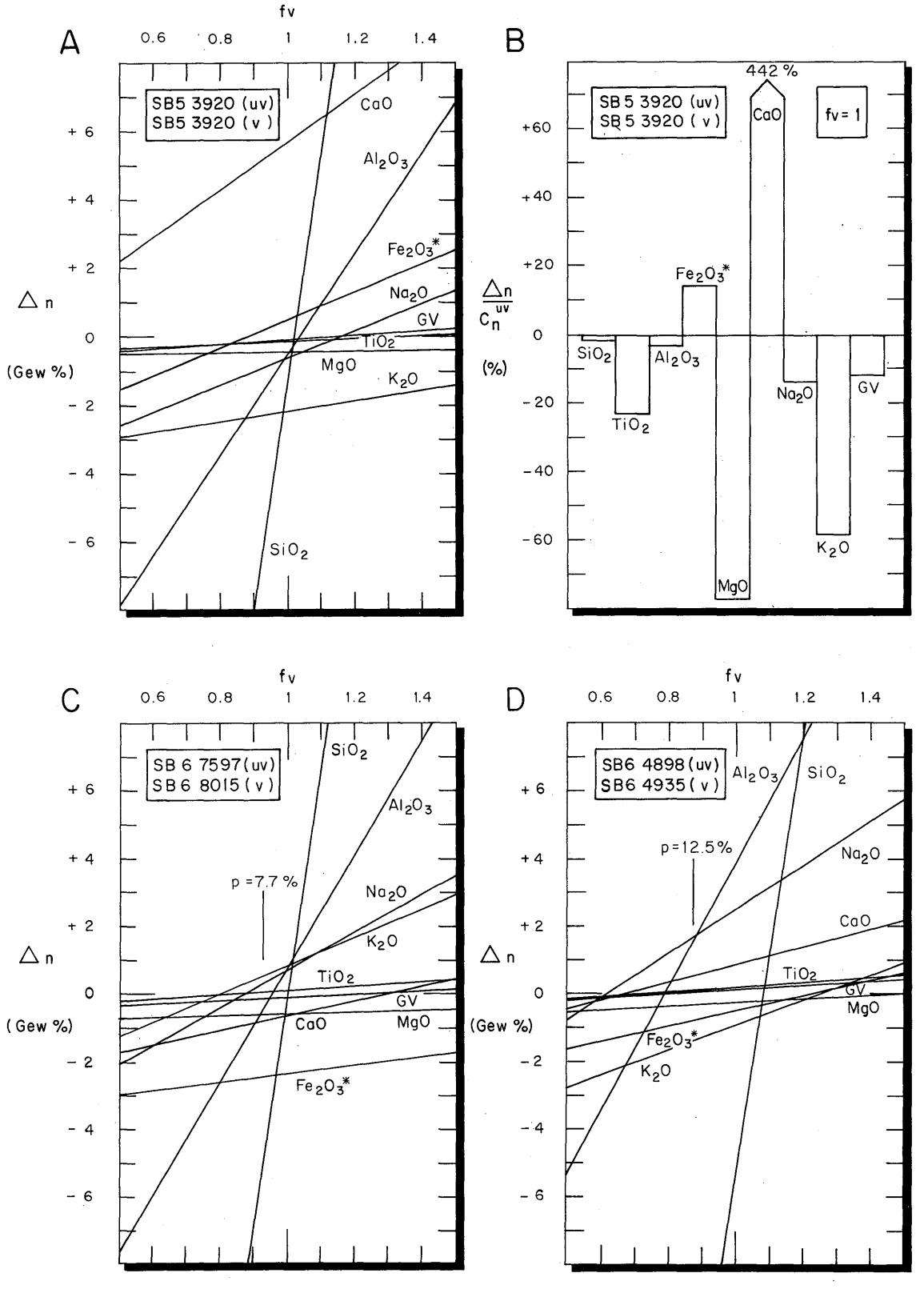

Figure 12: Diagrams according to GRESENS (1967)

The element migrations are greater in the immediate vicinity of clefts (Figure 12C and 12D), which is probably a result of strong convective fluid circulation. The characteristic increase in the porosity of the leached granites compensates the volume loss of the rock caused by element removal. The theoretical porosity calculated from the volumetric weight for the two examples given reached around 8 Vol-% (Figure 12C) and 13 Vol-% (Figure 12D). The increase in the porosity is an indication of the degree of leaching of the rock. Depending on the intensity of the leaching, the same element can be enriched or depleted (MARQUER et al. 1985). Examples of this are Al, Ca and K which are slightly depleted (Al, Ca) or enriched (K) at $f_v = 0.92$ (Figure 12C) but behave in exactly the opposite manner at $f_v = 0.87$ (Figure 12D). Si, Fe, Mg and Na always lie in the same range, i.e. they are either removed (Si, Fe, Mg) or enriched (Na).

This tendency corresponds to a dissolution of quartz and biotite (Si-, Fe-, Mg-decrease). At a low leaching level, part of the epidote is also dissolved (slight decrease in Ca and Al). With continuing leaching, epidote re-forms along with albite. In the

---

Figure 12: Diagrams according to GRESENS (1967) illustrating element migrations, shown for a comparison between chemically unaltered (ua) and altered (a) granodiorite (Fe_2O_3*, total iron expressed as Fe_2O_3; GV = loss of ignition). The analyses originate from STALDER (1981; Appendix 5).

A: Comparison between altered (to epidote) and unaltered GrGr ($_{ua}$ $_{a}$, not determined).
B: Enrichment and depletion of the most important oxide components following epidotization with constant volume ($f_v = 1$).
C,D: Comparison betweeen unaltered and hydrothermally leached GrGr immediately bordering a tension joint ($_{ua}$ = $_{a}$ = 2.72 g/cm³, STALDER 1981). The porosity (p) was calculated using the volumetric weight (VW) of the altered GrGr (C: VW_a = 2.51 g/cm³; D: VW_a = 2.36 g/cm³; STALDER 1981, Table 5, page 24). The volume factor (f_v) can then be estimated from the porosity (shown with vertical line).

case of moderate leaching, adularia replaces biotite (slight K increase, Figure 12C; STALDER 1964), which does not appear to be the case with a higher degree of leaching (K decrease, Figure 12D). The decrease in Mg and Fe is less marked in this case and indicates the growth of chlorite and epidote which retain part of the Mg and Fe released by the biotite dissolution.

The strong water circulation and the material migration associated therewith are characteristic of the tension joint stage and are probably responsible for sealing most of the discontinuities. The different elements required for joint filling come from the leaching of the granites. As a result of oversaturation, a drop in temperature and/or pressure release, the minerals precipitate out of the aqueous solutions and fill the interstices. The joints filled with powdery chlorite (K_3, NTB 81-07) and the calcite- or calcite-chlorite-bearing discontinuities certainly belong to this stage.

Hydrothermally leached areas represent preferential pathways for potential water circulation. In addition, the hydrothermal activity also leads to sealing of discontinuities.

3.3 Rock mechanical properties

3.3.1 Rock mechanical parameters

Table 7 gives the most important rock mechanical parameters, together with a few geophysical parameters.

	Central Aare granite Number of samples ( )	Grimsel-Granodiorite	Aplite	Lamprophyres
Volumetric weight [kg/m^3]	2660 ± 23.8 (105) /1/	2706 ± 13.6 (58) /1/	2599 ± 17.4 (25) /1/	2909 ± 31.0 (19) /1/
Porosity [Vol.%]	0.4 - 1.0 (3) /4/			
Uniaxial compressive strength [MPa]	169.1 ± 37.1 (54) /1/	116.9 ± 47.9 (28) /1/	225.6 ± 45.4 (13) /1/	127.0 ± 31.8 (9) /1/
Young's Modulus (E_{50}-Modul) [GPa]	53.3 ± 11.0 (54) /1/	47.3 ± 15.4 (28) /1/	60.2 ± 8.9 (15) /1/	42.4 ± 8.5 (9) /1/
Poisson's Ratio	0.37 ± 0.12 (54) /1/ 0.33 ± 0.03 /9/	0.33 ± 0.15 (28) /1/	0.40 ± 0.12 (13) /1/	0.33 ± 0.17 (9) /1/
Tensile strength (tensile splitting strength) [MPa]	9.06 ± 1.48 (42) /1/	9.54 ± 2.17 (24) /1/	9.27 ± 0.95 (9) /1/	12.55 ± 3.59 (6) /1/
Triaxial compressive strength [MPa]	263 ± 29.9 (4) (5MPa) 333 ± 20.6 (2) (10MPa) 410 ± 63.8 (3) (20MPa) /1/	230 ± 70.7 (2) (5MPa) 287 ± 24.7 (2) (10MPa) 355 ± 28.3 (2) (20MPa) /1/	297 (1) (5MPa) 395 (1) (10MPa) 455 (1) (20MPa) /1/	240 (1) (5MPa) 226 ± 44 (3) (20MPa) /1/
Angle of friction ((*): for fractures)	33 (1) (*) /1/	30 ± 2 (3) (*) 29 (1) /1/	34 (*) 36 /1/	32.5 ± 3.5 /1/
Pressure wave velocity-hand specimen [m/s]	3111 ± 278 (105) /1/ 3100 - 3500 dry 4650 - 4750 water-saturated /3/	3351 ± 388 (58) /1/	2948 ± 428 (25) /1/	2120 ± 480 (4) /1/
Pressure wave velocity-whole rock [m/s]	5600 ± 100 /2/ 5450 - 5500 /5/ 5200 /8/ 4900 - 5300 /9/	5600 ± 100 /2/ 5250 ± 100 /5/	5400 - 5700 /2/	5700 - 6100 /2/ 5500 - 6200 /5/ 5200 - 6250 /8/
Thermal conductivity [W/m·K]	2.58±0.19 (20) (wet) 3.34±0.35 (20) (dry) /4/	2.46±0.19 (16) (wet) 3.22±0.29 (16) (dry) /4/	3.31±0.35 (2) (wet) 5.32±0.49 (2) (dry) /4/	2.21±0.45 (3) (wet) 2.71±0.60 (3) (dry) /4/
Permeability [m/s]	$5 \cdot 10^{-17}$ (10MPa) /1/ $3.5\text{-}45 \cdot 10^{-12}$ (5-15MPa) /6/ $5 \cdot 10^{-12}$ (5-30MPa) /7/			

References	Laboratory	and	Report
/1/	EPFL		NTB 81-01
/2/	Prakla-Seismos GmbH		NTB 81-01
/3/	Geotest		NTB 81-07
/4/	ETHZ		22.12.81
/5/	Geotest		84041 20.6.84
/6/	GSF		Annual report 83
/7/	EIR		AN-42-84-24
/8/	BPB		Logs BOUS 85.001-3
/9/	WBK		Seismic tomography

Table 7: Rock mechanical parameters of the main rocks at the GTS.

Two important factors must be borne in mind when interpreting the data:

a) The majority of measurements were carried out on drill cores in the laboratory. Since the rock in situ is under greater stress, these results do not represent true in situ values.

b) The parameters refer to the intact **rock** on a small scale. The properties of the **whole rock body** will be affected by fracturing, changes in rock type etc. These factors also affect mainly the permeability.

3.3.2 Rock stresses

The stress measurements carried out by the BGR (Appendix 6) show that:

- there is an average difference of more than 10 MPa between the minimum and maximum horizontal stress
- the maximum horizontal stress lies between 18 and 45 MPa and the minimum principal stress between 15 and 32 MPa
- the maximum horizontal stresses are generally directed towards the SE, i.e. perpendicular to the main alpine schistosity S_2.

The stress, which is 4-5 times higher than the lithostatic pressure of around 9-12 MPa, indicates the presence of significant horizontal forces in the main compression direction NW-SE.

4 STRUCTURAL GEOLOGY

4.1 Measurement methods

4.1.1 Tunnel observations

The discontinuities occurring in the tunnels were mapped using a special geological compass constructed by GEOTEST. The principle of the compass is based on taking bearings of the surface using two light sources which are mounted on a board. The azimuth and the angle of dip of the board, which is aligned with the discontinuity plane, are then determined as usual. A second method is based on the exact transfer of the discontinuities onto a profile in the form of a tracing graph of the tunnel. The azimuth and angle of dip are then determined in a similar way to tracing the structures on a drill core (explained later). Appendix 7 gives an example of a tunnel map with the tracing graph of the discontinuities.

For the evaluation of the tunnel data, the GTS was divided into two areas. The N area comprises the laboratory tunnel up to the branch to the AU and VE areas and the WT area. The S area consists of the rear laboratory tunnel, the VE and the AU areas (Figure 1, page 2; Appendix 3). The division of the tunnel sections into two areas was based on the fact that the N area generally has a more complex pattern of brittle structures than the S area (Appendix 11).

4.1.2 Core observations

The identification of discontinuities in the boreholes was carried out with a drill core tracing graph (isometric sketch). The tech-

nique was developed by GEOTEST and is presented in detail in NTB 84-03 (pages 94-104). It can be summarised briefly as follows:

The drill cores have a line of orientation parallel to the borehole axis and all structures are traced onto a transparent film, i.e. the traces of the discontinuities are recorded. Using a template (adapted to the drilling diameter) on which the azimuth (Faz) and angle of dip (Faw) are calibrated, an apparent Faz/Faw pair can be determined for each surface. These values are then converted in order to obtain the true Faz and Faw (computer program ORKE, GEOTEST). The process corresponds to a triple rotation:

a) Rotating the orientation line of the drill core in an upwards direction,
b) Vertical positioning of the borehole axis,
c) Rotating the orientation line of the drill core in a northerly direction.

Appendix 8 provides an illustration of a drilling profile with all the brittle structures determined in this manner.
NAGRADATA (Nagra data-bank system for geological data) covers the brittle structures from only some of the boreholes drilled at the GTS. Although only 12 boreholes were processed, they nevertheless provide a good cover of the whole GTS area since they can be sequenced to form a N-S profile (Figure 1, page 2; Appendix 3). From N to S, these are:

N	BOUS 85001	BOSB 80003
	BOUS 85002	BOSB 80004
	BOSB 80001	BOSB 80005
	BOGS 84041A	BOSB 80006 + 83008
	BOUS 85003	S BOSB 83001
	BOSB 80002	

A problem to be taken into consideration when evaluating the data is the relatively small range of drilling directions for the different boreholes, with the exception of BOGS 84041A which was drilled vertically (Figure 13). The majority of the boreholes have a WNW to WSW orientation and there is a marked drop in the E-W to

NW-SE orientated discontinuities which can be identified; this is because of sub-parallelism to the drilling direction (this affects mainly S_3, K_2 and L; see chapter 4.4). These discontinuities can however be taken into account in the N-S to SSW-NNE tunnel sections where again different systems are less well represented (mainly S_4, K_4; see chapter 4.4).

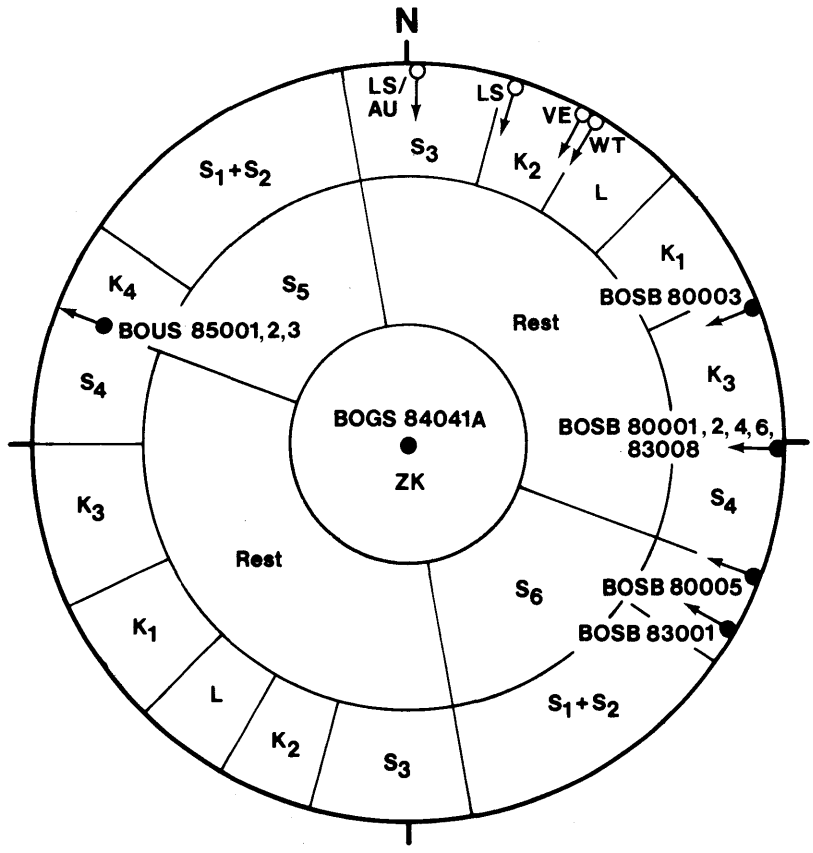

Figure 13: Stereographic projection (lower hemisphere) of drilling and excavation directions of the boreholes and tunnel sections used for the statistical evaluation of the discontinuities (LS: laboratory tunnel; WT: heater test tunnel; VE: ventilation tunnel; AU: decompressed zone tunnel).

Since the different boreholes cover a relatively small range of directions, a specific joint system could in fact be under-represented. The calculated percentage frequencies for the individual joint systems must therefore be interpreted with some caution.

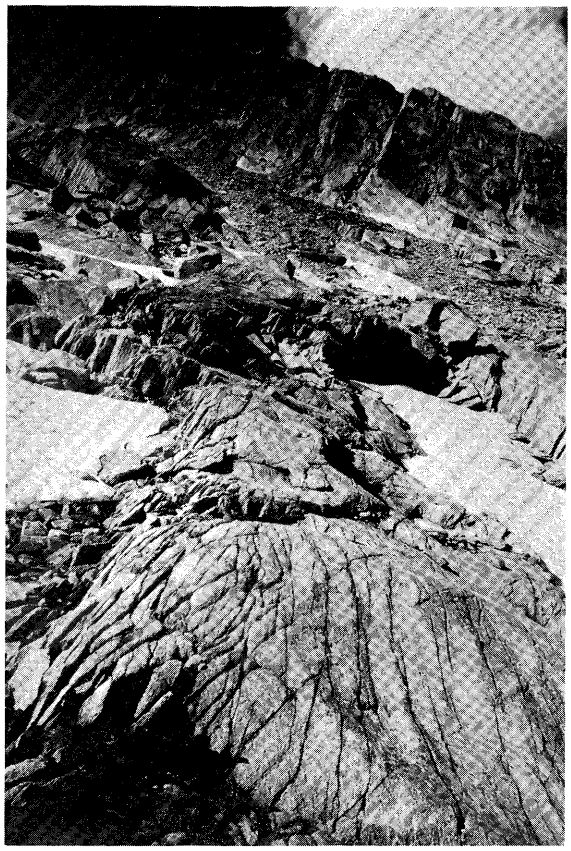

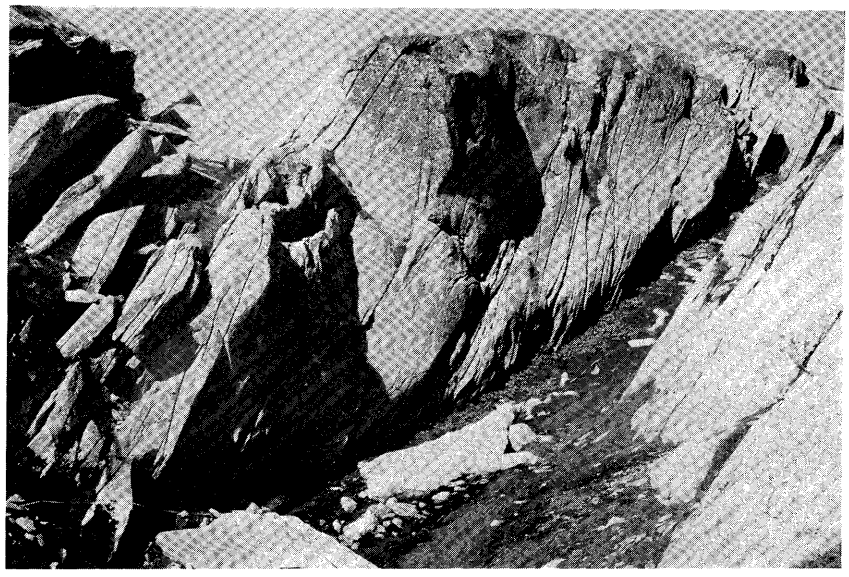

Figure 14: Photographs of the Juchlistock area

4.1.3 Surface mapping

A large part of the Juchlistock is easily accessible over a widely denudated rock surface (Figures 14A and 14B). It was therefore possible to obtain data on exposed brittle structures over a representative surface area.

Six profiles were planned; their specifications are given in Table 8 and their traces are shown on the structure map (Appendix 9). The profiles are divided into sections which are adapted to take account of the terrain. The brittle structures were mapped along these sections with a compass and measuring tape.

The main objectives of the mapping were:

- to obtain orientation measurements (azimuth and angle of dip) in a statistically relevant quantity comparable with underground measurements;
- to allow as exact a localisation of measurements as possible;
- to determine the orders of magnitude of joint lengths and discontinuity spacings;

with a view to provide complementary information on the geometry of structures in the Test Site area.

Figure 14: Photographs of the Juchlistock area

A Surface photograph of surface east of the Juchlistock at around 2450 m towards the peak area of the Juchlistock. The joints are clearly distinguishable from the polished rock surface. The rhombic pattern is a result of the intersection of vertical S_1+S_2 structures with K_2 structures.

B Surface photograph of surface south-east of the Juchlistock along measurement profile 2 (see Appendix 9) at around 2250 m. The profile lies in a gully, a so-called "Chäle", which corresponds here to a large K_2 disturbance.

Profile no.	Section no.	Length (m)	Direction	Altitude in m a.s.l. Start	End	included in NAGRADATA
1	101-105	225	E - W	1995	2070	
2	201-203	162		2085	2070	*
	211-231	1075	SE - NW	2070	2430	*
	241+242	65		2435	2460	*
3	301-331	900	S - N	2250	2145	*
4	401-413	600	W - E	2310	2155	*
5	501-526	1000	N - S	1790	1885	
6	601-616	770	NE - SW	1845	2260	*

Table 8: Details of the surface profiles

Since NAGRADATA is designed for the processing of drill-core measurements, the field profiles 2,3,4 and 6 had to be converted accordingly and were then included in the data-bank. The resulting pole diagrams, azimuth/dip logs and lists formed the basis for the information presented in chapter 4.6. In addition, the structures which were recognisable in the aerial photographs were identified using the field observations and the structure map (Appendix 9) was prepared using this information.

4.2 General definitions

The discontinuities occurring at the GTS are the products of both ductile deformation (foliation) and brittle deformation (fractures), as well as contacts between two different rock types (mainly lamprophyre/granite contacts).

The literature defines the different forms of tectonic discontinuity as follows (NTB 84-30, RAMSAY and HUBER 1987):

- **Foliation** (schistosity): those surfaces which are characterised by a preferred mineral orientation (mainly phyllosilicate platelets) corresponding to their grain form;

- **Fracture:** in general, any mechanical discontinuity in the rock which causes a loss of cohesion. If there is no differential displacement parallel to the fracture surface and the aperture remains small (i.e. not more than 1-2 mm), the structure is called a **joint.** Joints can be open or closed. In the latter case, circulating hydrothermal solutions have deposited minerals which have sealed the openings and the rock thus regains a certain cohesion. If there is a differential displacement parallel to the fracture surface, the structure is called a **fault** or a **displacement** or **shear** surface.

Further deformation phenomena are defined as follows and will always be used in this sense in the present report:

- **Shear zone:** planar or curviplanar zone with greater length than width surrounded by rocks with low deformation. A shear zone can be continuous (ductile) or discontinuous (brittle) (RAMSAY and HUBER 1987).

- **Mylonite:** fine-grained, banded and cohesive rock produced by local processes such as plastic gliding and dynamic recrystallisation. A mylonite generally shows high finite deformations (RAMSAY and HUBER 1987).

- **Cataclasite:** strongly deformed intact rock with massive, often chaotic texture. The deformation (cataclasis) which affects more or less the total rock volume occurs by way of fracturing of rock and mineral particles with simultaneous rotation and mechanical mixing of these fragments (HEITZMANN 1985, RAMSAY and HUBER 1987). Cataclasites generally form in the brittle-ductile transition range (HEITZMANN 1985).

- **Kakirite:** strongly brecciated, non-cohesive rock body penetrated by joint and shear surfaces. Deformation by cataclasis is restricted to these fracture zones and rock fragments are often surrounded by rock flour (fault gouges) (HEITZMANN 1985).

- **Fracture:** any mechanical discontinuity in a rock, be it a joint or a shear surface (KRAUSSE et al. 1978).

The nomenclature used in NTBs 81-07, 85-34 and 85-47 for tectonic discontinuities distinguishes between schistosity and jointing. Jointing is usually taken to include more or less planar surfaces which penetrate the rock and therefore includes joints in the narrower sense as well as shear surfaces. Tension joints are a special phenomenon since these are usually longitudinal fissures and cavities which are either open or filled mainly with quartz and chlorite.

The discontinuities included in NAGRADATA and used for evaluation purposes include only brittle structures. This covers the so-called fracture cleavage, i.e. fractures which lie parallel to the schistosity. However, these structures can be broken up as a result of drilling or core removal and do not necessarily correspond to an actual joint or shear fracture.

Since most discontinuities are healed, traces of earlier movements often have to be presumed because they occurred before or during the mineral precipitation. The occurrence of slickensides, polished joint surfaces and fault gouges generally indicates late to post-metamorphic movements which is clear from the deformed (late)-alpine mineral fillings. All this is the result of reactivation of old discontinuities during uplift. The movement can also affect fracture planes which were formed as joints. STECK (1968a) gives such an example for chlorite joints ($ZK_2 = K_3$).

Two types of joint fillings can be distinguished in the case of sealed discontinuities:

a) Actual joint coatings which were precipitated out from hydrothermal solutions. Typical minerals are quartz, feldspar, epidote, calcite, chlorite, and sphene. The joint thickness is generally a few mm, but can also be several cm.

b) Thin mineral enrichments of biotite, muscovite and chlorite, generally 0.5-2 mm thick. These mineral accumulations along surfaces where displacement took place reflect what happens on a large scale in shear zones and biotiteschists.

Borehole	Number of "open" discontinuities		Number of closed discontinuities		Total number of discontinuities
	Number	%	Number	%	
BOUS 85001	17	3.8	433	96.2	450
BOUS 85002	116	11.7	876	88.3	992
BOSB 80001	145	67.4	70	32.6	215
BOGS 84041A	61	22.3	213	77.7	274
BOUS 85003	56	9.2	556	90.8	612
BOSB 80002	17	26.2	48	63.8	65
BOSB 80003	13	22.8	44	77.2	57
BOSB 80004	16	72.7	6	27.3	22
BOSB 80005	70	54.3	59	45.7	129
BOSB 80006	24	15.9	127	84.1	151
BOSB 83008 / BOSB 83001	71	49.7	72	50.3	143
Total	606	19.5	2504	80.5	3110

Table 9: Number and percentage of "open" and closed discontinuities in 12 boreholes at the GTS

The evaluation of the data on jointing from 12 boreholes showed that only 20% of the joints are broken or not infilled; this value varies from borehole to borehole (Table 9).

4.3 Comments on the origin of the brittle structures

The structures which originated during the alpine structural overprinting are both ductile and brittle in nature (STECK 1968a, CHOUKROUNE and GAPAIS 1983). Whether the rock fractures or undergoes ductile deformation depends on the temperature and pressure conditions, on the properties of the mineralogical components and, to some extent, on the grain size of the individual minerals. Most of the deformed rocks at the GTS can be designated as protomylonites (> 50% clasts in a dynamically recrystallised matrix; HEITZMANN 1985). The occurrence of cataclasites or even kakirites indicates late tectonic stresses.

The deformation caused by joint formation is very small. The formation of joints during the main tectonic deformation phase can therefore be ruled out since this phase was accompanied by strong deformation. Although fractures could have been formed during the main deformation phases, they would have developed by dilation into veins or, as a result of shearing movements along the fracture surfaces, into displacement surfaces or faults. Joints form mainly as the result of the release of elastic strain energy accumulated in the rock during the closing phases of the orogenetic activity or above all during the course of late uplift in a region (RAMSAY and HUBER 1987). Since most of the structures occurring at the GTS originate from the time of the main alpine structural overprinting, they correspond rather to shear surfaces than to joints in the narrower sense (Table 10).

NTB 85-34		STECK (1968a)		CHOUKROUNE AND GAPAIS (1983)
Discontinuity system	Mean azimuth angle of dip	Discontinuity system	Explanation	Explanation
S_1	142/77	S_1	sinistral shear surface	conjugate to S_3/S_4
S_2	157/75		schistosity	main alpine schistosity
-	-	S_2	-	crenulation cleavage observed only in some mylonites
S_3	183/65	S_3	dextral shear surface	conjugate to S_1
-	-	S_4	-	sinistral shear surfaces, conjugate to S_3
K_1	233/80 partly inverted	-	-	-
K_2	199/70 partly inverted	S_3 p.p.	-	-
K_3	264/84	ZK_2	-	with chlorite-filled "cross-joints"
K_4	117/62 partly inverted	S_4 p.p.	-	-
K_5	336/42	S_6	-	SE-striking, relatively flat reverse faults conjugate to S_5
ZK (K_6)	sub-horizontal	ZK_1	-	alpine tension joints
-	-	S_5	NW-striking reverse faults	conjugate to S_6
L	216/80+242/80		-	lamprophyre directions, partly overlapping with K_1, K_2 or K_3

Table 10: Correlation of the discontinuity systems

Ductile and brittle structures can be produced simultaneously. The brittle behaviour depends mainly on the stress difference to which a rock is subjected (see PRICE 1966, BLES and FEUGA 1981, HANCOCK 1985, RAMSAY and HUBER 1987):

$$\sigma_{diff} = \sigma_1 - \sigma_3$$

σ_1: maximum principal stress
σ_3: minimum principal stress

The fracture formation occurs via (Figure 15A-C):

a) Increasing the stress difference, e.g. through tectonic stress (Fig. 15A);

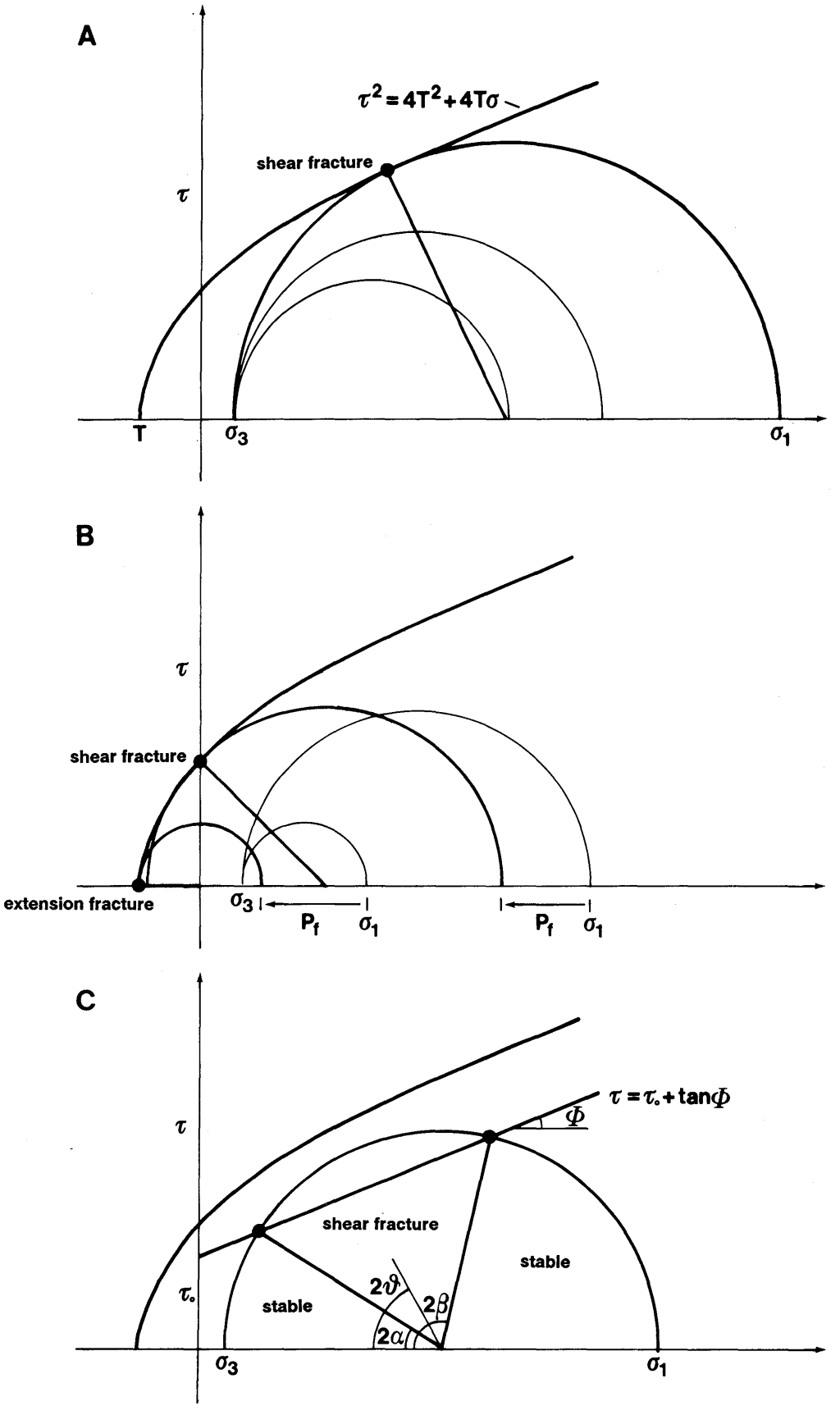

Figure 15: Mohr diagrams showing the theoretical aspects of fracture formation

b) Decreasing the principal stresses due to build-up of a counteracting pore pressure (P_f) without altering the stress difference. Two cases can be distinguished (Fig. 15B):

- the minimum effective principal stress (σ_3) exceeds the tensile strength of the rock and extension fractures form;
- the shear stress (τ) coupled with the normal stress exceeds the shear fracture limit and shear fractures are formed;
- The pore pressure may build up due to the decrease in the pore volume caused by tectonic stress or to mineral reactions and/or recrystallisations (textural changes). The fact that most of the discontinuities are healed indicates a hydrothermal fluid circulation. This again could have facilitated the formation of brittle structures.

Figure 15: Mohr diagrams showing the theoretical aspects of fracture formation (compiled after PRICE 1966, ETHERIDGE 1983, HANCOCK 1985, RAMSAY and HUBER 1987). The stability limit of the isotropic rock follows the fracture criterium of Griffith:

$$\tau^2 = 4T^2 + 4T\sigma$$

(τ, shear stress; σ, normal stress; T, tensile strength)

A Shear fracture formation by increasing the differential stress (σ_1-σ_3)

B Fracture formation due to reduction of the principal stresses with the effect of pore pressure (P_f):

σ_1-$\sigma_3 \leq 4T$ -> extension fracture

σ_1-$\sigma_3 > 4T$ -> shear fracture

C Reactivation of an existing discontinuity surface which follows the Coulomb-Navier fracture criterion:

$$\tau = \tau_o \bullet \tan\phi$$

(τ_o, cohesion; $\tan\phi$, coefficient of internal friction)
A shear fracture occurs only if $2\alpha \leq 2\vartheta \leq 2\beta$ (ϑ, angle between σ_1 and the discontinuity; α, β, boundary angle).

c) Reactivation of an old structure. The fracture formation is influenced by the angle relationships between the shear surfaces and the direction of the principal stress axes, as well as by the amount of these stresses. Whether or not a discontinuity surface will reactivate as a fracture, and thus whether it will glide or not, depends mainly on the following parameters: coefficients of static and dynamic friction and cohesion on the surface of the discontinuity. These parameters are generally smaller than those of the corresponding isotropic rock (Fig. 15C; RAMSAY and HUBER 1987).

While the first two of the abovementioned mechanisms - a) and b) - are responsible for the formation of all brittle structures, the last process c) leads to the reactivation of the most important structures and to the formation of cataclasites and kakirites. Open fissures arise from the reactivation of old structures and today these represent the most important water flow-paths.

4.4 Structures at the GTS (underground)

The aim was to confirm, supplement and, where necessary, to correct Nagra's earlier division of the discontinuities into 3 schistosity systems, 6 joint systems and an independent lamprophyre direction (NTB 81-07, 85-34, 85-47). Based on the fact that certain brittle structures show preference for fillings with certain minerals or mineral associations (e.g. chlorite on K_3 discontinuities), the discontinuities were divided according to mineral coatings. In order to discriminate between the brittle structure systems, the following **categories** were defined:

- **Of:** **"open" discontinuities**, i.e. those which are broken open or not filled;

- **Bi:** discontinuities filled or coated only with **biotite;**
- **Gli:** **mica-bearing discontinuities**, i.e. those with only biotite and chlorite, muscovite and chlorite, biotite and muscovite and/or biotite, muscovite and chlorite;
- **Chl:** **discontinuities** with only (powdered) **chlorite;**
- **Cc:** **discontinuities** with only **calcite** and/or with **calcite** and **chlorite;**
- **Ep:** **discontinuities** with only **epidote** and/or **epidote-quartz;**
- **Qz:** **discontinuities** healed only with **quartz.**

To complement the brittle structures, foliation measurements were also considered by way of comparison.

On the whole, the existing system for classifying the discontinuities could be confirmed. A clear division of the two main systems S_1 and S_2 is not always possible since the orientations of these systems often overlap one another. On the other hand, further evaluation of the brittle structure data allowed three new systems to be identified, the nomenclature of STECK (1968a) being adopted, i.e. S_4, S_5 and S_6.

4.4.1 Division of the discontinuities according to their orientation

For each of the 12 boreholes taken into consideration, as many pole diagrams as possible were drawn of the different categories of discontinuities. Pole sectors which should characterise actual discontinuity systems were then derived from the pole maxima.

The delimitation (in Figure 16) of the pole sectors at angles of dip of 60° and 25° is arbitrary. It is however based on the fact that between 84 and 94% of the surfaces (in boreholes and in the tunnel) in the steep systems have an angle of dip greater than 60°. Discontinuity systems with an angle of dip less than 60° which,

from the point of view of their azimuth, belong to a steep system, are not taken into account. This explains why the residual sectors often make up several percent (Figure 16).

The division based on azimuth and angle of dip is somewhat artificial since

- in the case of a curved surface, the orientation is always changing (CHOUKROUNE and GAPAIS 1983);
- the orientation of a system within a rock can change from area to area (STECK 1968a).

As a result of the evaluation, the Schmidt net was divided into pole sectors delimiting the individual discontinuity systems (Figure 16).

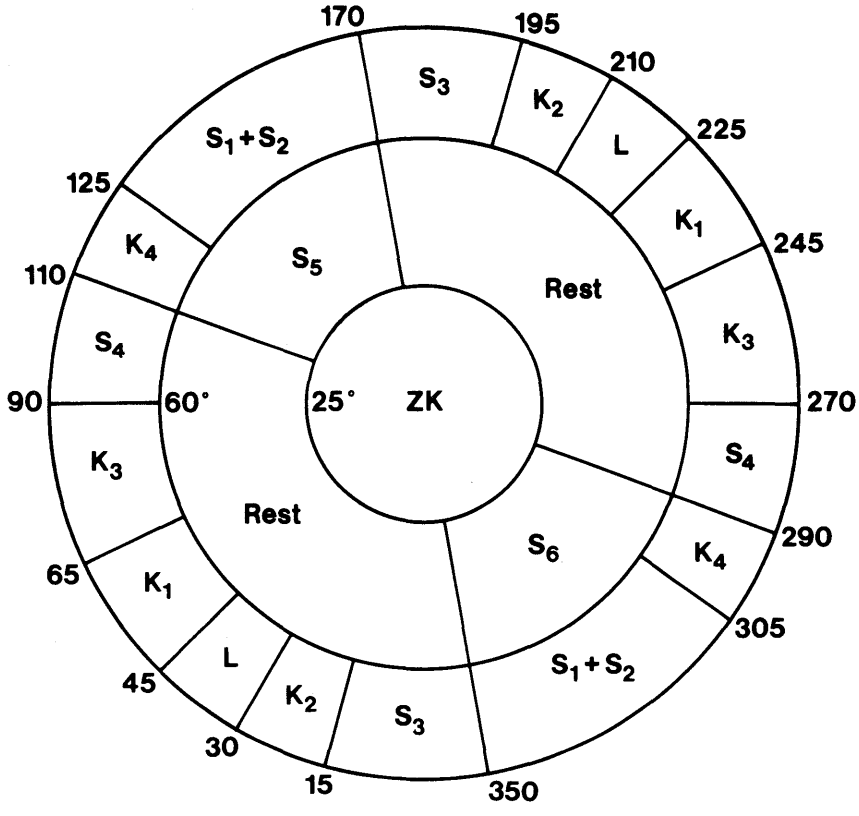

Figure 16: Division of the Schmidt net into pole sectors (Rest = residual sectors).

The pole sectors actually give discontinuity orientations. They can, however, be interpreted as a representative indication of an existing discontinuity system since they are generally clear in different pole diagrams, even when there are overlaps and connections between neighbouring sectors (Table 11).

	NTB 85-34		GTS/Boreholes		GTS/Laboratory Tunnel	
System	Mean azimuth/ angle of dip	Number of discontinuities considered	Mean azimuth (without inverted discontinuities)	Number of discontinuities considered	Mean azimuth (without inverted discontinuities)	Number of discontinuities considered
S_1	142/77	639	147	807	147	171
S_2	157/75	519				
S_3	183/65	271	183	306	185	44
K_1	233/80 partly inverted	292	235	147	234	20
K_2	199/78 partly inverted	124	203	73	202	31
K_3	263/84	144	257	191	260	31
K_4	117/62 partly inverted	163	119	113	114	9
K_5 (S_6)	336/42	isolated	315	62	335	8
ZK	sub-horizontal	73	sub-horizontal	38	sub-horizontal	1
S_4	-	-	100	118	108	4
S_5	-	-	141	212	151	8
L	216/80+242/80	186	219	82	218	25

Table 11: Average angles of dip and azimuths of the discontinuity systems at the GTS.

Only brittle structures were evaluated with NAGRADATA but, in order to characterise a discontinuity system as a schistosity, the ductile structures also have to be taken into account. The evaluation of the foliation measurements by GEOTEST resulted in only S_1-, S_2- and S_3 pole sectors being shown. Accordingly, only these three systems correspond to actual schistosities. Based on detailed observations at the surface, CHOUKROUNE and GAPAIS (1983) could distinguish S_2 as the main schistosity and S_1 and S_3 as conjugate shear surfaces.

The individual discontinuity systems are then characterised briefly and each is illustrated with a pole diagram. Figure 17 shows a comparison of the distribution of all brittle structures in the boreholes and the GTS tunnel.

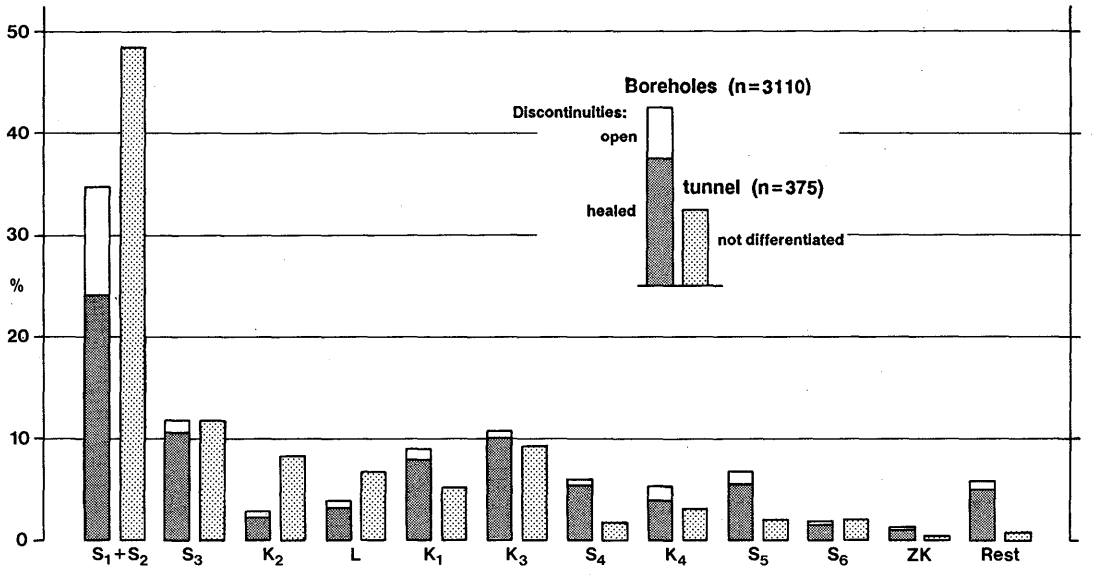

Figure 17: Distribution of all discontinuities in the boreholes and the laboratory tunnel according to pole sectors.

4.4.1.1 Systems S_1 and S_2 (Figure 18, Tables 10 and 11)

General: Although S_1 (shear surface) and S_2 (main schistosity) form two systems, they are treated together as they never occur separately. It is also impossible to assign the different structures clearly to S_1 or S_2 since their orientation varies within the rock and leads to overlaps.

Characteristics: With the exception of calcite-bearing surfaces, the systems S_1 + S_2 occur in all discontinuity categories (pp.60 and 61). Particularly noteworthy is the pronounced occurrence of these systems in the case of open fractures.

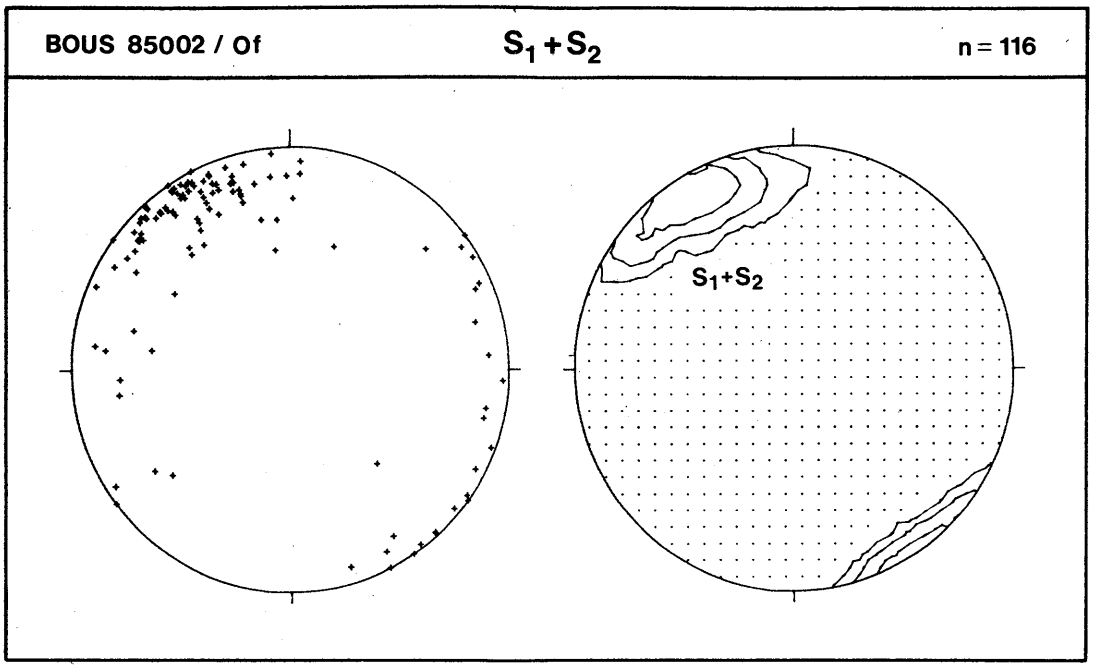

Figure 18: Pole diagram for S_1 + S_2. Contoured at 2-, 4-, 8- and 16-times homogeneous distribution.

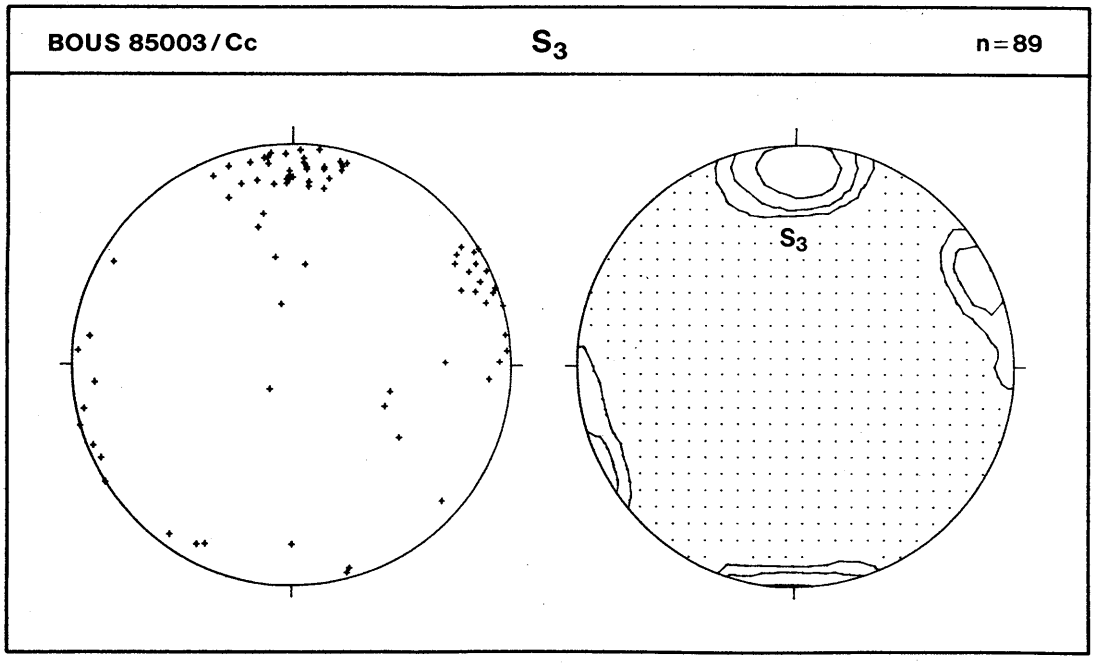

Figure 19: Pole diagram for S_3. Contoured at 2-, 4-, 8- and 16-times homogeneous distribution.

Frequency/distribution: S_1 + S_2 form by far the most frequently occurring discontinuity pair since S_2 corresponds to the main alpine schistosity and is often represented together with S_1 as fracture cleavage. S_1 + S_2 can be recognised in all the boreholes and in the laboratory tunnel, with the exception of borehole BOSB 80003. This can probably be explained by the sub-parallel direction of S_2 and of the borehole axis.

Example: Pole diagram for S_1 + S_2 for open fractures (Of) in borehole BOUS 85002.

4.4.1.2 System S_3 (Figure 19, Tables 10 and 11)

General: In contrast to S_1 + S_2, S_3 is much less clearly in evidence.

Characteristics: S_3 is indicated in all discontinuity categories, most clearly for epidote and quartz discontinuities. This confirms the surface observation by STECK (1968a) to the effect that S_3 is often characterised by milky quartz veins.

Frequency/distribution: Large S_3 disturbed zones are found only at the entrance to the GS-cavern and in the AU- and VE-areas.

Example: Pole diagram for S_3 for calcite- (and chlorite-) bearing discontinuities (Cc) in borehole BOUS 85003.

4.4.1.3 Systems K_2+L (Figures 20 and 21, Tab. 10 and 11)

General: K_2 and L are treated together here because they rarely

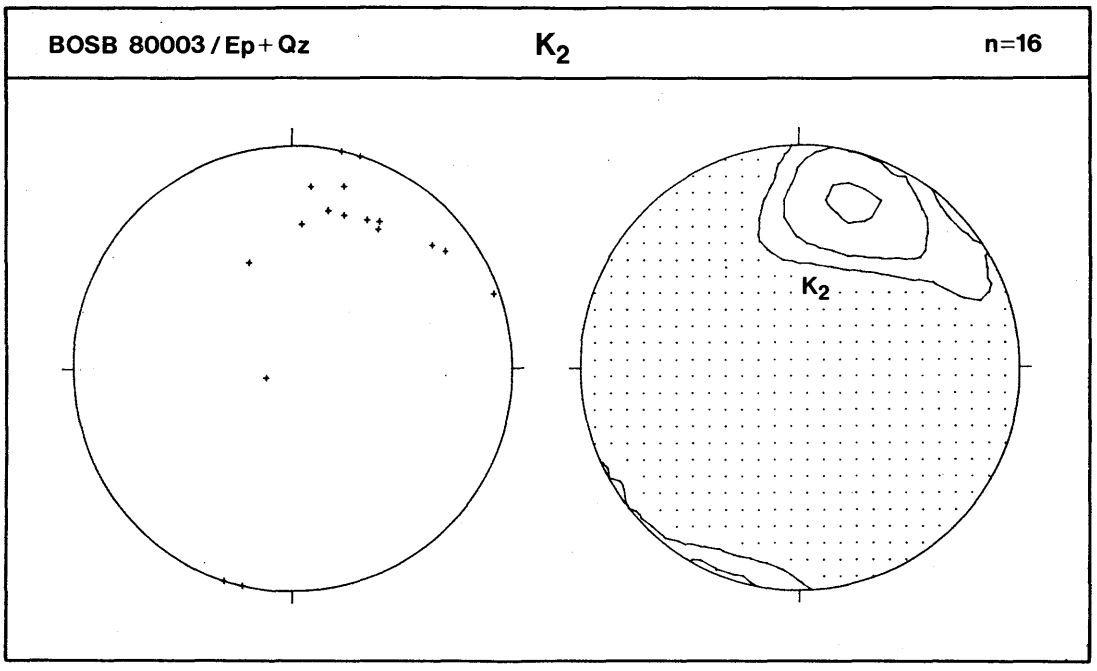

Figure 20: Pole diagram for K_2. Contoured at 2-, 4-, 8- and 16-times homogeneous distribution.

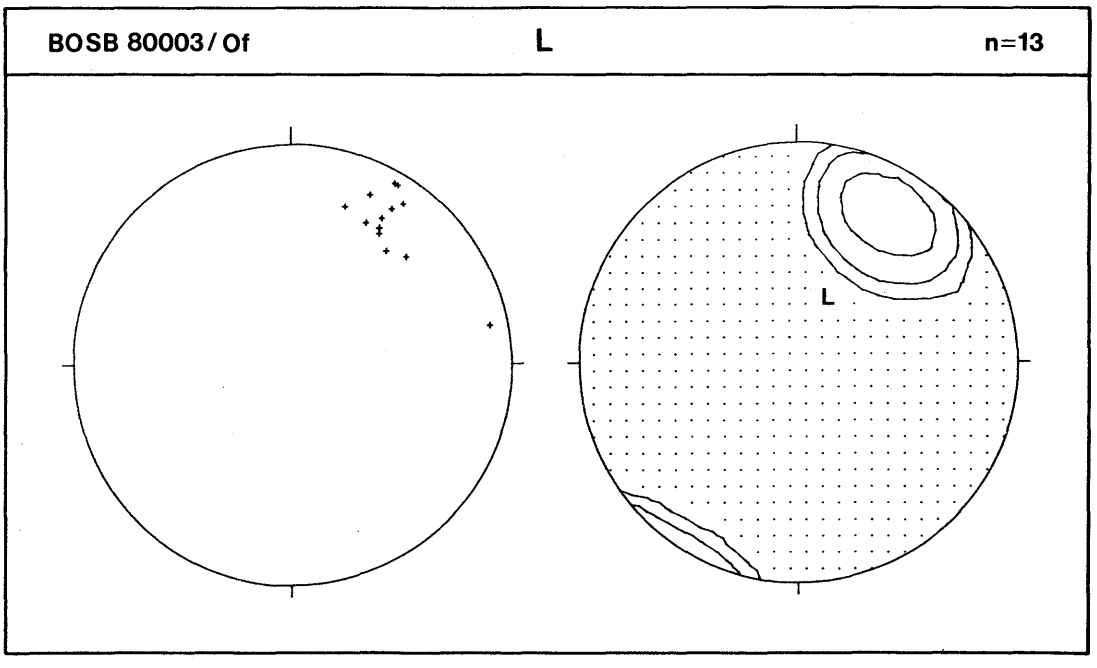

Figure 21: Pole diagram for L. Contoured at 2-, 4-, 8- and 16-times homogeneous distribution.

occur separately. In addition, L indicates only one of two lamprophyre direction maxima since the other overlaps with K_1/K_3. L need not correspond to a brittle structure system but can also simply represent a direction. This interpretation is supported by the fact that, in the vicinity of L or along contacts with lamprophyres, K_2 generally adapts to the L-direction. No link could be established between L and K_1.
Whether K_2 always represents an independent system is often not clear since S_3 overlaps to a large extent with K_2.

Characteristics: K_2 occurs most clearly where L is strongly represented.

Frequency/distribution: K_2 and L occur much less frequently in the boreholes than in the tunnel (Figure 17, p. 64). This is almost certainly a result of cutting effects since most of the boreholes are sub-parallel to K_2. K_2+L could be recognised most clearly in the boreholes BOSB 80003 and 80004 since these cross a lamprophyre-rich zone.

Examples: Pole diagrams for K_2 for discontinuities healed with epidote, quartz and/or feldspar (Ep + Qz) in borehole BOSB 80003 (Figure 20);
Pole diagram for L for open fractures (Of) in borehole BOSB 80003 (Figure 21).

4.4.1.4 System K_1 (Figure 22, Tables 10 and 11).

General: It is very probable that K_1 does not represent actual cross-jointing but rather, together with K_3, a system conjugate to S_2.

Characteristics: K_1 is shown most often by epidote-filled discontinuities.

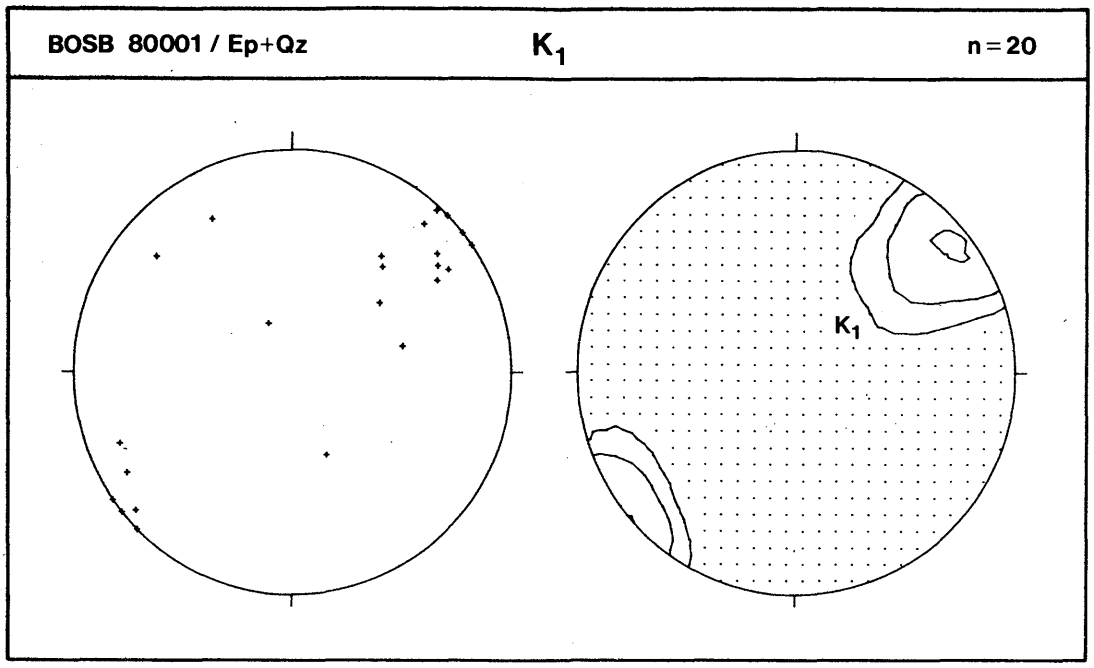

Figure 22: Pole diagram for K_1. Contoured at 2-, 4-, 8- and 16-times homogeneous distribution.

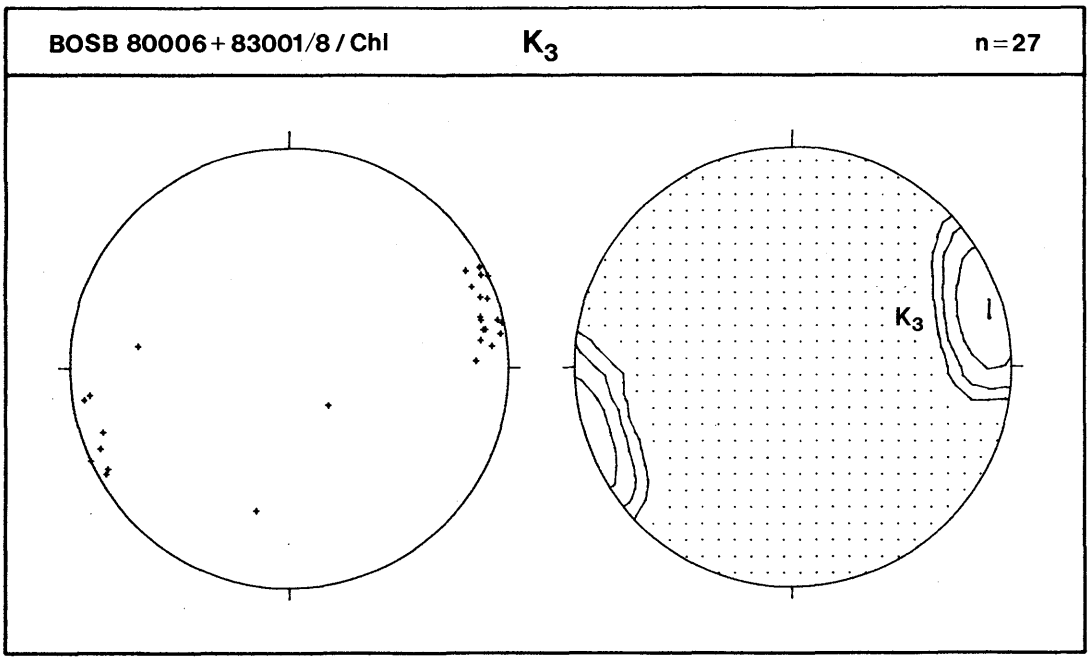

Figure 23: Pole diagram for K_3. Contoured at 2-, 4-, 8- and 16-times homogeneous distribution.

Frequency/distribution: Although K_1 is a secondary system, it is fairly widespread. It is most clearly represented in borehole BOSB 80001 since it is also shown there by open discontinuities.

Example: Pole diagram for K_1 for epidote and/or quartz discontinuities (Ep + Qz) in borehole BOSB 80001.

4.4.1.5 System K_3 (Figure 23, Tables 10 and 11)

General: The K_3-system corresponds to brittle structures which have the greatest longitudinal extent (up to several decametres), as seen from surface observations (STALDER 1964, STECK 1968a).

Characteristics: At the surface, K_3 is evidenced mainly by chlorite joints. At the GTS, however, K_3 is characterised by all mineral coatings identified on joint surfaces. K_3 can only be designated as actual cross-jointing to the main alpine schistosity (S_2) when it overlaps with K_1, which is only partly the case. Otherwise, together with K_1, it forms a conjugate pair of brittle structures with respect to S_2.

Frequency/distribution: As the third most common system (Figure 17), K_3 is represented in almost all the boreholes and in the laboratory tunnel. The clearest occurrence is in borehole BOUS 85002.

Example: Pole diagram for K_3 for the chlorite discontinuities (Chl) in the boreholes BOSB 80006, 83001 and 83008.

4.4.1.6 System S_4 (Figure 24, Tables 10 and 11)

General: S_4 (terminology for structures both of a brittle and ductile nature; STECK 1968a) does not represent an actual schistosity. Whether S_4 represents an independent system at all can not be determined with any degree of certainty. On the one hand, it could form a system with K_4 and, on the other hand, even small changes in direction of the K_3 system lead to considerable overlapping with S_4.

Characteristics: S_4 is evidenced only slightly by discontinuity coatings. The clearest evidence for this system is given by brittle structures healed with mica, chlorite, calcite or epidote.

Frequency/distribution: S_4 can be observed clearly only in the boreholes BOUS 85002 and 85003. It occurs less frequently in the tunnel than in the boreholes, which could be explained by the fact that S_4 is sub-parallel to the tunnel.

Example: Pole diagram for S_4 for discontinuities filled with epidote (Ep) in borehole BOUS 85003.

4.4.1.7 System K_4 (Figure 25, Tables 10 and 11)

General: K_4 can never be separated as such due to overlapping mainly with S_1 and, to a lesser extent, with S_4. It could even represent a single system together with S_4 which, together with S_3/K_2, forms a system pair conjugate to the main schistosity (S_2).

Characteristics: The system K_4 is represented, even if only to a small extent, in all discontinuity coatings. The presence of K_4 in

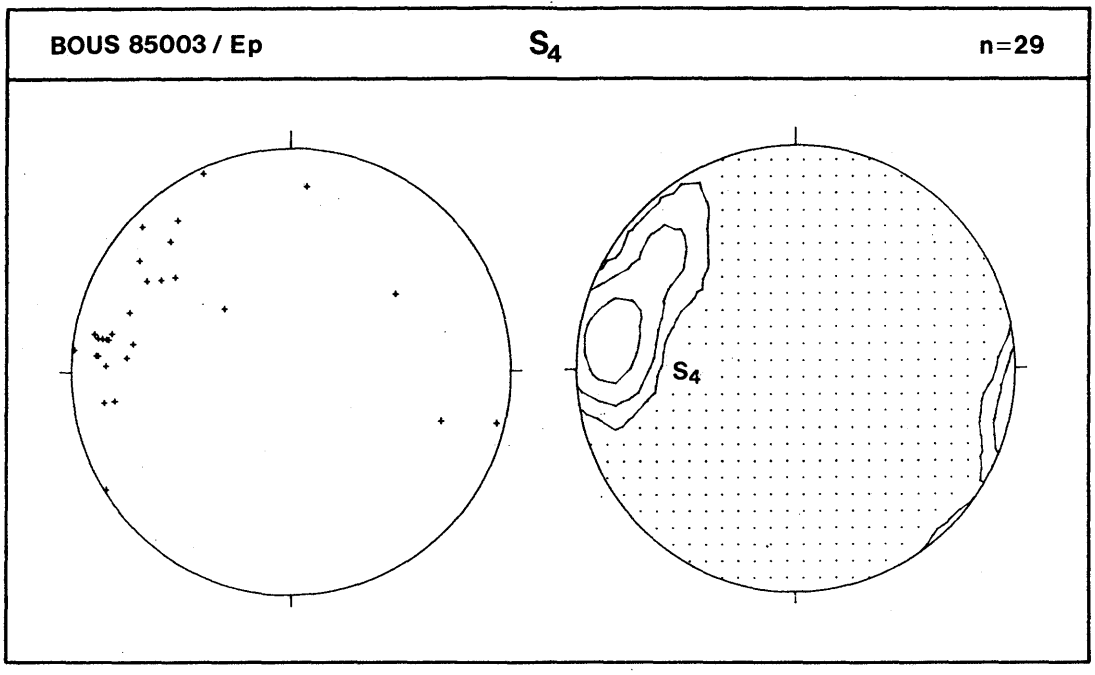

Figure 24: Pole diagram for S_4. Contoured at 2-, 4-, 8- and 16-times homogeneous distribution.

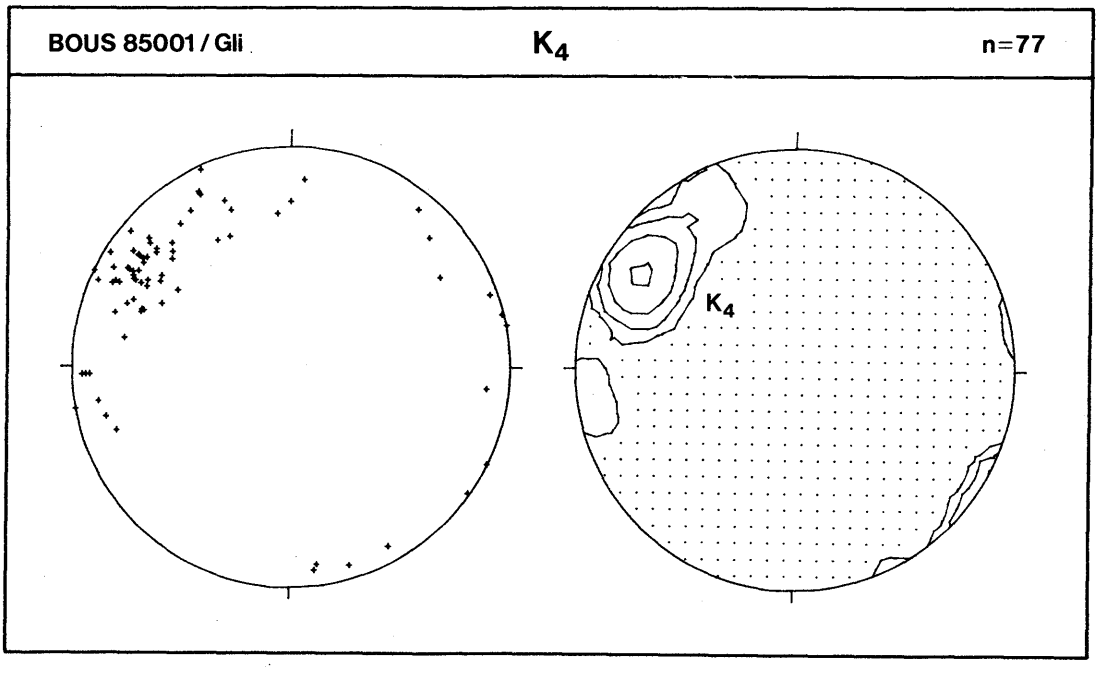

Figure 25: Pole diagram for K_4. Contoured at 2-, 4-, 8- and 16-times homogeneous distribution.

open fractures is notable. These brittle structures, which are represented otherwise by S_1+S_2 and S_3, indicate either that part of K_4 really corresponds to the system S_1 or could be a result of the systems S_1 and S_4 bordering on one another.

Frequency/distribution: K_4 occurred most clearly in the boreholes BOSB 80006, 83001 and 83008. It can also be identified in the boreholes BOUS 85001 and 83003. The fact that K_4 occurs less often in the tunnel than in the boreholes could be due to the fact that both directions are sub-parallel.

Example: Pole diagram for K_4 of the mica-bearing discontinuities (Gli) in borehole BOUS 85001.

4.4.1.8 System S_5 (Figure 26, Tables 10 and 11)

General: S_5 (terminology for shear surfaces according to STECK 1968a) is not actually a schistosity. It is difficult to decide whether it represents an independent system since S_5 surfaces show an S_1+S_2- and K_4-azimuth but are distinguished from these systems by a clearly smaller angle of dip.

Characteristics: Because it occurs so rarely, the system S_5 has no characteristic, statistically relevant discontinuity fillings.

Frequency/distribution: S_5 could best be distinguished as a separate system in the boreholes BOSB 80006, 83001 and 83008.

Example: Pole diagram for S_5 for the quartz joints (Qz) in the boreholes BOSB 80006, 83001 and 83008.

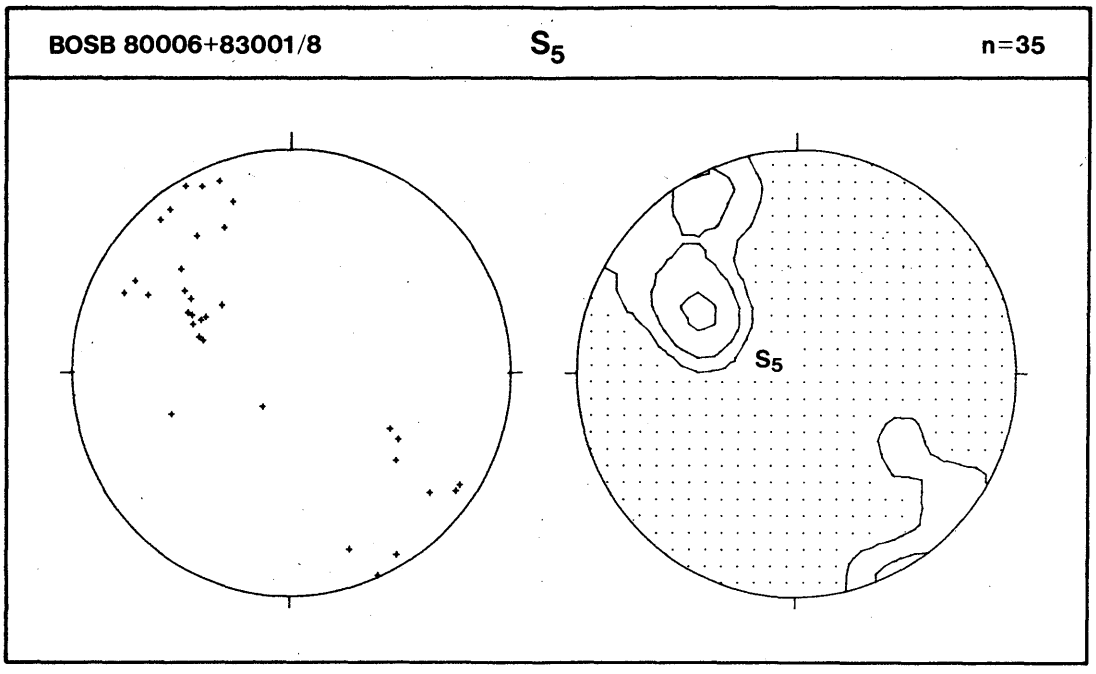

Figure 26: Pole diagram for S_5. Contoured at 2-, 4-, 8- and 16-times homogeneous distribution.

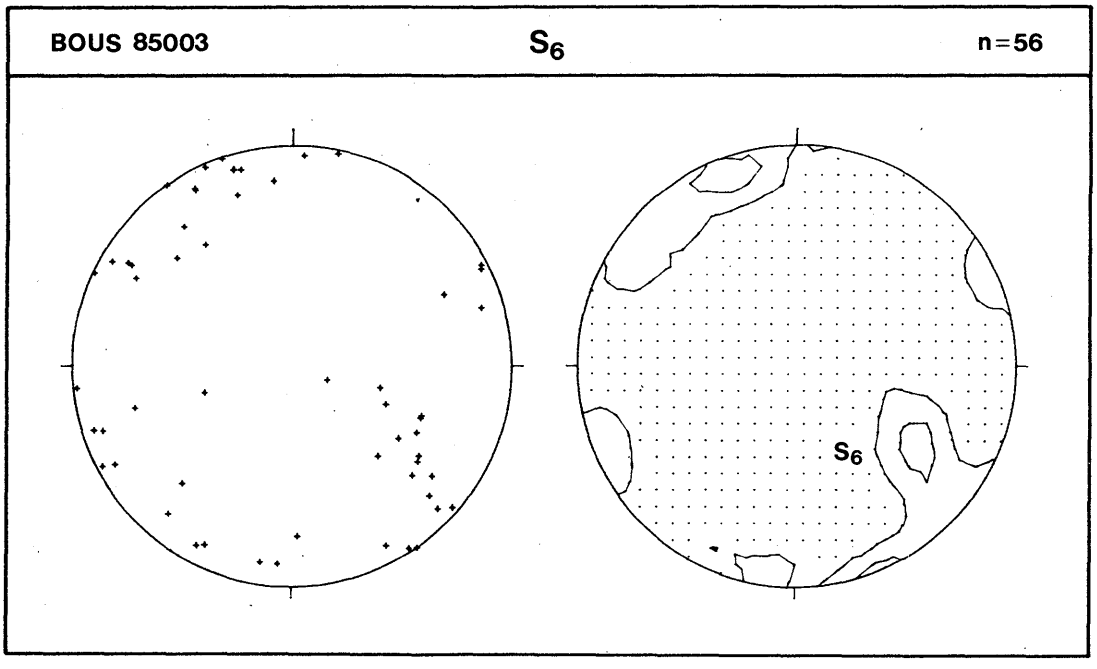

Figure 27: Pole diagram for S_6. Contoured at 2-, 4-, 8- and 16-times homogeneous distribution.

4.4.1.9 System S_6 (Figure 27, Tables 10 and 11)

General: S_6 (terminology for shear surfaces according to STECK 1968a) is not clearly defined as a system at the GTS. It was however identified as it can sometimes (although rarely) be recognised clearly at the surface (STECK 1968a).

Characteristics: System S_6 could in fact represent overturned S_1+S_2 structures, particularly where S_6 is indicated by biotite discontinuities or open joints. Only quartz discontinuities give any indication of the independent nature of this system.

Frequency/distribution: S_6 is most clearly identifiable in the boreholes BOSB 80006, 83001 and 83008, as well as in BOUS 85003.

Example: Pole diagram for S_6 for the open joints (Of) in borehole BOUS 85003.

4.4.1.10 System ZK (Figure 28, Tables 10 and 11)

General: Tension joints occur only rarely but form the most noticeable, and often the most attractive, brittle structures. They are very rarely found in boreholes, which is due to the horizontal or slightly inclined course of the latter.

Characteristics: Tension joints are indicated clearly only by quartz veins.

Frequency/distribution: Tension joints are evidenced most clearly by discontinuities filled with quartz in the boreholes BOUS 85001 and 85003. At the GTS, the largest tension joint was encountered in the measuring tunnel in the AU area.

Example: Pole diagram for ZK for quartz discontinuities (Qz) in borehole BOSB 85001.

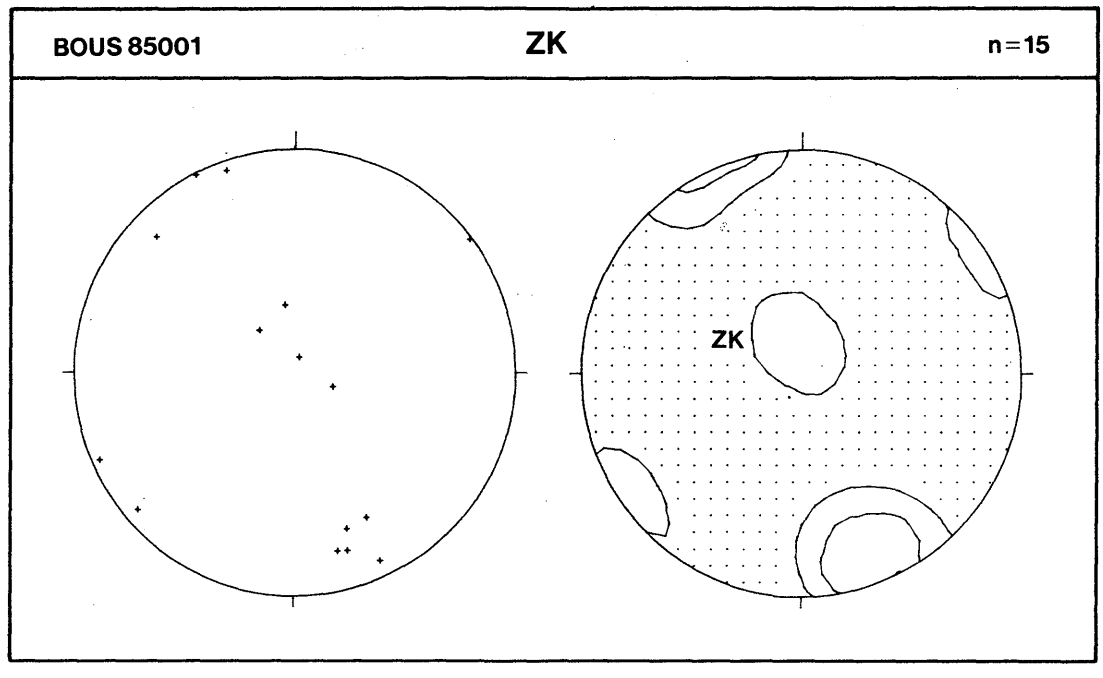

Figure 28: Pole diagram for ZK. Contoured at 2-, 4-, 8- and 16-times homogeneous distribution.

4.4.1.11 Discontinuity distribution in the boreholes

The statements made up till now on the individual discontinuity systems are based on the evaluation of pole diagrams. The necessary caution to be applied when interpreting the systems identified in this way is mentioned in the summary (Chapter 4.4.5).

Greater differences in the distribution patterns of the brittle structures result when the discontinuities are identified according to borehole (Figure 29). This division clearly shows the

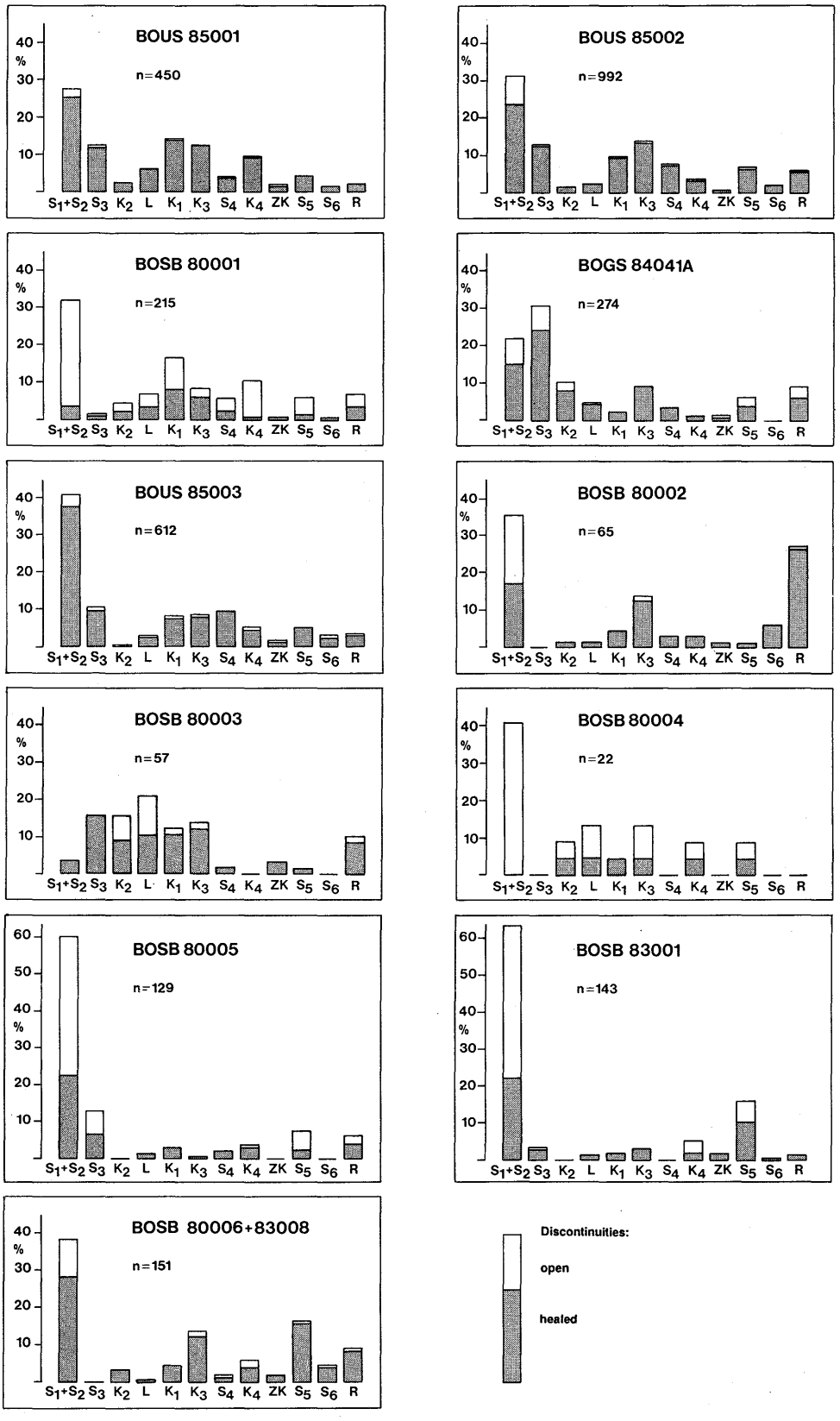

Figure 29: Discontinuity systems divided according to boreholes

heterogeneity of the distribution of the systems within the rock body. The differences in restricted areas show the heterogeneity of the deformation. S_1+S_2 remain the dominant systems in all boreholes, except for BOGS 84041A which crosses an S_3 fracture zone and BOSB 80003 which crosses a lamprophyre-rich zone where K_2/L dominates. The following discontinuity systems are predominant in the whole GTS (boreholes and tunnel)(Figures 17 and 29):

- S_1+S_2
- S_3
- K_2/L
- K_3
- K_4/S_4
- K_1

S_5, S_6 and ZK occur significantly less often. S_1 and S_3, K_2/L and K_4/S_4 can be interpreted as equivalent systems. K_3 occurs partly as cross-jointing to S_2, but also to some extent with K_1 as a conjugate system to S_2.

4.4.2 Mineralisation of the fractures at the GTS

When distinguishing the characteristic mineral coatings on the different fracture surfaces, only the dominant fillings were taken into consideration. The division into 6 categories (see pp. 60 and 61) comprises, depending on the borehole, between 55 and 95% of all brittle structures (Figure 30). This division is nevertheless taken as representative for evaluation purposes because the fillings not taken into account (residual) are generally mixtures of different minerals (e.g. epidote + chlorite, quartz + chlorite). These mineral associations do not indicate a new discontinuity system since they can certainly be assigned to at least one (as a rule to more) of the filling categories already distinguished.

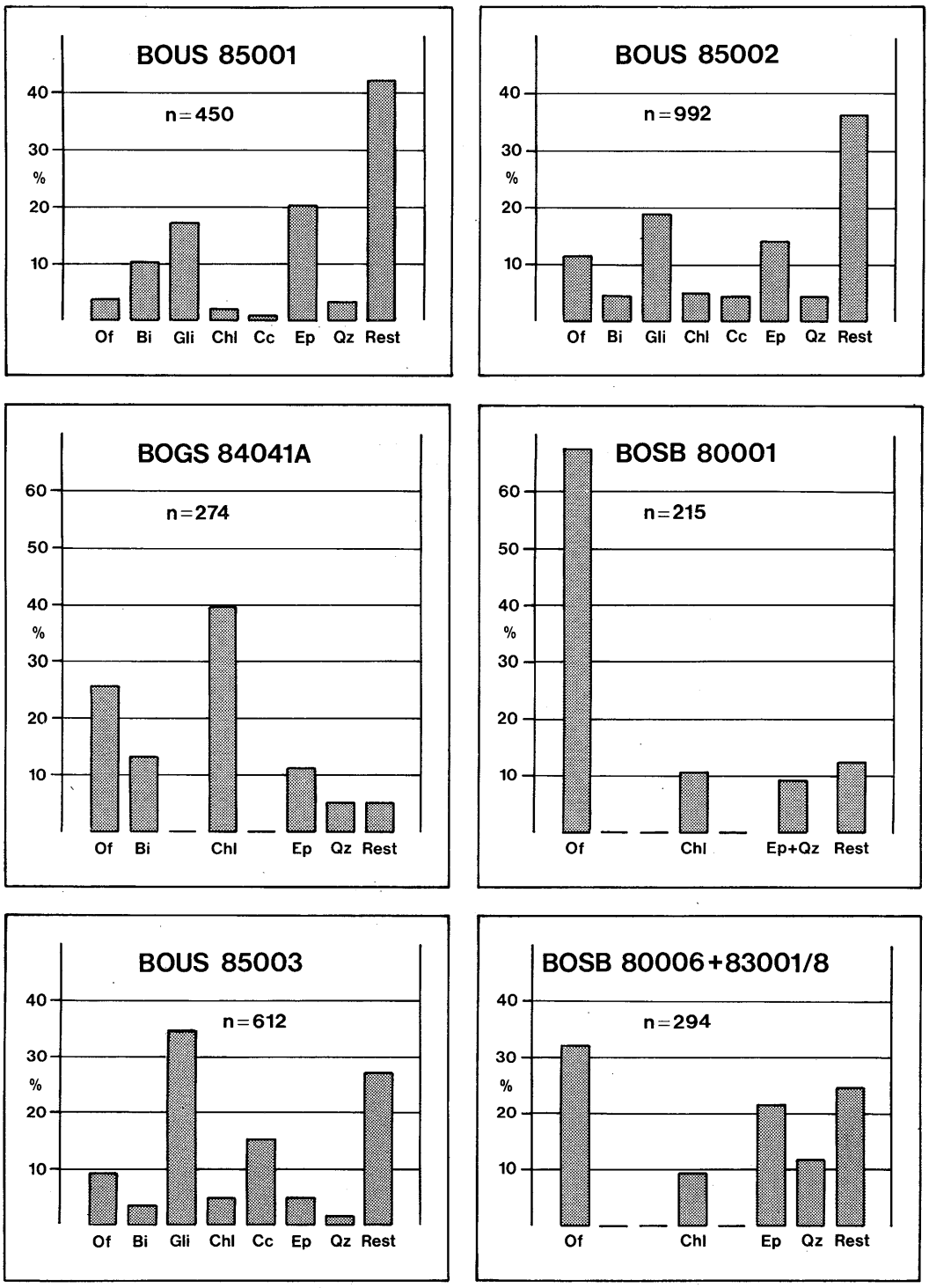

Figure 30: Division of discontinuities according to mineral coatings. Abbreviations: Of: "open" fractures; Bi: biotite-bearing fractures; Gli: mica-bearing fractures; Chl: chlorite-bearing fractures; Cc: calcite-bearing fractures; Ep: epidote-bearing fractures; Qz: quartz-bearing fractures; Rest: residual fractures.

The distribution of the individual discontinuities according to mineral coatings shows clear differences in frequency. In addition, the individual frequencies of filling categories vary significantly in the different boreholes. Although a characteristic mineral filling can occur preferentially in a specific system, this does not imply exclusivity, since a system is always characterised by several mineral coatings.

The nature of the filling is influenced to some extent by the host rock of a brittle structure. This is clear in the case of the calcite fractures which occur almost exclusively within, or in the vicinity of, lamprophyres (e.g. BOUS 85003).

The variation of category frequencies between the boreholes is also the result of the experience gained during drilling in interpreting the degree of filling of a discontinuity. This applies in the first instance to the so-called "open" fractures which, on closer observation, could also have been interpreted as biotite- or mica fractures (e.g. in BOSB 80001). Since this affects mainly the "open" fractures and the biotite or mica fractures, comparisons of these fracture frequencies should be carried out semi-quantitatively.

4.4.3 Degree of connectivity of the brittle structures

The degree of connectivity of a brittle structure corresponds to the ratio of the surface trace on the tunnel wall or drill core to the amount of complete separation of the rock body. It represents a measure for the longitudinal extent of a joint since this parameter cannot be determined more accurately underground without considerable simplification.

Statistical evaluation was carried out only for the tunnel data (Figure 31; NTB 85-34). The evaluation based on the earlier divi-

sion of discontinuities is still valid since this was, at best, only supplemented and not brought into question.

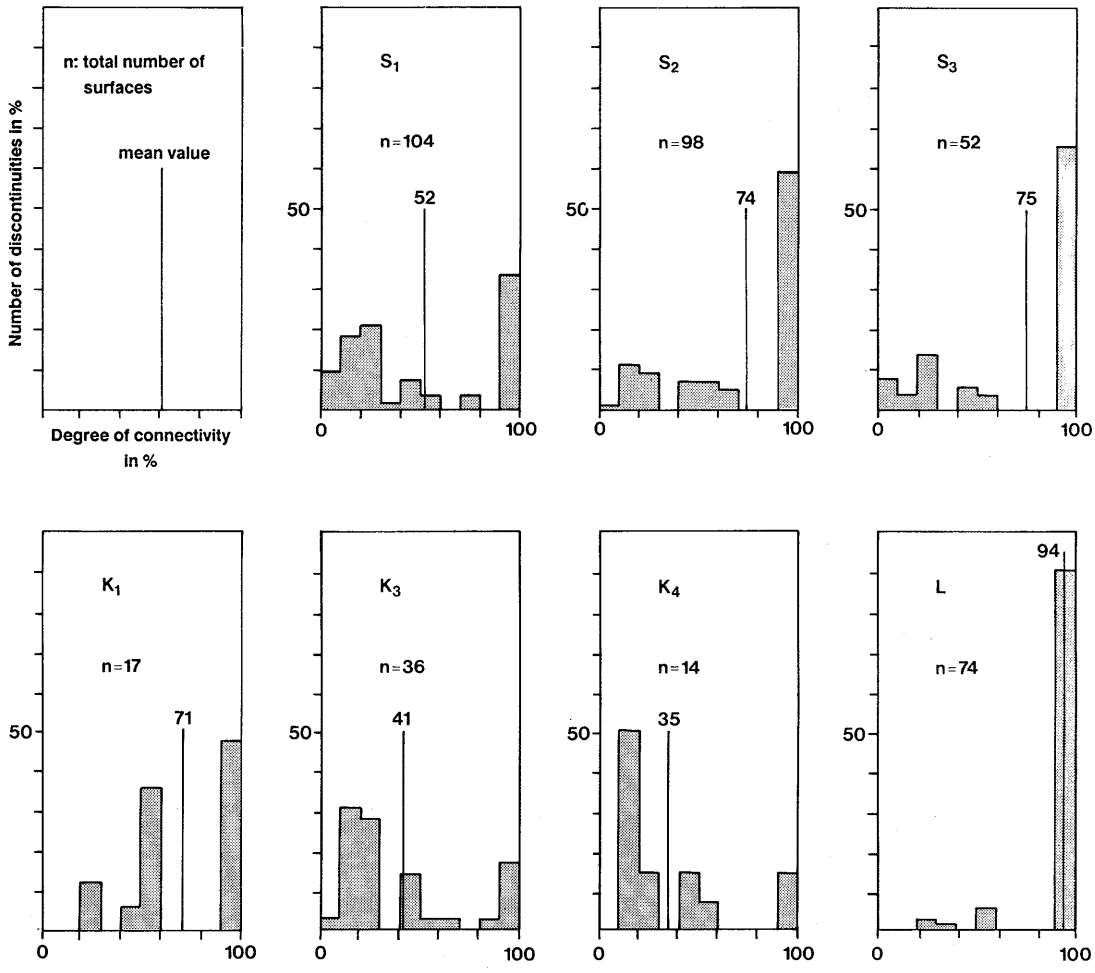

Figure 31: Degrees of connectivity of the individual discontinuity systems in the laboratory tunnel. This Figure is based on NTB 85-34; the division used there into systems S_1 and S_2 is based on a S_1/S_2 boundary with 150° direction of dip. The two histograms must therefore be interpreted with caution. In this Figure, L comprises all lamprophyre/ZAGr and GrGr contacts, irrespective of their direction.

Only systems with a high degree of connectivity are potentially important aquifers. As can be seen from Figure 31, the

granite/lamprophyre contacts (L) show the highest degree of connectivity (94%). This is not surprising as individual lamprophyres can be correlated over several hundred metres. Figure 31 also shows that the systems corresponding to a schistosity (S_1+S_2 and S_3) also have a high average degree of connectivity (> 70%).

In the case of healed fractures, the brittle structures occurring in the lamprophyres and those characterised by calcite coatings always have a high proportion of non-connected surfaces (in BOUS 85003 30-60%). These features point to feather joints produced by shear movements during the deformation of the lamprophyres.

4.4.4 Discontinuity spacings

Appendices 10A and 10B give details of the discontinuity spacings according to GTS-areas (tunnel and boreholes). When dividing the discontinuities, the earlier system according to NTB 85-34 was used.

No new evaluation of discontinuity spacings was carried out. The following information is therefore based on NTB 85-34.

The individual discontinuities in a system tend to occur in sets, which is clear from the Poisson distribution of the fractures (Figure 32). Of the 7 systems taken into consideration (S_1+S_2, S_3, K_1, K_2, K_3, K_4; Appendices 10A and 10B), S_3 has the greatest tendency to close set spacing and K_3 the smallest. For all systems, the spacing between two surfaces of the same system is in the range of one metre or more in less than 5% of all discontinuities.

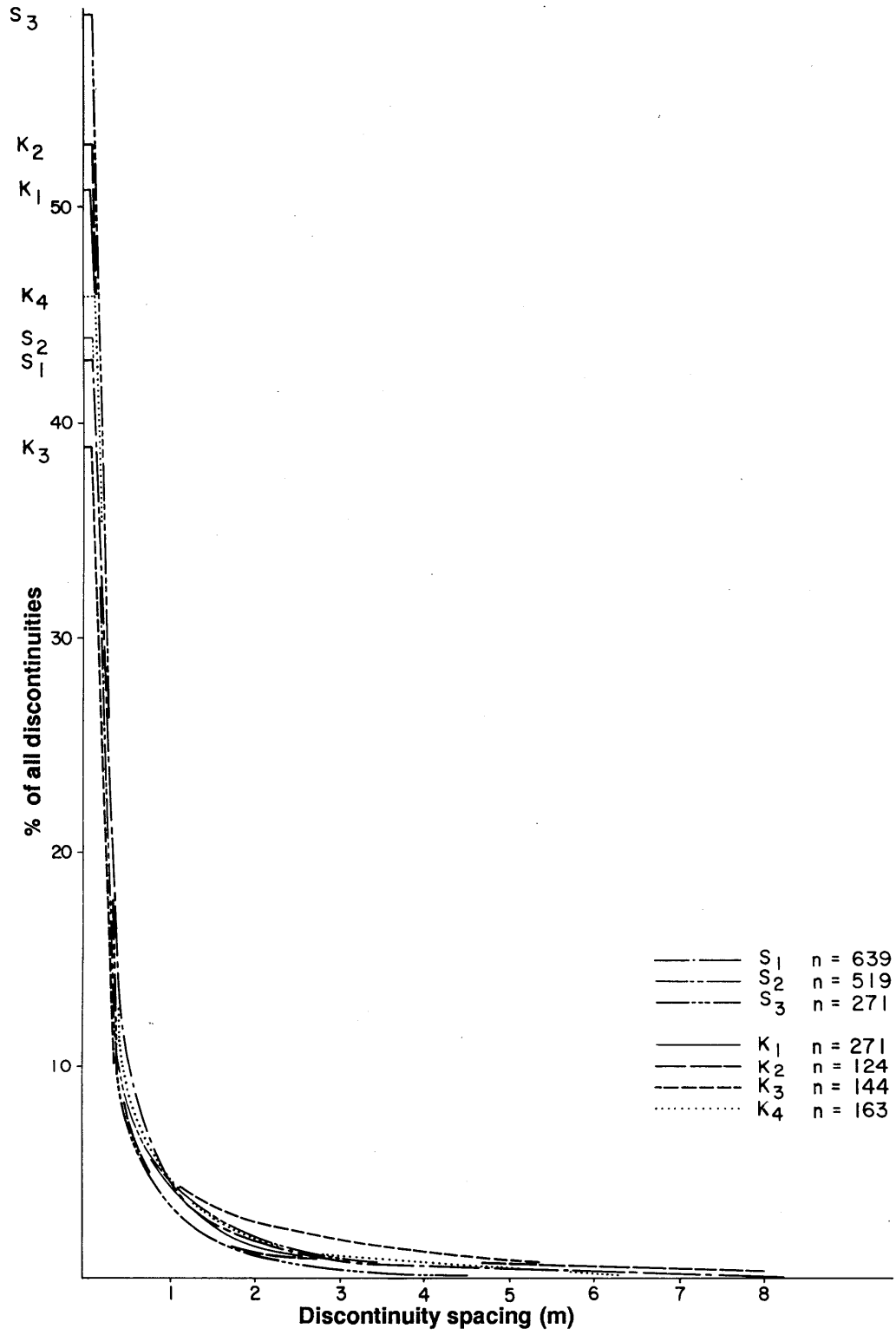

Figure 32: Discontinuity spacings: mean values for the whole GTS

4.4.5 Summary overview

Whether each of the 12 pole sectors distinguished actually corresponds to a discontinuity system is questionable. Overlaps of 10 to 20° in both the direction of strike and the dip are widely found and can lead to deception as to the existence of a system. The individual discontinuities therefore form a so-called fracture spectrum (HANCOCK 1987) which is characterised by a scatter of azimuths.

Despite this reservation, Table 12 shows the systems which clearly exist.

System	Comments
S_2	Main schistosity (azimuth strongly overlapping with S_1; the two systems cannot be separated on the basis of orientation alone)
S_1 and S_3	equivalent system pair (conjugate)
S_4/K_4 and K_2/L	equivalent system pair (+ orthogonal)
K_1 and K_3	equivalent system pair (conjugate)
ZK	tension joints

Table 12: Systems shown to exist at the GTS

S_5, and particularly S_6, are not clearly evidenced although they were described by STECK (1968a) and by CHOUKROUNE and GAPAIS (1983, only S_5).

The dominant discontinuity systems are shown in Figure 33 as a block diagram.

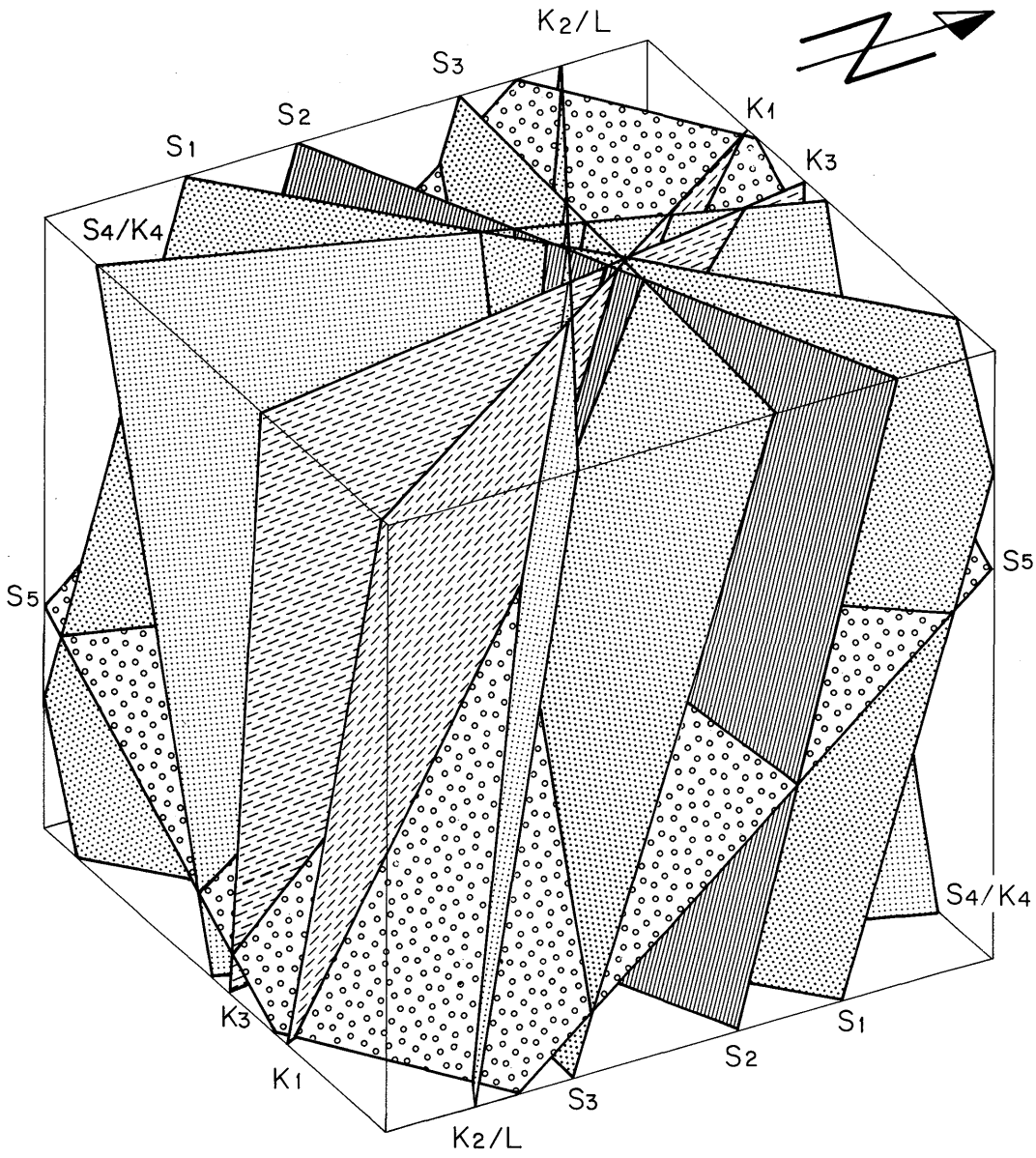

Figure 33: Block diagram of the dominant fracture systems. For a better overview, the sub-horizontal system ZK and the hypothetical system S_6 were left out.

The long chlorite-filled fractures which are typical of K_3 sometimes correspond to cross-jointing to S_2. In such cases, the azimuth lies between typical K_3 and K_1 directions; otherwise K_3 and K_1 form a system pair conjugate to the main schistosity.

S_4 and K_4, as well as K_2 and L, were treated together. The reason for this lies in the proximity of these pole sectors to one another. Because of the small differences in azimuth and angle of dip, they cannot be distinguished clearly as two systems.

Appendix 11 shows the most important discontinuities according to borehole and GTS-section (tunnel). The variations in azimuth and angle of dip within the GTS can be seen clearly. There are also significant differences within this detailed division as the dominant fracture systems differ from place to place. This situation is caused to a considerable extent by the influence of the drilling direction on the relative frequency of the individual fracture systems.

The apparent absence of a system in a section can also be misleading if the other systems are represented by a significantly larger number of brittle structures. Although actually present, the apparently absent system is suppressed and thus not identified.

Finally, the absence of a system does not necessarily mean that it has no significance. A system which is of secondary importance percentage-wise can nevertheless be fairly significant because, e.g., it has a large number of open fractures or a considerable longitudinal extent. The lamprophyre contacts which have L- and K_1-directions are a typical example of this since they are often accompanied by open and water-bearing joints.

The variations in the orientation of discontinuity systems are certainly influenced by local heterogeneities. Lamprophyre contacts form the most important mechanical discontinuities which can alter the regional stress field and determine the local one. The formation of certain brittle structures is influenced in this manner since the main stresses on which the formation of a tectonic discontinuity depends can alter in direction and strength.

Underground, i.e. in tunnels and boreholes, the systems are represented in the following order of frequency (Figures 17 and 33, p. 64 and 85):

S_1+S_2	36.2%	K_2/L	7.6%
S_3	11.8%	S_5	6.3%
K_3	10.6%	S_6	2.0%
K_4/S_4	10.6%	ZK	1.1%
K_1	8.6%	Rest	5.2% (Fig. 13, p. 49)

Open joints are found mainly in the systems S_1+S_2, which clearly dominate. The remaining open fractures are distributed over the other discontinuity systems, the frequency being given in Figure 29.

4.5 Surface structural geology

4.5.1 Orientation of the discontinuity systems

60% of all the measured values can be assigned to four systems. Since, in a jointed zone, **one** measured value can correspond to several planes, more than 90% of all discontinuities are ultimately taken into account.

The frequency distribution of the measured values is, as can be seen from Table 13, very uneven. Even after the correction necessitated by the direction of profile 6 (S_1 and S_2 values not taken into account), the system S_1+S_2 still dominates by far. Within the area investigated, there are no marked trends with regard to frequency distribution of discontinuity systems.

The systems S_1+S_2 and S_3 correspond more or less exactly to the corresponding division underground (see Figure 20, p. 67). Pole

diagrams can be used to separate S_1 and S_2 from one another; the boundary of these systems is at an azimuth of dip of 150°. On the surface, K_2 and K_3 were extended by the interlying systems L and K_1 which are statistically difficult to recognise. In order to calculate the true thicknesses and discontinuity spacings, a weighted mean value was taken from the pole diagrams.

System	Proportion of measured values	Azimuth/angle of dip [β / α]		Corresponds underground to the system	Comments
		Range of variation	Weighted mean value		
S_1+S_2	65%	β 135-171; 325-342 α 63-88; 85-90	155/70	S_1+S_2	Values for profile 6 not taken into account
S_3	5%	β 172-198 α 70-90	188/81	S_3	
K_2	10%	β 199-229 α 72-90	210/75	K_2 und L	L statistically inseparable
K_3	20%	β 230-267 α 72-90	258/80	K_1 und K_3	K_1 statistically inseparable

Table 13: Main discontinuity systems at the surface (60% of all measured values)

The range of variation of the discontinuities S_1+S_2 lying subparallel to the main schistosity is similar both on the surface and underground. In profiles 2 and 3, 20- to 150 m-long sections can be identified which are dominated either by S_1 (azimuth of dip < 150°) or by S_2 (azimuth of dip > 150°). S_2 appears to occur more frequently in the vicinity of K_2- or K_3 fracture zones.

In several pole diagrams, an accumulation of the pole points of all four systems along a great circle with a linear intersection of 187/80 can be seen (Figure 34). This direction corresponds to the intersection lines between any discontinuities on this great circle. The intersection lines within the 4 systems, and thus between

the majority of the discontinuities, run mostly parallel and dip steeply to the south.

ZK should be mentioned as a further relevant discontinuity system which is, however, statistically very poorly represented. It comprises the slightly NE-dipping tension joints which occur mainly in the southern section of profiles 2 and 3.

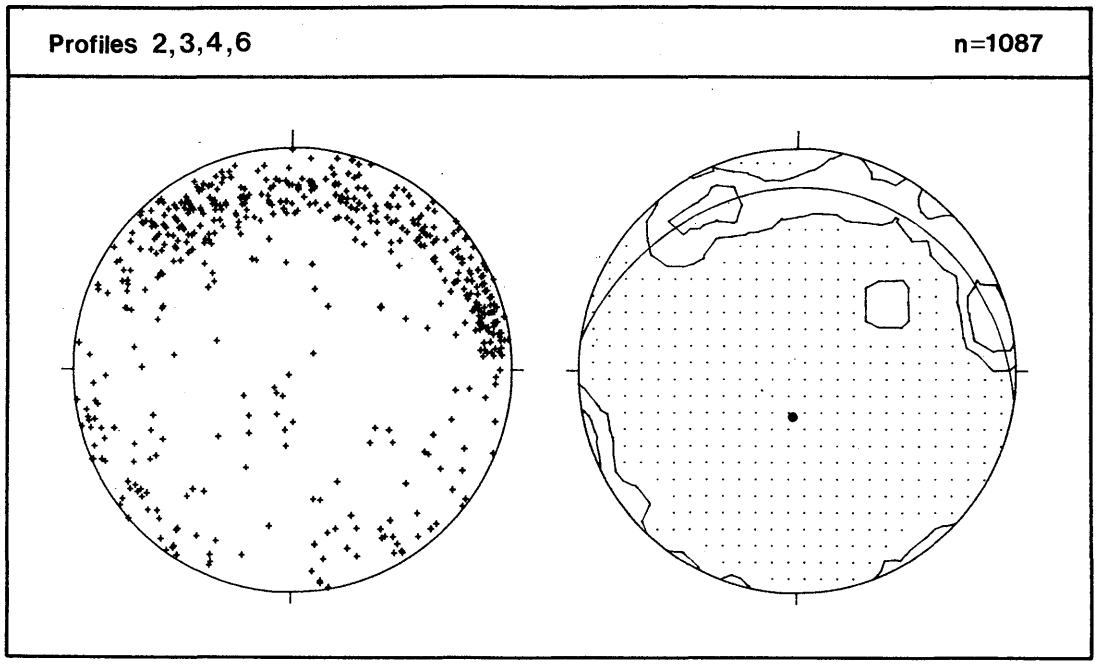

Figure 34: Pole diagram for the orientation data of zones with 2-15 joints/m (profiles 2, 3, 4 and 6; contoured at 2-, 4-, 8- and 16-times homogeneous distribution). The Figure gives an example of accumulation of surface poles "along" a great circle. The axis of the great circle (187/80) is shown by a point.

4.5.2 Mineralisation of the fractures at the surface

Because of the strong weathering, minerals can only rarely be recognised and identified as joint fillings. Table 14 gives the

mineral fillings observed for the different discontinuity systems. There are no data which would allow a more extensive evaluation.

Minerals / System	Chl	Chl+Qz	Qz	Qz+Ep
S_1+S_2	-	x	o	x
S_3	x	-	x	-
K_2	o	x	x	-
K_3	x	-	-	-
ZK	-	x	x	-

Table 14: Mineral fillings of the joint systems (o = individual measurement; x = several measurements and - = no measurement.

4.5.3 Connectivity and extent of the discontinuities

Almost all the discontinuities recorded in the range of the profile lines are non-cohesive surfaces penetrating through the rock body. On the one hand, there are joints whose original apertures have been largely obscured by weathering and gravitation and are therefore no longer measurable. On the other hand, there are shear surfaces along which weathering processes have cleared out the intensively fractured area and their original thicknesses are no longer measurable.

The third group to be mentioned are the healed joints. In so far as they are several mm thick or recognisable due to weathering, they were taken into consideration and make up less than 2% of all discontinuities.

In the field, the extent of the discontinuities was divided into four categories as follows:

Length	2.5 m	10 m	25 m	
Category	1	2	3	4

The interruption of the discontinuities could only be observed directly in relatively few cases because of erosion or Quaternary cover. In most cases, the interruption takes the form of intersection with another system. Single joints in particular can gradually disappear and be lost in the undisturbed intact rock.

Appendix 12 gives the pole diagrams corresponding to the extent of the surface structures. For the four main discontinuity systems, a rough division of lengths can be made as in Table 15.

System	Extent				Σ
	2.5 m	10 m	25 m		
S_1+S_2	1	5	18	40	64
S_3	1	2	1	2	6
K_2	-	2	6	2	10
K_3	1	3	4	12	20
Σ	3	12	29	56	100%

Table 15: Estimated distribution of the extent of discontinuities in the four main systems

44% of the discontinuities (zones) have an extent of < 25m. S_3 and K_2 in particular are dominated by this proportion of discontinuities which end or are lost within the visual range of the profile lines.

It is evident that the fault zones which extend over greater distances are not clearly defined with one measurement (in the region of the profile line). An example of this is profile 6 in the Geisschälen (S_2 disturbance, Appendix 9). Morphologically the gully is eroded along a 154/74-oriented "discontinuity". The azimuths and angles of dip for the most jointed areas measured over the 800 profile metres vary between 134-172/60-90 (Figure 35). From 33 measured values, a general profile of 155/77 can be determined.

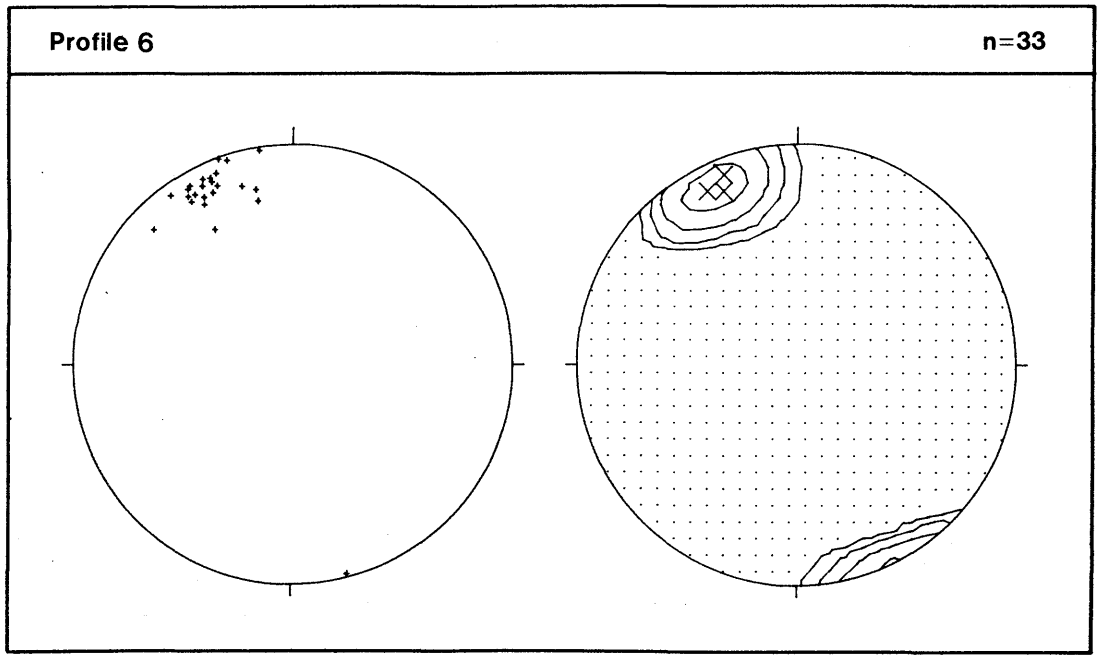

Figure 35: Pole diagram for measured values of strongly jointed zones in profile 6. Contoured at 2-, 4-, 8- and 16-times homogeneous distribution.

4.5.4 Discontinuity spacings

During the field studies, it was decided to distinguish three degrees of jointing and to include these in NAGRADATA (Table 16).

Field measurements			NAGRADATA	
Category	Discontinuity spacing	Measured values	Input	CODE
virtually no jointing	50 cm	for each joint: - intersection point on profile - azimuth/angle of dip	 * *	KLUF
slightly jointed	5 cm	on profile: beginning and end of zone joint density (joints/m) azimuth/angle of dip, average	* number *	KLPA
strongly jointed		on profile: beginning and end of zone joint density azimuth/angle of dip, average	* not covered *	ZSOG

Table 16: Division into jointing categories. Abbreviations: KLUF: single joint; KLPA: parallel joints; ZOSG: strongly jointed zone (NAGRACODE, NTB 84-03).

The division is based on morphological criteria:

- a zone with more than 20 joints/m appears in the rock body as a channel,
- areas with less than 2 joints/m appear at first sight as unjointed.

4.5.4.1 Frequency distribution of the 3 jointing categories in the 4 main systems

Using Appendix 13, the following distribution can be made:

- zones with ≥ 20 joints/m are almost entirely restricted to S_1+S_2;
- zones with < 20 joints/m can be divided into 4 main discontinuity systems (S_1+S_2, S_3, K_2, K_3).

4.5.4.2 Determination of true discontinuity spacings

Azimuth/dip-logs and lists of discontinuity systems were drawn up from the values in NAGRADATA and the following parameters were then calculated (Figure 36):

a = thickness of joint zone
b = thickness of interlying "unjointed" zone
c = joint spacing within a (only for zones of 2-20 joints/m).

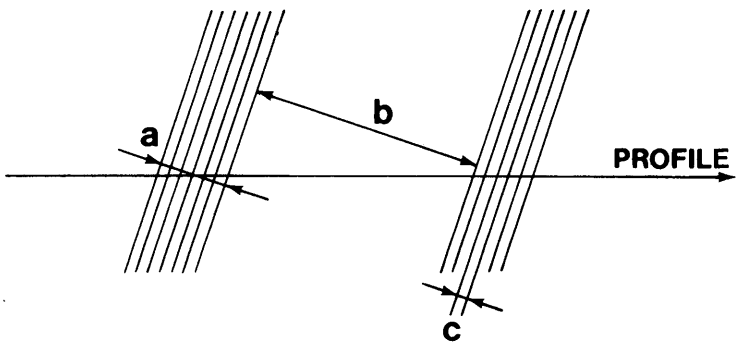

Figure 36: Scheme of calculated discontinuity spacings

The values a and b are presented in Appendix 13 as a histogram in thickness classes of 0.5 m and in Appendix 14 as an empirical distribution function. Appendix 15 shows the frequency of c-values and their dependence on a.

Only those sections of the total profile lengths which could be interpreted without any gaps were evaluated; this led to a decrease of 30% in the profile lengths. The results obtained from 2300 m of profile are still considered to be representative.

The simplest characterisation of the a-, b- and c-values determined for the 4 main discontinuity systems is the central value (median). If necessary, thickness ranges for a and b, which correspond to a specific percentage of the measured values, can be read directly from the summation curves in Appendix 14. The following values characterise the different systems:

- **S_1+S_2 zones with ≥ 20 joints/m**

  Medians: a = 2.5 m
  b = 10 m

  The values for b are 2.5-4 times greater than for a.

- **S_1+S_2 zones with 2-20 joints/m**

  Medians: a = 2.5 m
  b = 4.0 m
  c = 0.16 m

  The a-values are in the same range as for zones with ≥ 20 joints/m. The b-values are up to 3 m greater than a and are thus very similar to a.

- **Zones with 2-20 joints/m in:**

		S_3	K_2	K_3
Medians:	a =	1.8	1.2	1.0 (m)
	b =	12.0	9.5	13.9 (m)
	c =	0.10	0.2	0.26 (m)

It is typical for all three systems that more than 60% of the a-values are less than 2.0 m and the b-values are significantly more than a.

There is no apparent link between a and c in any of the 4 discontinuity systems (see Appendix 15). At the most, for S_1+S_2 and K_3, areas within which 90% of the data lie could be defined mathematically.

Table 17 gives the results for the discontinuity spacings and compares them with the extents.

System	Azimuth/angle of dip, range of variation	Weighted mean value	CODE	Discontinuity spacings Limit [m]	Median [m] a	b	c	Estimated distribution (%) Extent 2.5m	10m	25m	
S_1+S_2	135-171 /63-88	155/70	ZOSG	0.05	2.5	10.0	-				12
	325-342 /85-90		KLPA		2.5	4.0	0.16	<1	3	15	20
			KLUF	0.5	-	-	-		2	3	8
S_3	172-198 /70-90	188/81	ZOSG	0.05	-	-	-				<1
			KLPA		1.8	12.0	0.18	1	2		
			KLUF	0.5						1	2
K_2	199-229 /72-90	210/75	ZOSG	0.05	-	-	-				<1
			KLPA		1.2	9.5	0.2		1	4	
			KLUF	0.5					1	2	2
K_3	230-217 /72-90	258/80	ZOSG	0.05	-	-	-		<1		
			KLPA		1.0	13.9	0.26		1	1	2
			KLUF	0.5					1	3	10

Table 17: Characterisation of jointing categories in the 4 main systems. Abbreviations: ZOSG: strongly jointed zone; KLPA: parallel joints; KLUF: single joint (NAGRACODE, NTB 84-03).

Compared with the structural map (Appendix 9), the low proportion of strongly jointed zones with a long extent in the systems K_2 and K_3 is notable. This is caused on the one hand by the profile line and, on the other hand, by the fact that these structures are treated as lamprophyres in the area investigated.

4.5.5 Indications of movement

The recording of structures within a narrow zone along a profile line gives only incidental information on movements in the discontinuity systems. Only a few isolated indications of movement can therefore be obtained from the field observations. These are sketched in Figures 37 and 38 and compiled in Table 18. Apparently movements occurred in different phases and in varying directions along larger fault zones.

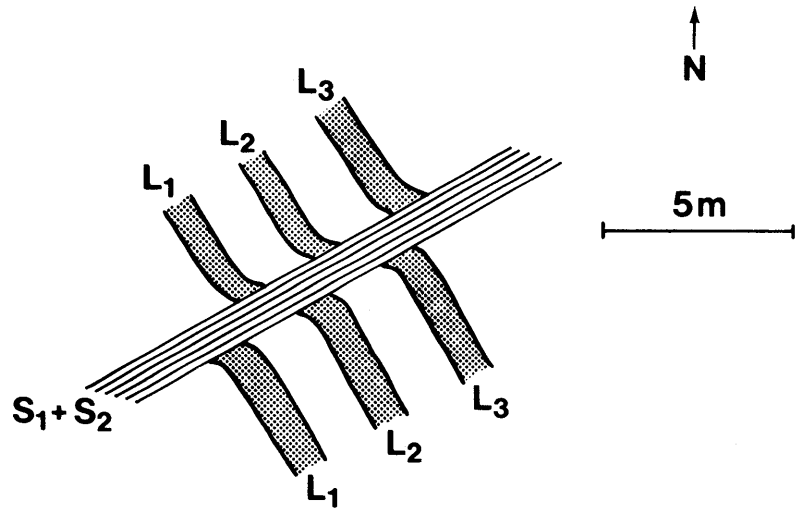

Figure 37: Sketch of an intersection of three lamprophyre dykes with a strongly jointed zone in S_1+S_2. Coordinates: ca. 667,000/159,770 (difficult to access). This phenomenon could only have been caused by multiple opposing shearing movements.

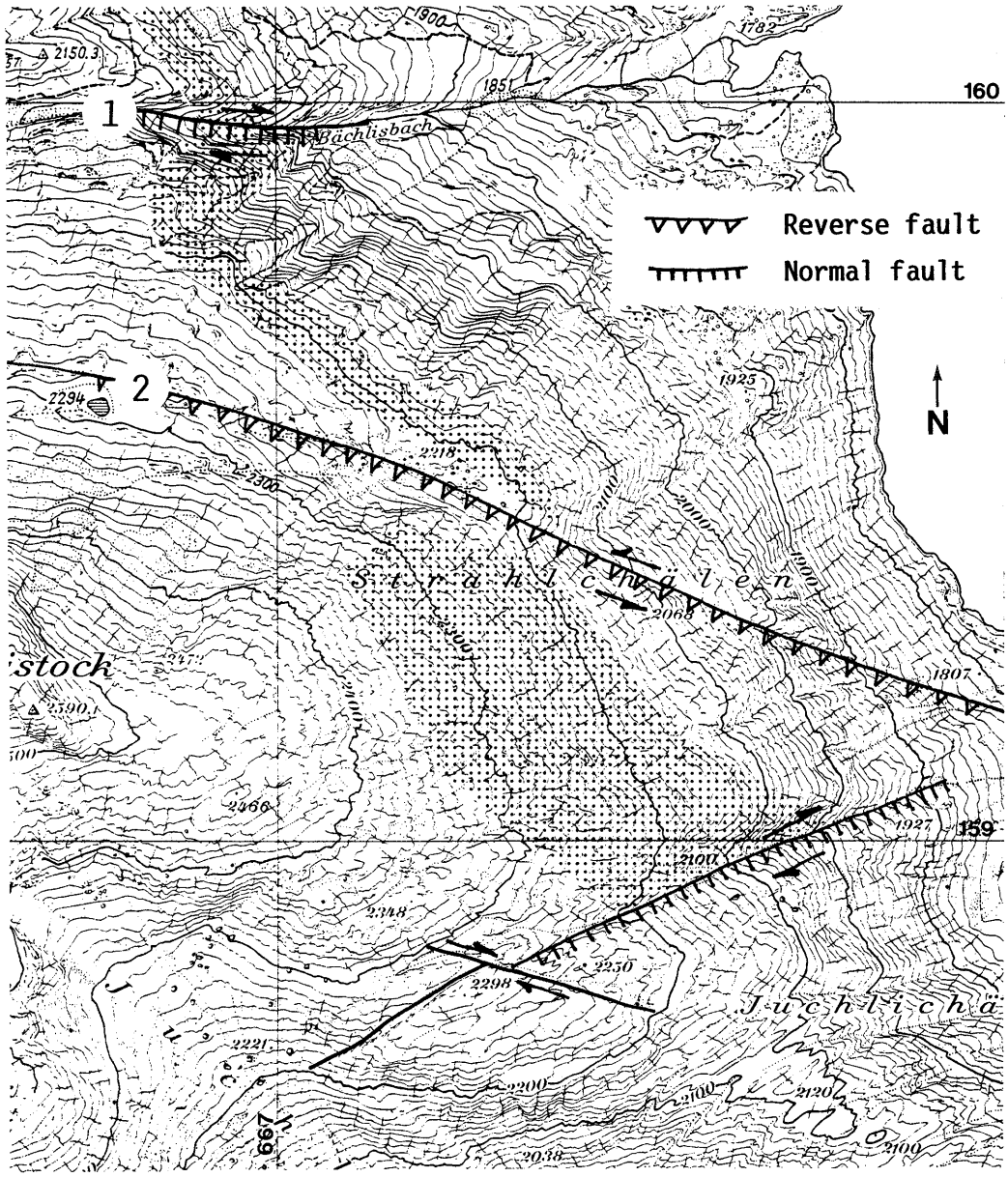

Figure 38: Large-scale delimitation of the lamprophyre-rich area (dotted) by disturbed zones east of the Juchlistock (scale 1:10,000). The movements along fault zones 1 and 2 are interpreted hypothetically on the basis of drag structures observed in the field. Such a phenomenon can be explained only by multiple movements in different directions.

System	Locality	Phenomenon	Interpretation
S_1+S_2	Profile 4, 85 m	displacement in rock texture	sinistral fault
	225 m	displacement in rock texture	dextral fault
	Geisschäle	- lack of lamprophyres	normal fault
	whole profile 6	- dragging of lamprophyres	dextral fault
		- azimuth of lineations: sector SW	sinistral fault
	Figure 41	- displacement of lamprophyres (K_2 or K_3)	reverse fault
		- dragging of lamprophyres	sinistral fault
	Bächlisbach	- displacement of lamprophyres (K_3)	sinistral or normal fault
		- dragging of lamprophyres	dextral fault
K_2	Geisschäle	- displacement of the Geisschäle (S_2) at level 2280	dextral fault
	profiles 6 and 2	- azimuth of lineations	dextral fault
S_3(?)	Strahlchäle	- displacement of lamprophyre-rich rock area	dextral or normal fault
	see Figure 42	- dragging of lamprophyres	sinistral fault
	profile 3, 450 m	- azimuth of feather joints in lamprophyre	sinistral fault

Table 18: Indications of movement along discontinuities

4.6 Structural map of the Juchlistock

4.6.1 General overview of the Juchlistock area

In the Juchlistock area, a rhombic network of 2 main structural directions can be recognised (Figure 39):

- the direction corresponding to the main schistosity, striking around 60° NE (discontinuity system S_1 + S_2) and obliquely angled thereto
- the 60° NW-striking direction of the main jointing (discontinuity system K_2).

Landscape elements in the S_1+S_2 direction from north to south are:

- Bächlisbach
- Brüngrat-Juchlistock
- Geisschälen
- Juchlichälen - central part of Lake Grimsel
- Spittellamm.

These graben and the mountain ridge have a very rugged appearance.

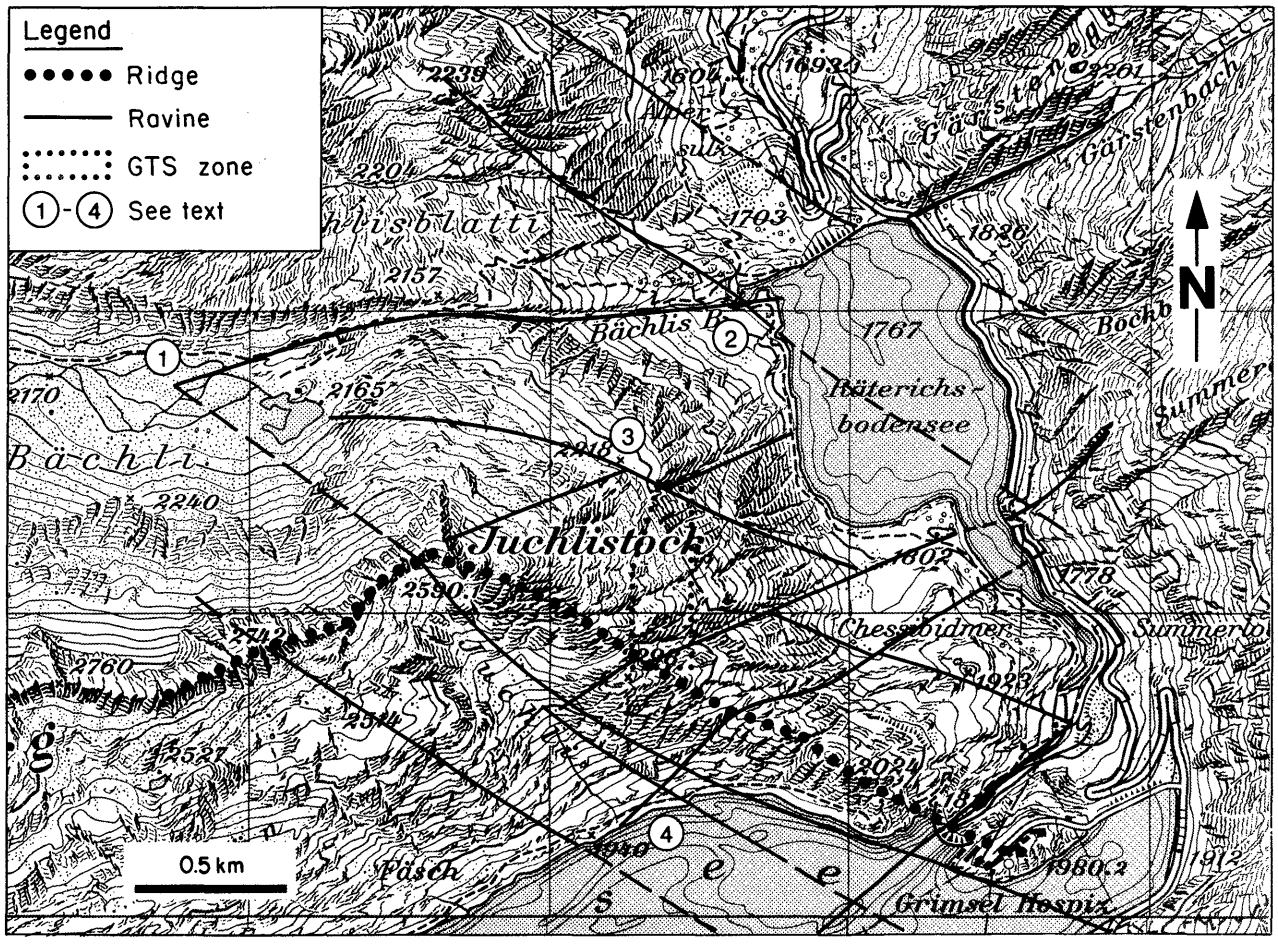

Reproduziert mit Bewilligung des Bundesamtes für Landestopographie vom 11.12.84

Figure 39: Morphologically recognisable main structures in the Juchlistock area.

Landscape elements in the K_2-direction from south-west to north-east are:

- Juchli - Lake Grimsel (- Grimsel pass)
- the ridge from the Juchlistock to the Grimsel hospice
- the Strahlchäle (somewhat oblique)
- Räterichsboden lake - east end of the Bächlisblatti
- Course of the river Aare.

The graben and mountain ridge are - partly due to glaciation - less noticeably eroded.

The GTS lies in a rock body which is clearly penetrated by S_1+S_2 structures and can be defined along intensively fractured zones:

Bächlisbach in the N
Spittellamm in the S
} S_1+S_2 structures

Juchli in the W
Course of river Aare in the E
} K_2 structures

Some areas in which the S_1+S_2 and K_2 structures intersect with one another are particularly marked:

1) the Bächlisboden,
2) the NW corner of the Räterichsboden lake,
3) the snow-field at Pt. 2218 on the Strahlchäle,
4) Lake Grimsel in the section Juchlichälen - Spittellamm/Juchli.

The rock bodies are prismatic and dip steeply to the south, forming a kind of "chimney" with increased jointing. Areas 2) and 3) mentioned above were penetrated by the main access tunnel and have proved to be strongly water-bearing. The immediate vicinity of area 3) is the subject of underground seismic investigations.

Joints running parallel to the valley incisions (valley joints) are interpreted as a syn- to post-glacial "sheeting" effect caused by pressure relief (STALDER 1964).

The transition from Central Aare granite in the N to Grimsel granodiorite in the S of the Juchlistock is recognisable neither in nature nor from aerial photographs as a change in the structure of the rock body. This change occurs smoothly in a transition zone which is some decametres wide and extends, obliquely to the main schistosity, from immediately north of the Juchlistock to the end of the Räterichsboden lake.

Lamprophyres are found frequently in the higher part of the mountain flank between the Juchlistock and the Räterichsboden lake. Their occurrence is restricted to the following areas:

- between Bächlisbach and Strahlchälen in a ca. 100 m - wide strip along level 2200,
- between Strahlchälen and Geisschälen from level 2000 to 2350.

South of the Geisschälen, no more lamprophyres are exposed.

4.6.2 Comments on the structural map

The structural map (Appendix 9) is a compilation of field measurements, tunnel mapping and interpretation of aerial photographs with reference to structures and water conditions in the rock body in the area of the GTS.

Based on the measurement profiles and supplemented partly by isolated measurements, the main surface structures were assigned to the different discontinuity systems. The division of structures outwith the measurement profiles is largely interpretative since it is based on photogeological analyses.

The course of the lamprophyres was first mapped and then completed using aerial photographs. Over wide stretches in the field, it is often only the structure and not the actual dyke rock that is recognisable.

The mapping of surface waters relates to the situation in late summer after so-called complete snow-melt. A significant contribution to the hydrological data was made by the information on water influxes in the main access tunnel and in the laboratory zone (GTS) which indicate areas in the rock which have a significantly higher permeability.

4.7 Comparison of structures observed on the surface and underground

4.7.1 Comments on measurement methods

Acquisition of structural data in surface profiles, on tunnel walls and in drill cores are approaches which investigate a rock body on very different scales and under very different conditions. The possibilities and the best methods for identifying structures differ significantly and the final consistent presentation of the data in NAGRADATA was achieved only by making relevant adaptations of information from three different collections of raw data.

The following paragraphs will comment on the extent to which the results of the three different recording methods can be compared with one another (if at all), how far they complete one another and what information is still required.

4.7.2 Quantities of data

A comparison can be drawn between the number of measured values obtained in the boreholes, the GTS tunnel and on the surface.

The selected structures covered by NAGRADATA are divided as follows:

	Total length (m)	Number of discont. planes	Number of discont./m'
Boreholes	1410	3100	2.2
GTS tunnel	750	500	0.7
Surface profiles	3300	4800	1.5

The relatively low number of measured values from the tunnel measurements can be explained partly by the careful drilling methods employed. In blasted tunnels (e.g. GS- and BK-areas), the number of measurable discontinuities is significantly greater than in comparable stretches which were excavated by tunnelling machine.

4.7.3 Frequency distribution of discontinuity systems

With regard to the location of discontinuities, comparable frequency distributions were obtained from boreholes, tunnels and at the surface. The same four systems dominate everywhere (Table 19):

	S_1+S_2	S_3	$K_2(+L)$	K_1, K_3
Surface	65	5	10	20
GTS tunnel	54	13	17	16 (6/10)
Boreholes	48	16	9	27 (12/15)

Table 19: Frequency distribution for joints within the four main discontinuity systems

The rarer occurrence of S_3-structures at the surface can be explained as follows:

- The S_3-structures are less marked at the surface and therefore more difficult to recognise. The relative absence of S_3 could be a local phenomenon since STECK (1968a) and CHOUKROUNE and GAPAIS (1983) frequently observed S_3-structures.

- The spatial orientation of the GTS tunnel sections could have led to a situation which is more favourable for identifying S_3-structures.

- Thanks to the very efficient logging techniques used on drill cores, the S_3-structures are well-defined, despite the fact that the driling directions often form an acute angle to S_3.

It is worth noting that, from a statistical point of view, a large-scale regional phenomenon can not be identified in any of the three measurement fields. The Grimsel area is characterised mainly by S_1+S_2 and K_2 structures (see chapter 4.6) and it would therefore be expected that K_2 would dominate over K_3.

4.7.4 Mineralisation of joints

The identification of joint coatings allows a more refined and reliable division of the discontinuities into systems. The data from core-logging could not be supplemented by data from tunnel or surface measurements. At the surface, most joint coatings have been removed by weathering.

4.7.5 Discontinuity apertures

It is often difficult to tell from studies of drill-cores whether a fracture in the core is due to a non-cohesive discontinuity in the rock or to the actual drilling process. The surface observations can be of assistance here. The connectivity or intactness of the rock can be seen from the surface and is accentuated by weathering and pressure relief.

The comparison between surface and underground findings will also have to be taken into account when considering the long-term behaviour of the rock body.

4.7.6 Extent of the discontinuities

The surface observations provide a basic framework for determining the extent of discontinuities, the validity of which has still to be verified for laboratory conditions. The interpretation of isolated exposures underground can be improved with the mapping of typical intersection patterns at the surface.

4.7.7 Discontinuity spacings

Discontinuity spacings were calculated from surface profiles (for the whole area) and from selected boreholes (for individual areas of the GTS). The measurements are not yet directly comparable:

- Depending on the tectonic style of the rock, the following values were determined from surface data for the four main systems:
    a) Thicknesses of less jointed zones;
    b) Thicknesses of jointed zones;
    c) Discontinuity spacings within jointed zones.

  A jointing pattern can be built up using these values.

- The discontinuity spacings for the different systems were calculated from core-logs. The occurrence of the joints in sets can

be derived from this information. In a further analysis, the values a) to c) above will have to be calculated.

Since the underground data were measured along complete profiles (i.e. those not obscured by vegetation or detritus), they generally provide more reliable information on the thicknesses of less jointed zones. It is generally assumed that evaluation of surface profiles gives minimum values for these thicknesses.

4.7.8 Movements

Evidence of movements along discontinuities is found fairly frequently. However, movement directions are difficult to define and the opportunities for determining the amount of displacement are rare. Either no age sequence at all, or often only one which is contradictory, is all that can be recognised from many joint intersections.

Surface measurements provide statistically proven movement directions only for the Geisschäle (an S_2-fracture zone). At other locations, evidence of multi-phase movements in different directions can be found.

Appropriate tunnel mapping underground should provide more information on movements than that which could be derived from the drillcores.

4.8 Preliminary approaches to modelling the Juchlistock

With regard to modelling the structures in the vicinity of the GTS, approaches exist in three different dimensions.

In the Grimsel area there is a **regional** structural pattern which outlines the Juchlistock as a unit. In the area of the Juchlistock, a **local** structure pattern can be derived from surface and tunnel measurements, which controls the conditions at the GTS. This in turn forms the framework for a **small-scale** model developed from surface and underground observations, from which the form and volume of an "average" unjointed rock body can be derived.

4.8.1 Large-scale disturbed zones

As already mentioned in Chapter 4.6.1, the Grimsel area is characterised by a network of large-scale structures which generally strike 60° NE and 60° NW. Based on this, the Juchlistock can be defined along four marked lineaments which are characterised morphologically by increased erosion (Figure 39, p. 100); they are as follows:

- Grimsel Lake - course of river Aare and Räterichsboden lake which form the south and east boundaries,

- The Bächlisbach which forms the north boundary,

- The morphologically less clear line Bächlisboden - Juchli - Grimsel lake which forms the west boundary.

Discontinuities in the S_1+S_2 direction dominate in this rock body.

4.8.2 Correlation of structures in the tunnel and at the surface

Strongly jointed zones in the tunnel can be correlated with morphologically marked structures at the surface (see longitudinal profile in Appendix 16). If the longitudinal profile is supplemented by the spatial course of the jointed zones recognisable from the surface, the block diagram in Appendix 17 results. A separation of prisms delimited by K- and S-zones (usually K_2 and S_2) can clearly be seen. The lamprophyres appear as an element running obliquely to this in the laboratory zone. They are generally intersected by S_1+S_2 structures and are dragged along K_2 structures.

The change from Central Aare granite in the north to Grimsel granodiorite in the south is not associated with any noticeable change in the structural pattern. This lithological transition was therefore not taken into consideration in this block diagram.

4.8.3 Discontinuity spacings

When evaluating the surface data, a classification of jointing was suggested which divided the rock into strongly-, slightly- and non-jointed zones. In so far as this division, which is based on surface factors (weathering, erosion) can be applied underground, drill-core and tunnel data are to be analysed accordingly.

With regard to the 4 main discontinuity systems, these data provide information on the thicknesses of the differingly jointed areas and on the frequency of joint intersections.

5 WATER CIRCULATION IN THE GTS

5.1 Circulation pathways of the water in the rock

Direct observation of the circulation pathways of groundwater was possible in the unventilated laboratory tunnel shortly after it had been excavated. The water inflow points were charted systematically (Appendices 3 and 8).

The water flow is concentrated almost exclusively in discontinuities. Table 20 and Figure 40 show the frequency of water flow for the individual discontinuity systems.

Place of observation	Total investigated		Number of discontinuities considered	Number of water-bearing discontinuities		Number of water-bearing discontinuities in S_1, S_2, L	
	Tunnel m'	Surface m^2		Total	per m^2 tunnel wall	Total	Proportion of water-bearing discontinuities
Laboratory tunnel (excavated)	773	8500	320	114 (35%)	0.013	91 (28%)	80%
BK/GS cavern (blasted)	65	820	175	11 (6%)	0.013	8 (4.5%)	73%

Table 20: Water flow from discontinuities in the laboratory tunnel (L = lamprophyre/granite contact).

The systems S_1+S_2 and the lamprophyre/granite contacts clearly dominate. Hardly any water was observed in the tunnel for the discontinuities K_1, K_2 and K_3. In the cavern blasted for the fracture system flow test, there was local water flow in the K_1 discontinuities which are in direct contact here with a close-by S_1+S_2 fracture zone.

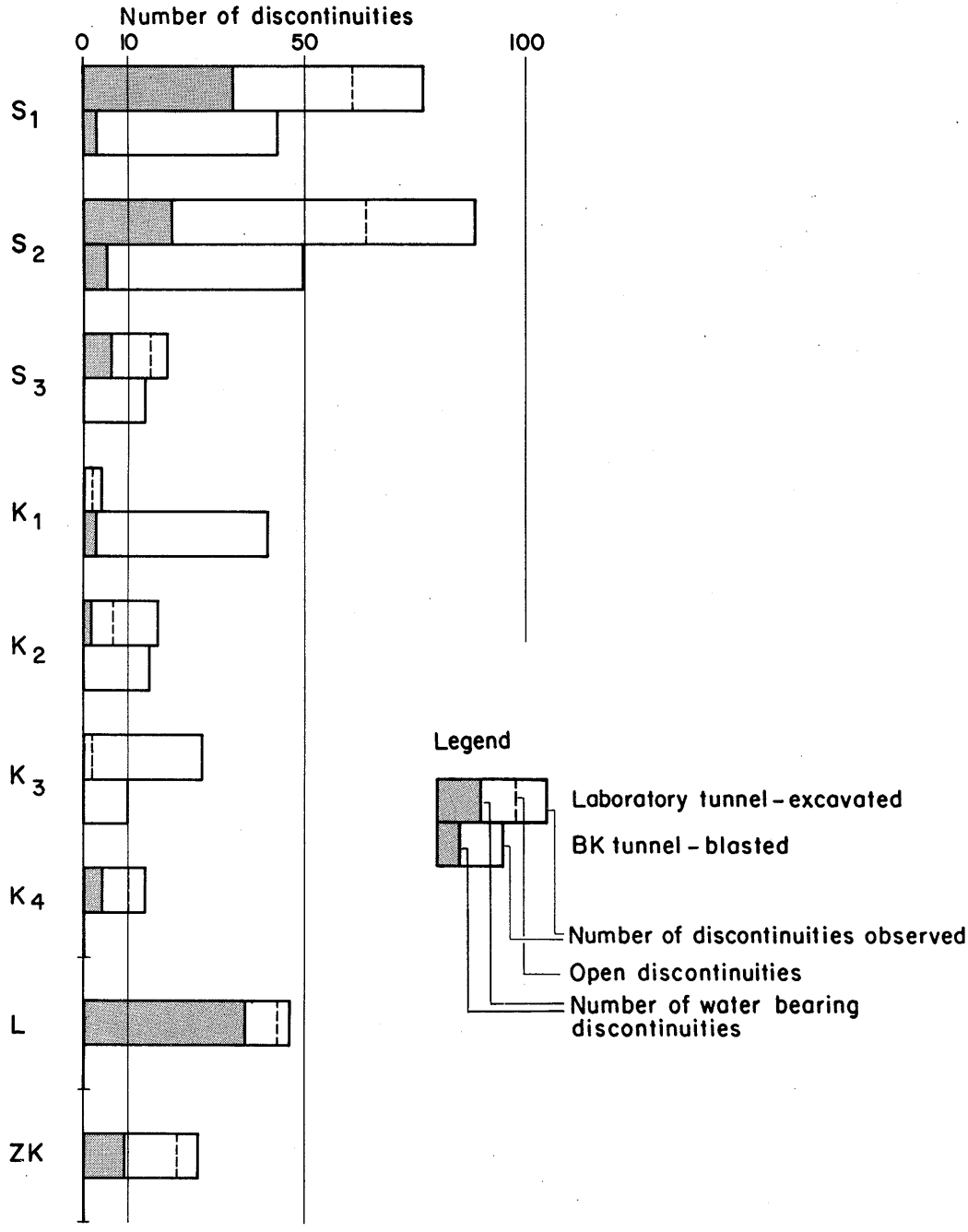

Figure 40: Water flow in the discontinuity systems in the laboratory tunnel.

S_1+S_2 and L form, for the most part, steep fracture zones which penetrate the whole of the Juchlistock massif. At the surface,

these systems often form marked graben and channels (so-called "Chälen", Figure 14B, p. 50) due to the increased incidence of weathering. Snow-melt and rain-water can penetrate into the mountain at these locations or lake-water can infiltrate into the ground below the storage lakes. These systems form the main infiltration pathways for the water into the mountain but this does not mean that only these systems are wet. It must rather be assumed that the whole rock body with all its joint systems is water-bearing. However, many joints appear to be dry because they are closed or healed and their permeability is so low that the wetness is hardly detectable.

It is surprising that the tension joints, which are restricted in extent, are very often water-bearing. There are various reasons for this:

- The tension joints are linked with large porous, hydrothermally leached rock zones and drain these as soon as they are encountered;

- The tension joints can be linked with other more dominant discontinuity systems.

Tension joints often occur in the vicinity of lamprophyre contacts. Since the lamprophyres are preferential water pathways, it is not surprising that the tension joints in their vicinity are very wet.

5.2 Groundwater discharge

The most significant groundwater exfiltration points in the main access tunnel of the KWO and at the GTS were observed systematically over a period of 5 years (1983-1987). The profile in Appendix 16 gives an overview of the measurement locations and the data are presented in Appendices 18 and 19.

5.2.1 Water flow into the main access tunnel

Table 21 gives the results of measurements of water exfiltration.

Groundwater exfiltration (Tm)	Average exfiltration (M) (ℓ/min)	Dev. (S) (ℓ/min)	S in % of M (%)	min. exfiltration measured (ℓ/min)	max. exfiltration measured (ℓ/min)	T (average) (°C)	abs. T Variation (±°C)	Vertical overburden (m)	Type of hydrograph curve
Hauptzugangsstollen									
709	1.46	0.06	5	1.3	1.6	9.1	0.9	250	1
927	0.14	0.01	7	0.1	0.13	10.6	2.3	310	1
1698	1.10	0.03	3	0.98	1.18	9.4	0.8	420	1
1755	1.12	0.06	5	0.9	1.2	9.3	0.6	360	1
1792	0.24	0.01	4	0.2	0.28	8.9	0.6	300	1
1845	0.27	0.02	7	0.2	0.32	8.7	0.9	250	1
1846	0.33	0.04	12	0.25	0.42	8.7	0.8	250	2
2076	6.2	1.1	18	4.2	8.4	7.6	0.8	100	2
2171	0.45	0.05	11	0.35	0.56	7.8	0.6	85	2
2244	1.35	0.20	14	1.1	2.4	7.8	0.7	80	2
2280	1.26	0.16	13	1.1	2.0	7.5	1.0	80	2
2288	2.10	0.19	9	1.7	2.5	7.0	0.8	80	2
2300	0.32	0.09	28	0.23	0.55	7.7	0.6	80	2
2302	0.75	0.14	19	0.4	1.1	7.7	0.6	80	2
2314	0.39	0.29	75	0.03	1.95	7.6	0.6	80	2
Test Site									
A95	0.31					10.9	1.4		
BK left	0.16					11.6	1.5		
BK right	1.07					11.7	0.9		
L217	0.0001					-	-		

Table 21: Statistical evaluation of the groundwater exfiltration and temperatures (measurement period 1983-1987; measurements initially weekly, later monthly).

With regard to quantities of water discharge, two different types of hydrograph curve can be distinguished (Appendix 18):

- **Type 1** is characterised by very small, almost undetectable variations in the measurement error range. The corresponding water exfiltration points lie beneath a large rock overburden of more than 250 m. External influences such as climate or changes in water-level in the lakes do not have any noticeable effect on the water exfiltration.

- **Type 2** shows more or less clear periodical variations. These are manifested as a significant increase in water flow in the second half of the year due to the effects of the snow-melt which begins in June. Most of the groundwater discharge points affected lie within the sphere of influence of Lake Grimsel. A rise in the level of the lake causes an increase in water pressure and leads to increased wetting of the fracture zones which lead into the lake. Both factors could be the reason for the increase in exfiltration in autumn. The water discharge points for type 2 lie beneath an overburden of less than 250 m.

The groundwater temperatures increase considerably with increasing overburden. In the range of influence of Lake Grimsel, they are around 7°C and, in the GTS, around 10°C.

5.2.2 Water discharge in the GTS

When planning the GTS, a "dry" rock zone was consciously selected. The geological profile in Appendix 16 shows clearly that water flow observed at the GTS is generally low. The areas flanking the fracture system flow test, BOSB 80001 and the decompressed zone test/ventilation test are an exception. In these areas, fracture zones with large quantities of water were encountered.

GTS ZONE				Discharge ℓ/min	Specific discharge	
	Borehole	Tunnel	Metres		ℓ/min per m'	per open discontinuity
Fracture system flow		BK		1.4		
	BOSB 80001		0-80	0.03	0.0003	
			80-85	0.07	0.014	0.004
			85-90	0.02	0.0045	0.006
			90-95	1.4	0.28	0.05
			95-100	0.65	0.13	0.04
Heating test	BOSB 80002		3-10	0	0	0
			10-35	0	0	0
			35-36	0.0002	0.00009	0.0002
			36-49	0	0	0
			49-58	0.015	0.0016	0.0009
			58-73	0	0	0
			73-76	0.002	0.001	0.002
			76-95	0.004	0.0002	?
			95-100	0.0006	0.0001	0.00008
	BOSB 80003		5-16	0.001	0.0001	?
			17-36	0.0008	0.00004	?
			37-42	0.005	0.001	0.0003
			43-73	0.0013	0.00004	0.0001
			74-75	0.012	0.012	0.003
			76-93	0.0013	0.00007	?
			94-100	0	0	0
	BOSB 80004		0-100	0.06	0.0006	0.003
Excavation effects		AU		0.25		
Ventilation test	BOSB 80005		0-100			
	Total			0.17	0.0017	0.0017
	BOSB 80006		65-75	0.003		
			75-85	0.0016		
			85-95	0.0003		
			175-185	0.0125		
			185-195	0.023		
	Total		0-195	0.05	0.0003	0.001
	BOSB 83001		30-40	0.0001		
			45-55	0.0005		
			90-100	0.0001		
			130-140	0.45	0.045	0.016
	Total		0-140	0.5	0.0035	0.007
Underground seismics	BOUS 85001		0-150	0.02	0.0001	0.0012
	BOUS 85002		0-150	0.65	0.0043	0.0056
	BOUS 85003		0-150	5.1	0.0340	0.0911

Table 22: Water discharge observed at the GTS. The measurements in the boreholes were carried out in packed-off sections. 0 indicates sporadic, very low and not exactly measurable discharge. The specific discharge per joint was calculated using drill-core logs. In areas marked ?, no open joints were identified.

Table 22 gives the results of discharge measurements. The amounts are:

- 0-12 ml/min • m' borehole (in BOSB 80001 up to 280 ml/min • m')
- 0.1-3 ml/min per open discontinuity (in BOSB 80001 up to 50 ml/min)

5.2.3 Variations in discharge in the GTS

As can be seen from Appendix 19, the discharge from boreholes BOSB 80002, 80003 and 80004 remains constant over long time periods. In contrast to this, in the wet zones at BOSB 80001, 80005, 80006, 83001 and A 96, there is a more or less abrupt drop in the discharge. This drop is caused on the one hand by the drainage effect of excavation work in the immediate vicinity of the boreholes in question (ventilation tunnel at BOSB 80005, 80006 and 83001) and, on the other hand, by direct drainage of the rock body concerned (BOSB 80001 and AU 95). At BOSB 80001, a decrease in the joint apertures as a result of settlement of the rock (due to temporary removal of the hydraulic pressure of over 40 bars) could be a reason for the decrease in discharge.

LITERATURE REFERENCES

ABRECHT, J. and SCHALTEGGER, U. (1988): Aplitic intrusions in the Central Aar massif basement: Geology, petrography and Rb/Sr data. Eclogae geol. Helv. 81, p. 227-239.

BERNOTAT, W.H. and BAMBAUER, H.U. (1982): The Microline/Sanidine transformation isograd in metamorphic regions. SMPM 62, p. 231-244.

BLES, J.L. et FEUGA, B. (1981): La fracturation des roches. Manuels et méthodes N° 1, BRGM, Orléans.

BOWERS, T.S., JACKSON, K.J. and HELGESON, H.C. (1984): Equilibrium Activity Diagrams. Springer-Verlag.

BUSSY, F. (1987): Intéractions physico-chimiques entre le granite du Mont-Blanc et ses enclaves. SMPM 67, p. 380-384.

CHOUKROUNE, P. and GAPAIS, D. (1983): Strain pattern in the Aar Granite (Central Alps): orthogneiss developed by bulk inhomogeneous flattening. J. Struct. Geol. 5, p. 411-418.

DE LA ROCHE, H., LETERRIER, J., GRANDCLAUDE, P. and MARCHAL, M. (1980): A classification of volcanic and plutonic rocks using R1-R2 diagram and major element analysis: its relations with current nomenclature. Chem. Geol. 29, p. 183-210.

DEMPSTER, T.J. (1986): Isotope systematics in minerals: biotite rejuvenation and exchange during Alpine metamorphism. EPSL 78, p. 355-367.

DESCOEUDRES, F. und EGGER, P. (1981): Sondierbohrungen Juchlistock-Grimsel: Felsmechanische Laboruntersuchungen. Unpubl. NAGRA-interner Bericht.

ETHERIDGE, M.A. (1983): Differential stress magnitudes during regional deformation and metamorphism. Upper bound imposed by tensile fracturing. Geology 11, p. 231-234.

FREY, M., JÄGER, E. und NIGGLI, E. (1976): Gesteinsmetamorphose im Bereich der Geotraverse Basel-Chiasso. SMPM 56, p. 649-659.

FREY, M., BUCHER, K., FRANK, E. and MULLIS, J. (1980): Alpine metamorphism along the geotraverse Basel-Chiasso - a review. Eclogae geol. Helv. 73, p. 527-546.

GRESENS, R.L. (1967): Composition-volume relationships of metasomatism. Chem. Geol. 2, p. 47-65.

GUBLER, E. (1976): Beitrag des Landesnivellements zur Bestimmung vertikaler Krustenbewegungen in der Gotthard-Region. SMPM 56, p. 675-678.

HANCOCK, P.L. (1985): Brittle microtectonics: principles and practice. J. Struct. Geol. 7, p. 437-457

HANCOCK, P.L. (1987): Premises and procedures in brittle tectonics. Acta Naturalia de l'"Ateneo Parmense", 23, p. 135-138.

HEITZMANN, P. (1985): Kakirite, Kataklasite, Mylonite - Zur Nomenklatur der Metamorphite mit Verformungsgefügen. Eclogae geol. Helv. 78, p. 273-286.

HOERNES, S. and FRIEDRICHSEN, H. (1980): Oxygen and Hydrogen isotopic composition of Alpine and pre-Alpine minerals of the Swiss Central Alps. Contrib. Mineral. Petrol. 72, p. 19-32.

HÜGI, TH. (1956): Vergleichende petrologische und geochemische Untersuchungen an Graniten des Aarmassivs. Beitr. zur geol. Karte der Schweiz, N.F. 49.

HÜGI, TH. (1967): Geologischer Führer der Schweiz. Wepf, Basel.

KAMMER, A. (1985): Bau und Strukturen des nördlichen Aarmassivs und seiner Sedimente. Unpubl. Diss., 1. Teil, Univ. Neuchâtel.

KEUSEN, H.R. und WEIDMANN, U. (1986): Das NAGRA-Felslabor Grimsel. SMPM 66, p. 492-502.

KEUSEN, H.R. und SCHULER, P. (1987): FLG-Rohdatenbericht. Unpubl. NAGRA-interner Bericht.

KRAUSSE, H.F., PILGER, A., REIMER, V. und SCHÖNFELD, M. (1978): Bruchhafte Verformung. Clausthaler tektonische Hefte 16.

LABHART, T.P. (1977): Aarmassiv und Gotthardmassiv. Sammlung geologischer Führer, Band 63.

MARQUER, D., GAPAIS, D. et CAPDEVILA, R. (1985): Comportement chimique et orthogneissification d'une granodiorite en faciès schistes verts (Massif de l'Aar, Alpes Centrales). Bull. Minéral. 108, p. 209-221.

MEYER, J. (1988): Petrographic and mineralogical characterization of the fault zones AU 96 m and AU 126 m at FLG. Unpubl. NAGRA-interner Bericht.

MILNES, A.G. and PFIFFNER, O.A. (1977): Structural development of the Infra-helvetic complex, eastern Switzerland. Eclogae geol. Helv. 70, p. 83-95.

MILNES, A.G. and PFIFFNER, O.A. (1980): Tectonic evolution of the Central Alps in the cross section St.Gallen-Como. Eclogae geol. Helv. 73, p. 619-633.

NTB 81-07 (1981): Sondierbohrungen Juchlistock-Grimsel. NAGRA, Baden.

NTB 84-03 (1984): NAGRADATA: Benützerhandbuch Band 1. NAGRA, Baden.

NTB 84-30 (1984): Das Kristallin des Südschwarzwaldes. NAGRA, Baden.

NTB 85-34 (1985): Felslabor Grimsel: Rahmenprogramm und Statusbericht. NAGRA, Baden.

NTB 85-47 (1985): Felslabor Grimsel: Übersicht und Untersuchungsprogramme. NAGRA, Baden.

PAHL, A., BRÄUER, V. HEUSERMANN, ST. KILGER, B. und LIEDTKE, L. (1986): Results of engineering geological research in granite. 5th Int. Congr. of the IAEG, Oct. 20-25, Buenos Aires.

PASTEELS, P. (1964): Mesures d'âges sur les zircons de quelques roches des Alpes. SMPM 44, p. 519-543.

POTY, B.P, STALDER, H.A. and WEISBROD, A.M. (1974): Fluid inclusion studies in quartz from fissures from Western and Central Alps. SMPM 54, p. 717-752.

PRICE, N.J. (1966): Fault and joint development in brittle and semi-brittle rock. Pergamon Press, London.

RAMSAY, J.G. and HUBER, M.I. (1987): The techniques of modern structural geology. Volume 2: folds and fractures. Academic Press.

RICHTER, R. and HOERNES, S. (1988): The application of the increment method in comparison with experimentally derived and calculated O-isotope fractionations. Chemie der Erde 48, p. 1-18

SCHAER, J.-P. et JEANRICHARD, F. (1974): Mouvements verticaux anciens et actuels dans les Alpes suisses. Eclogae geol. Helv. 67, p. 101-120.

SCHALTEGGER, U. (1987): Geochemie und Rb-Sr-Systematik der Aarmassiv-Granite zwischen Grimsel und Reusstal. SMPM 67, p. 462-466.

SCHENKER, F. and ABRECHT, J. (1987): Prä-aargranitische Anatexis, variszische Kontaktmetamorphose und alpidische Regionalmetamorphose im Oberhasli (zentrales Aarmassiv, Schweiz). SMPM 67, p. 13-26.

STRECKEISEN, A. (1976): To each plutonic rock its proper name. Earth-Science Reviews 12, p. 1-33.

STALDER, H. (1964): Petrographische und mineralogische Untersuchungen im Grimselgebiet. SMPM 44, p. 187-398.

STALDER, H.A. (1981): Sondierbohrungen Juchlistock-Grimsel: Mineralogische Untersuchungen. Unpubl. NAGRA-interner Bericht.

STECK, A. (1968a): Die alpidischen Strukturen in den zentralen Aare-Graniten des westlichen Aarmassivs. Eclogae geol. Helv. 61, p. 19-48.

STECK, A. (1968b): Junge Bruchsysteme in den Zentralalpen. Eclogae geol. Helv. 61, p. 387-393.

STECK, A. (1984): Structures de déformations tertiaires dans les Alpes centrales. Eclogae geol. Helv. 77, p. 55-100.

STECK, A., RAMSAY, J.G., MILNES, A.G. et BURRI, M. (1979): Compte rendu de l'excursion de la Société Géologique Suisse et la Société Suisse de Minéralogie et Pétrographie en Valais et en Italie nord du 2 au 5 octobre 1978. Eclogae geol. Helv. 72, p. 287-311.

STRECKEISEN, A. (1981): Provisional remarks on chemical classifications. IUGS Subc. igneous rocks, circ. 34, contr. 90.

VOLL, G. (1976): Recrystallization of quartz, biotite and feldspars from Erstfeld to the Leventina Nappe, Swiss Alps, and its geological significance. SMPM 56, p. 641-647.

WÜTHRICH, H. (1965): Rb-Sr-Altersbestimmungen am alpin metamorph überprägten Aarmassiv. SMPM 45, p. 875-971.

Petro-Tectonic Sketch-Map of **Aar - and Gotthard Crystalline Complexes** F. Schenker and R. Oberhaensli 1985

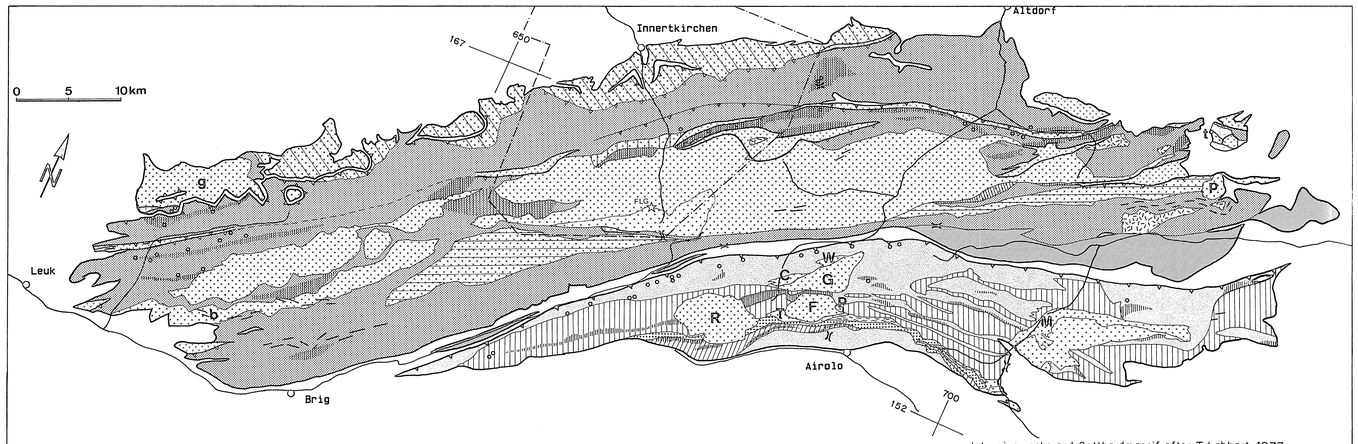

Ausschnitt Beilage 2

AAR CRYSTALLINE COMPLEX

- Southern Aargranites
- Giufsyenite
- Puntegliasgranite
- Grimselgranodiorite
- Baltschiedergranite
- Tödigranite
- Central Aargranites
- Diorites
- Mittagfluhgranite
- Gasterngranite

- Carboniferous metasediments
- Volcanosedimentary sequences*

- Lauterbrunnen - Innertkirchen crystalline complex
- Hercynian basement
- Relicts of Caledonian metamorphic rocks

- Alpidic thrusts
- Hercynian thrusts
- Acid dikes (? subvolcanic)
- Meta-ultramafic rocks

* Stadienobjekt der Autorenteile ergestellte Abgrenzung dieser Gesteine ist provisorisch

GOTTHARD CRYSTALLINE COMPLEX

- Rotondogranite
- Tremolagranite
- Prosagranite
- Fibbiagneiss
- Gamsbodengneiss
- Cacciolagranite
- Winterhornleucogranite
- Crystallinagranodiorite
- Medelsergranite

- Granitoide gneisses
- Scoresciagneiss
- Giubine series
- Prato series
- Hercynian basement
- Relicts of Caledonian metamorphic rocks

TAVETSCH COMPLEX

NAGRA **TECHNICAL REPORT NTB 87-14E**

GEOLOGICAL OVERVIEW MAP
OF THE AAR- AND GOTTHARD-MASSIFS

GRIMSEL TEST SITE | DAT: | **ENCLOSURE 1**

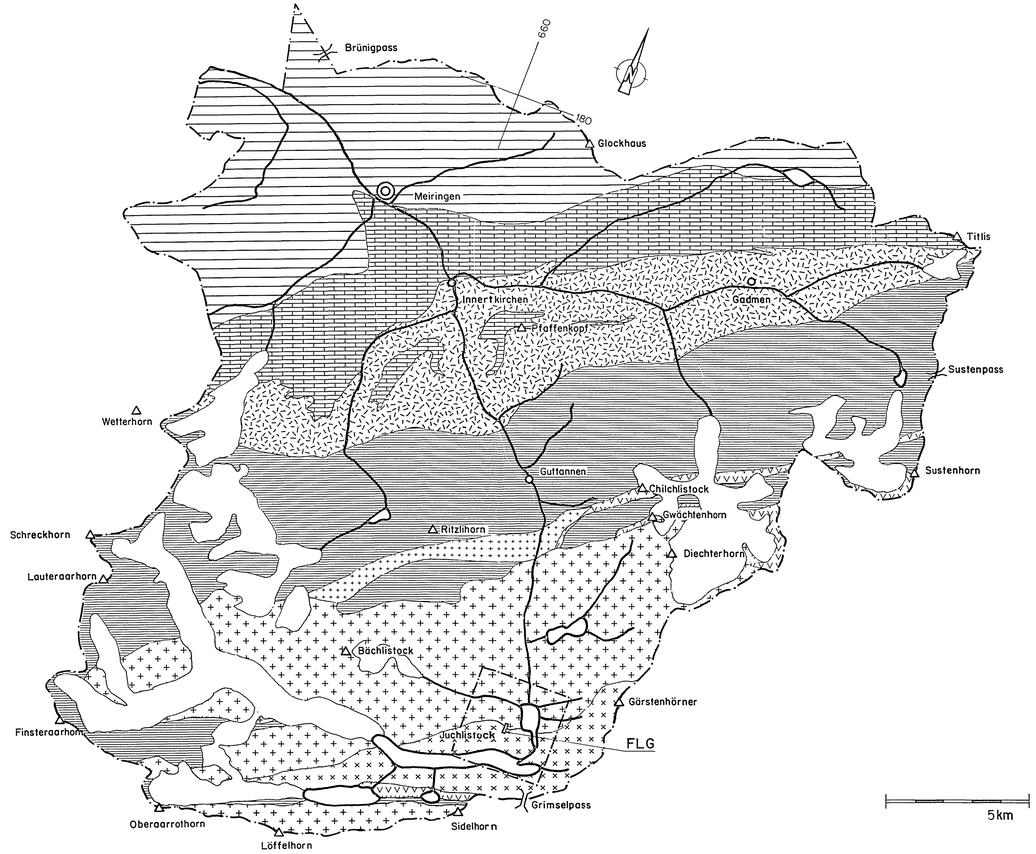

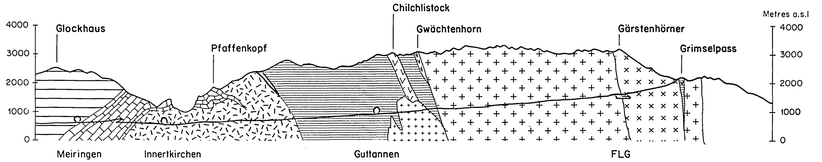

Geological - tectonic profile along the Grimsel Pass 1 : 100'000

Legend :

- Glacier, firn, lakes
- Sediments of the Wildhorn nappe (Jurassic, Cretaceous)
- Autochthonous and parautochthonous sediments (Triassic - Lower Tertiary)
- Innertkirchen crystalline at the contact with the "Altkristallin", partly accompanied by a thin zone of Carboniferous metasediments
- "Altkristallin", mainly light gneisses and dark biotite schists, with occasional amphibolites and lime silicate rocks
- Volcanoclastites (pyroclastites and metasediments), provisional distribution according to F. Schenker and R. Oberhänsli 1985 and F. Schenker (dissertation) 1986
- Mittagfluh granite
- Central and Southern Aare granite
- Grimsel granodiorite

Sources :

Stalder (1979) : Geologie und Mineralogie des Oberhasli
Schweiz. Alpenposten (1961) : Grimselpass
Schenker (1986) : Dissertation Uni Bern

NAGRA	TECHNICAL REPORT NTB 87-14 E
GEOLOGICAL MAP AND PROFILE OF THE HASLITAL	
GRIMSEL TEST SITE	DAT.: ENCLOSURE 2

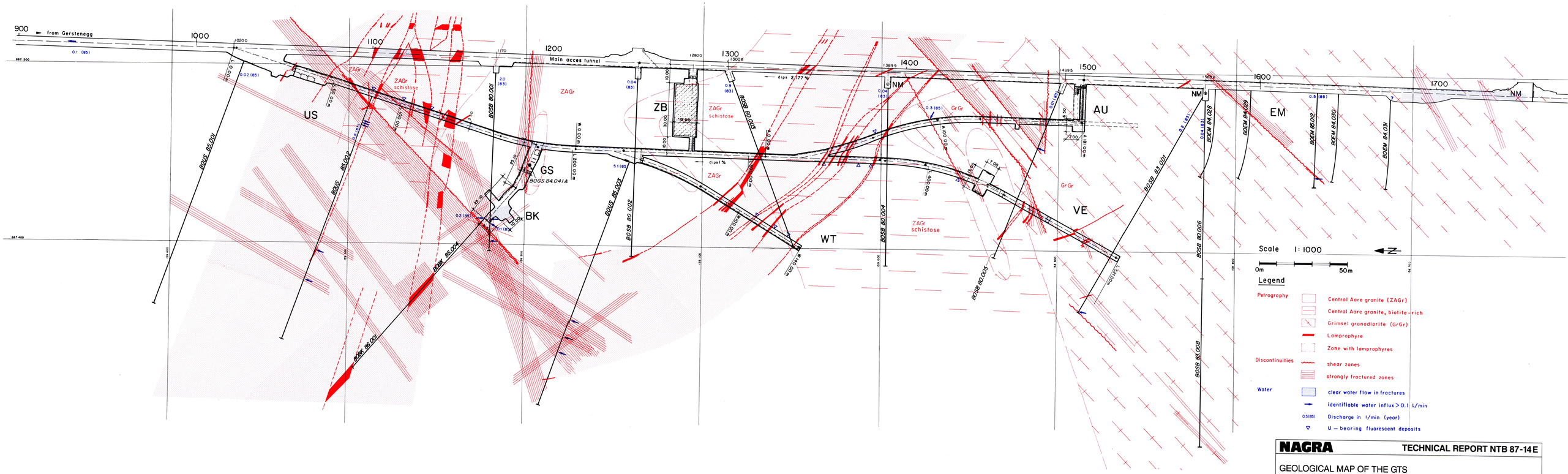

NAGRA TECHNICAL REPORT NTB 87-14 E

GEOLOGICAL MAP OF THE GTS

GRIMSEL TEST SITE | DAT.: | ENCLOSURE 3

	Central Aare granite ZAGr	Grimsel granodiorite GrGr	Aplite	Lamprophyre Kersantite	 Spessartite
Occurence (large-scale)	WSW-ENE-striking granitic body >100 km long and max. 8-10 km wide (550 km^2 surface area): forms core zone of the Aar Massif.	restricted to the Grimsel area, around 20 km long and max. 3 km wide (30-40 km^2 surface area), gradual transition to ZAGr to the S.	widespread dykes cm to dm thick in ZAGr, up to m thick in GrGr.	dykes occurring less frequently in ZAGr than in GrGr	
Macroscopic characteristics	light metagranite, fine- to medium-grained, equigranular to weakly porphyritic, massive to clearly parallel texture; few blocks.	dark metagranite to metagranodiorite, relatively coarse-grained, prophyritic massive or more frequently parallel-textured (augen gneiss type); rich in basic blocks.	light dense fine-grained granitic rock.	dark dense fine-grained rock occurring exclusively as dykes. Kersantite: biotite ≫ hornblende, spessartite: hornblende > biotite; almost exclusively kersantite in the Grimsel rock.	
Mineralogical composition	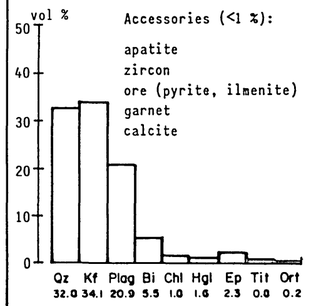 Light components: 88 vol %	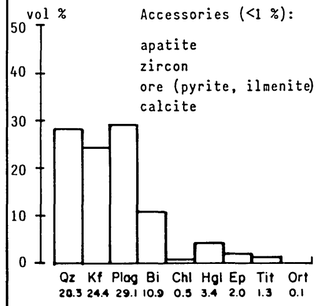 Light components: 82 vol %	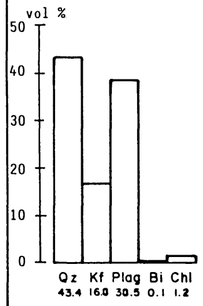 Light components: 99 vol %	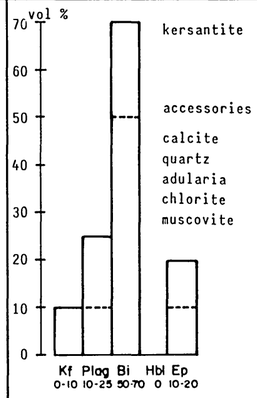 Light components: 10–35 vol %	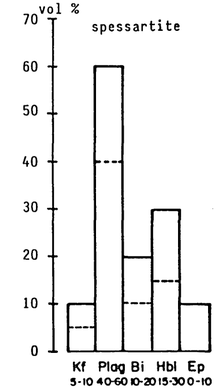 Light components: 45–70 vol %
Microscopic characteristics	Qz : deformed, sometimes largely recrystallised Kf : microcline, partly replaced by muscovite Plag: altered to albite ± epidote ± muscovite Bi : deformed and recrystallised, partly chloritised Chl : alteration product of biotite; fine-grained Chl-aggregates in tension joints and altered adjoining rock Hgl : accumulated on S-surfaces, with Chl and Ep in bands; replaces Kf in strongly deformed rock areas Ep : secondary, mainly an alteration product of Plag				

NAGRA	TECHNICAL REPORT NTB 87-14 E
PETROGRAPHY OF THE ROCKS	
GRIMSEL TEST SITE	DAT.: ENCLOSURE 4

	Central Aare granite					Grimsel-Granodiorite						Aplite	Lamprophyre			Hydrothermally altered granodiorites			
	SB 1 74.98 m	SB 2 14.00 m	SB 2 74.00 m	SB 3 93.00 m	SB 4 72.20 m	SB 5 35.96 m	SB 5 39.20 m	SB 6 48.98 m	SB 6 59.00 m	SB 6 75.97 m	SB 5 39.20 m 1)	SB 3 34.11 m	SB 3 38.02 m 2)	SB 3 71.90 m 3)	SB 4 28.70 m 4)	SB 6 48.98 m 5)	SB 6 49.35 m 6)	SB 6 75.97 m 5)	SB 6 80.15 m 6)
	Wt.%	Wt.%	Wt.%	Wt.%	Wt.%	Wt.%	Wt.%	Wt.%	Wt.%	Wt.%	Wt.%	Wt.%	Wt.%	Wt.%	Wt.%	Wt.%	Wt.%	Wt.%	Wt.%
SiO_2	74.65	69.56	74.67	68.65	71.22	67.95	67.76	69.90	65.35	66.57	66.66	75.84	48.09	51.03	57.08	69.90	64.22	66.57	66.86
TiO_2	0.20	0.41	0.16	0.42	0.41	0.58	0.61	0.44	0.51	0.56	0.47	0.11	1.44	1.22	0.85	0.44	0.65	0.56	0.66
Al_2O_3	13.14	14.72	12.78	15.21	13.88	15.04	15.20	14.48	17.03	16.10	14.73	12.29	16.89	15.43	14.55	14.48	18.28	16.10	16.94
Fe_2O_3 total	1.39	2.98	1.13	2.97	2.60	3.44	3.58	2.71	3.30	3.61	4.10	0.81	9.93	9.12	6.61	2.71	2.22	3.61	1.21
MnO	0.04	0.10	0.04	0.09	0.07	0.07	0.07	0.06	0.08	0.08	0.09	0.02	0.20	0.17	0.14	0.06	0.05	0.08	0.03
MgO	0.24	0.69	0.18	0.69	0.56	1.27	0.54	0.76	0.91	0.88	0.12	0.04	7.85	7.50	5.62	0.76	0.53	0.88	0.25
CaO	1.01	2.08	0.93	1.97	1.84	1.85	1.29	1.71	2.56	2.83	6.99	0.89	6.30	7.49	7.14	1.71	2.59	2.83	2.18
Na_2O	3.88	4.52	3.69	4.59	3.87	4.01	4.57	3.98	4.90	4.84	3.95	3.32	3.74	1.66	2.67	3.98	6.48	4.84	5.57
K_2O	4.70	3.47	4.83	4.03	3.91	4.03	3.77	4.59	3.56	3.35	1.57	5.33	1.45	3.91	2.81	4.59	3.66	3.35	4.21
P_2O_3	0.07	0.13	0.05	0.13	0.12	0.19	0.19	0.14	0.16	0.18	0.15	0.03	0.47	0.37	0.33	0.14	0.18	0.18	0.18
Cr_2O_3	<0.01	<0.01	<0.01	<0.01	<0.01	<0.01	<0.01	<0.01	<0.01	<0.01	<0.01	<0.01	0.04	0.05	0.03	<0.01	<0.01	<0.01	<0.01
NiO	0.01	0.01	0.01	0.01	0.01	0.01	0.01	0.01	0.01	0.01	0.01	0.01	0.02	0.03	0.02	<0.01	<0.01	<0.01	<0.01
Loss of ignition	0.31	0.49	0.38	0.60	0.53	0.81	0.78	0.45	0.84	0.60	0.69	0.24	2.79	1.50	1.72	0.45	0.60	0.60	0.49
ignition	98.92	99.15	98.84	99.35	99.01	99.24	99.36	99.22	99.20	99.60	99.52	98.92	99.21	99.48	99.57	99.22	99.46	99.60	98.58
Volumetric weight [g/cm^3]																2.70	2.36	2.72	2.51

1) Grimsel granodiorite with alteration to epidote
2) Spessartite
3) Kersantite
4) Spessartite/Kersantite
5) unaltered rock
6) altered rock

NAGRA **TECHNICAL REPORT NTB 87-14 E**

GEOCHEMICAL ANALYSES (MAIN ELEMENTS)

GRIMSEL TEST SITE | DAT.: | **ENCLOSURE 5**

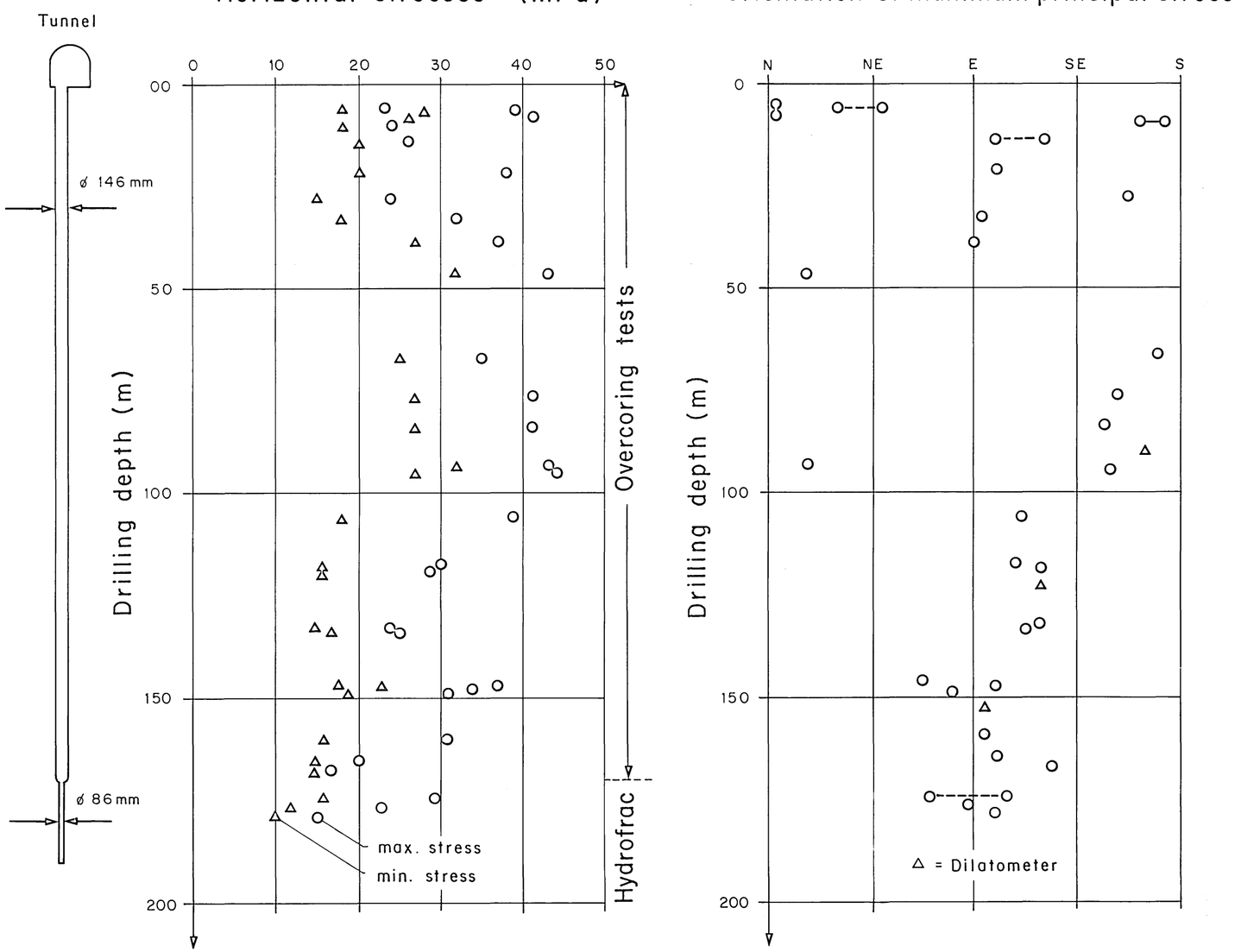

NAGRA	TECHNICAL REPORT NTB 87-14 E
STRESS MEASUREMENTS IN BOREHOLE BOGS 84 041 A (BGR, PAHL et al. 1986)	
GRIMSEL TEST SITE	DAT.: ENCLOSURE 6

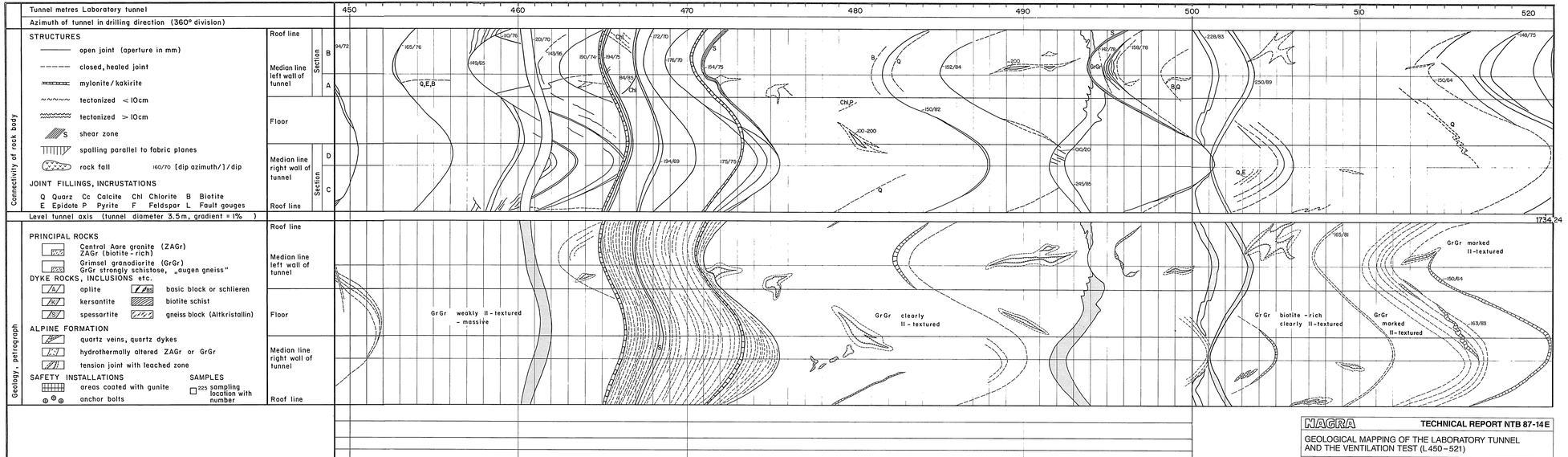

NAGRA	TECHNICAL REPORT NTB 87-14E
GEOLOGICAL MAPPING OF THE LABORATORY TUNNEL AND THE VENTILATION TEST (L 450 – 521)	
GRIMSEL TEST SITE	DAT: ENCLOSURE 7

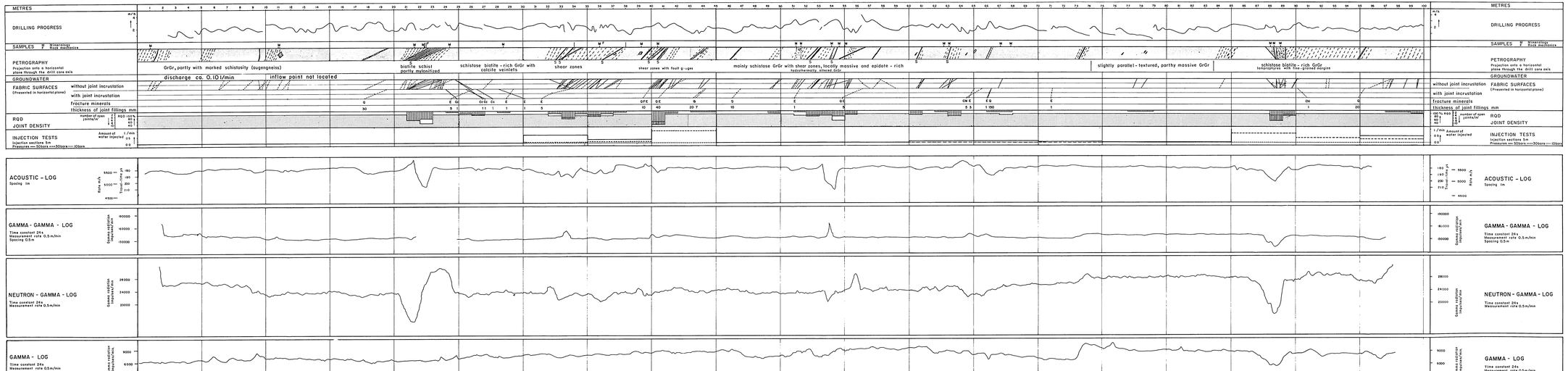

EXPLORATORY BOREHOLE	BOSB 80.005
Coordinates borehole mouth	667'488.86 / 158'900.30
	1738.45 m.a.s.l.
Type of drilling	rotary core drilling
Borehole diameter	86 mm
Drilling direction	291°
Tilt	1°
Drilling period	3.9. - 18.9.1980
Drilling contractors	SIF - Groutbor
Geological mapping	Geotest AG
Borehole logs	Prakla - Seismos GmbH
Log dates	24./26.11. and 2.12.1980

Legend

Principal rocks

- Central Aare granite (ZAGr)
- ZAGr biotite-rich
- Grimsel granodiorite (GrGr)
- strongly schistose GrGr, „augen gneiss"

Dyke rocks, inclusions

- Aplite
- Kersontite
- Lamprophyres (L)
- Spessartite
- Basic blocks or schlieren

Alpine formations

- Quartz veins, dykes
- Hydrothermally altered ZAGr or GrGr
- Alpine tension joint
- Shear zone
- strong jointing

Fabric planes

- open joints with dip direction
- closed joints with dip direction

Fracture fillings

Q	quartz	B	biotite	Ti	sphene
E	epidote	Chl	chlorite		
Cc	calcite	F	feldspar		
P	pyrite	Ms	muscovite	Le	fault gouges

NAGRA **TECHNICAL REPORT NTB 87-14E**

DRILLING PROFILE OF BOREHOLE BOSB 80 005

GRIMSEL TEST SITE | DAT: | **ENCLOSURE 8**

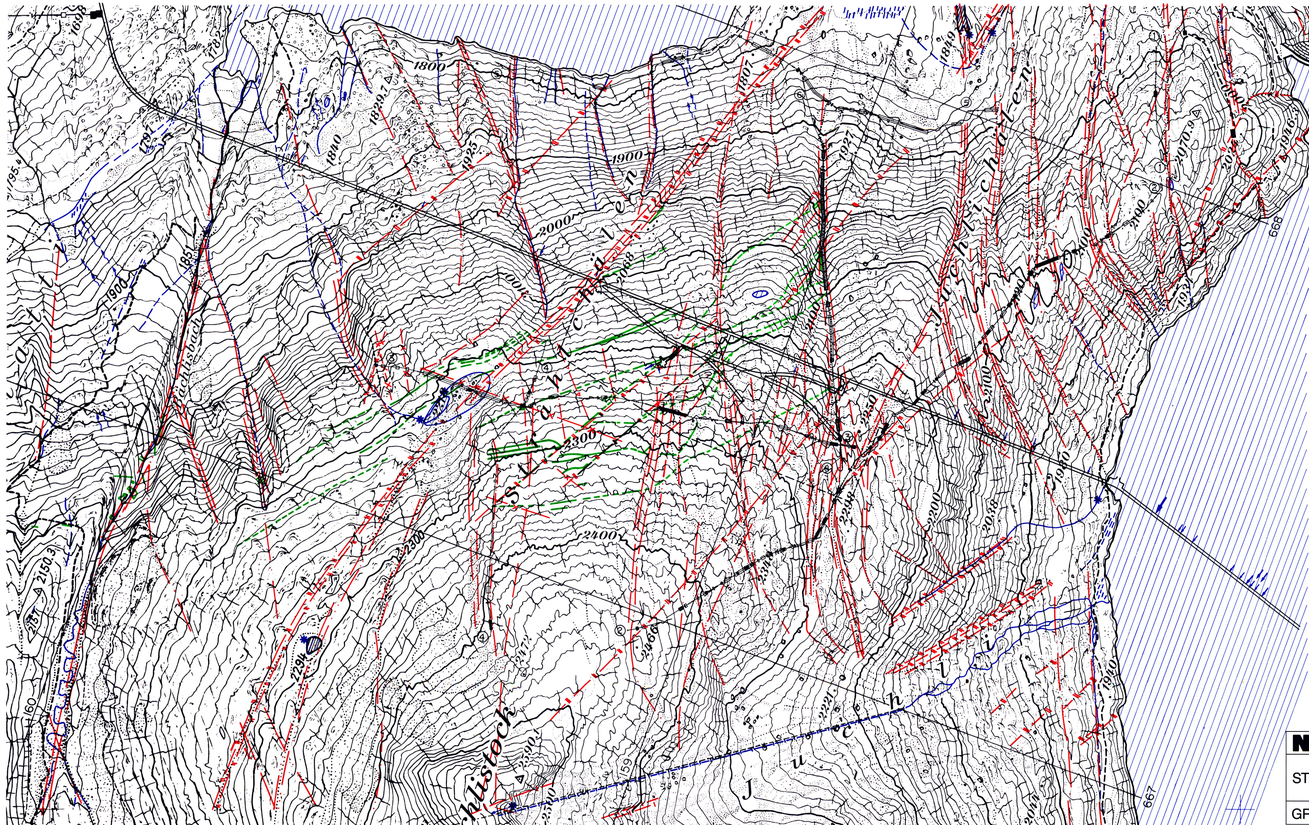

NAGRA	TECHNICAL REPORT NTB 87-14E
STRUCTURAL MAP OF THE JUCHLISTOCK	
GRIMSEL TEST SITE	DAT.: ENCLOSURE 9

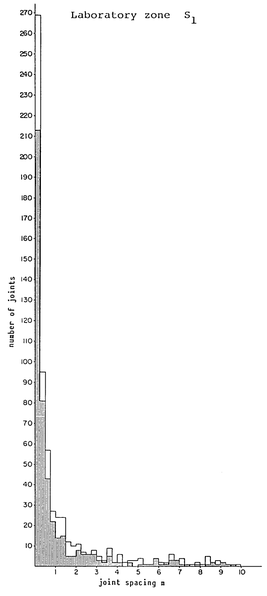

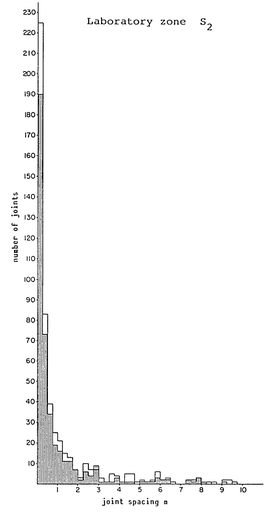

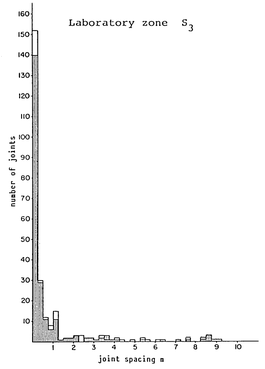

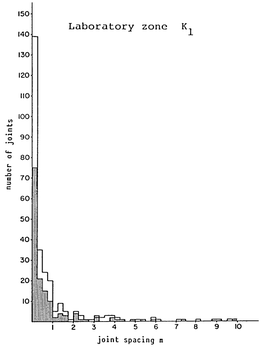

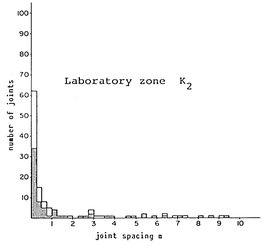

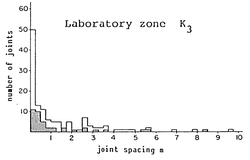

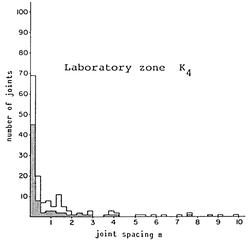

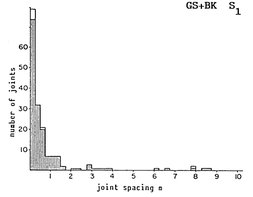

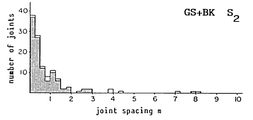

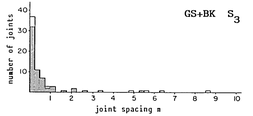

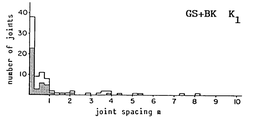

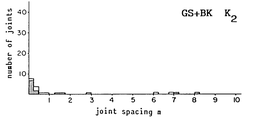

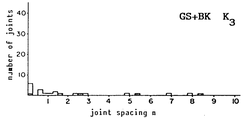

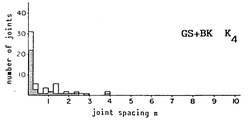

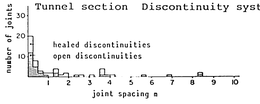

NAGRA	TECHNICAL REPORT NTB 87-14 E
DISCONTINUITY SPACINGS IN THE LABORATORY TUNNEL ZONE AND IN THE GS AND BK AREAS	
GRIMSEL TEST SITE	DAT.: ENCLOSURE 10A

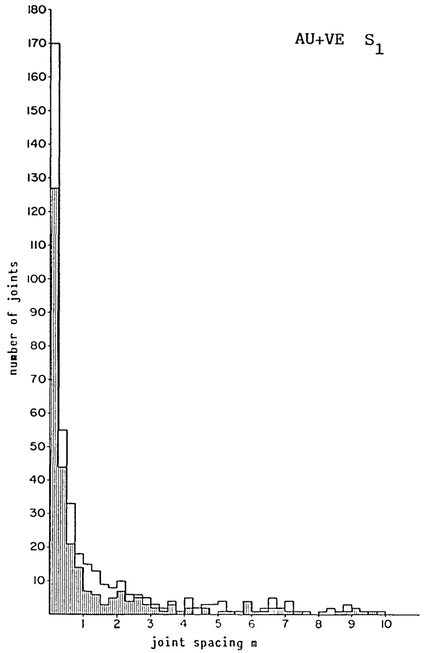

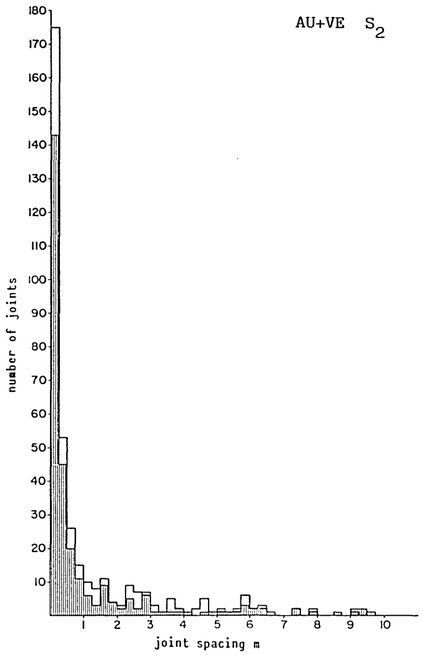

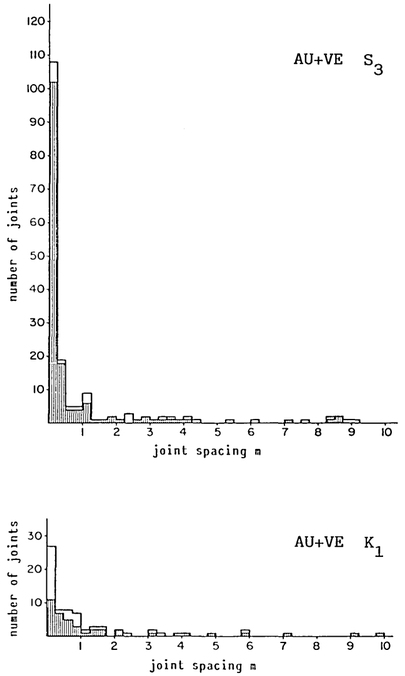

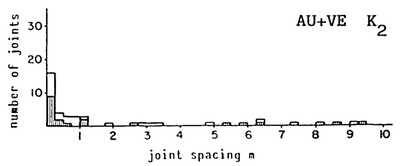

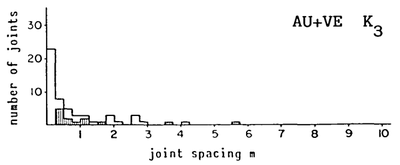

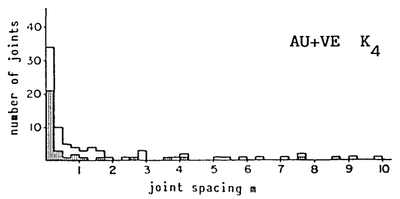

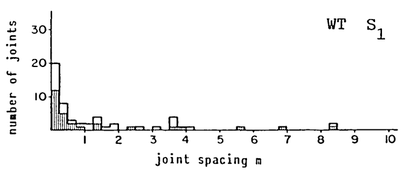

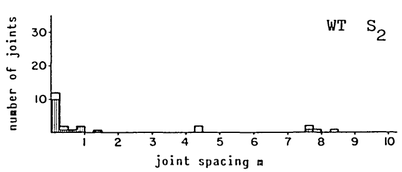

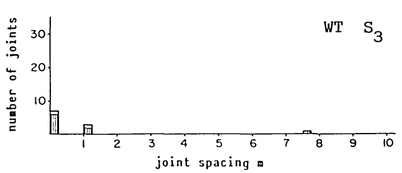

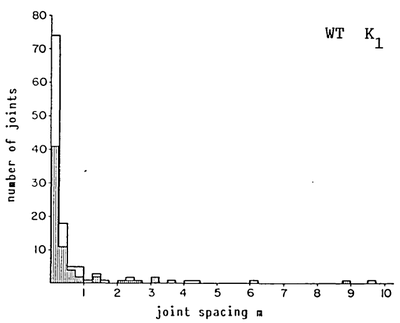

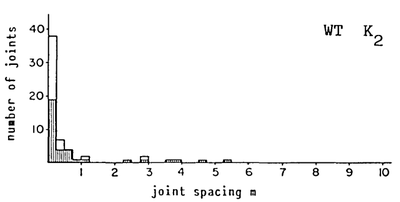

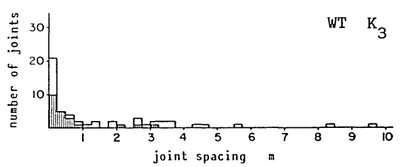

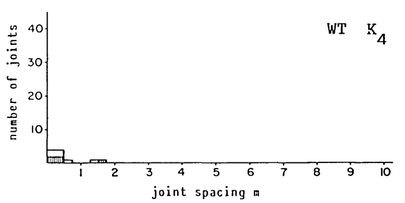

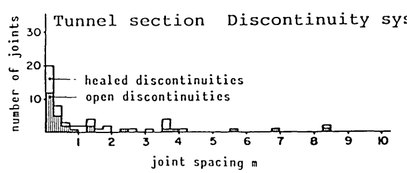

NAGRA	TECHNICAL REPORT NTB 87-14 E	
DISCONTINUITY SPACINGS IN THE AU, VE AND WT AREAS		
GRIMSEL TEST SITE	DAT.:	ENCLOSURE 10B

BOUS 85001

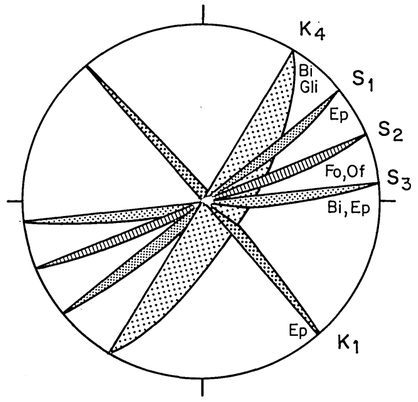

BOSB 80001

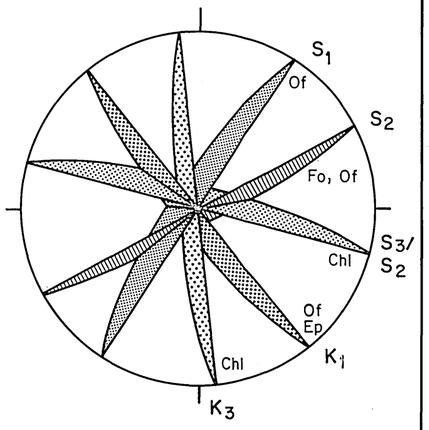

BOUS 85003

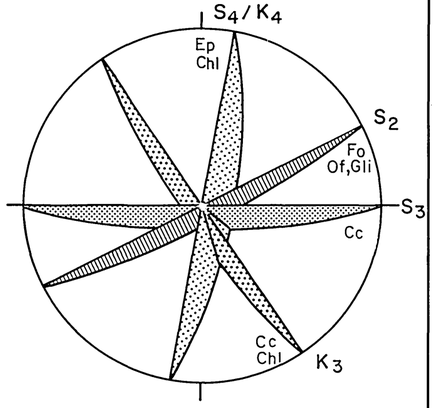

BOSB 80005

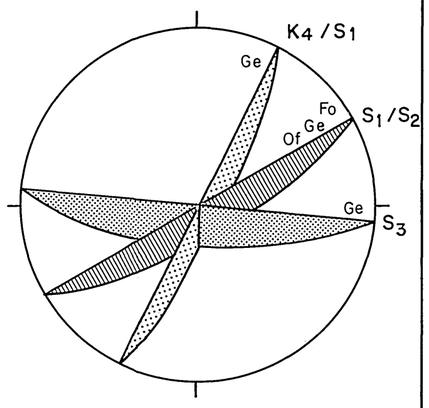

GTS N-ZONE

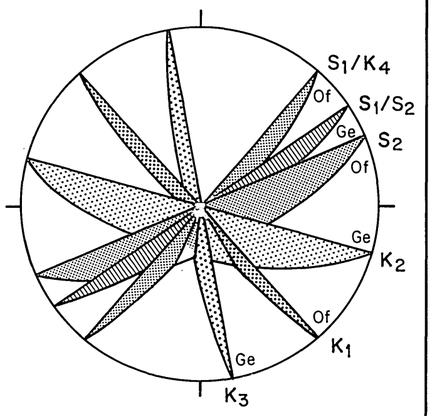

BOUS 85002

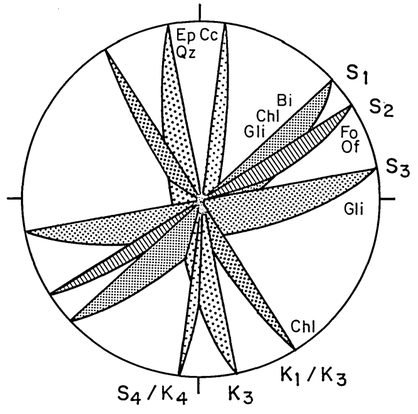

BOGS 84041A

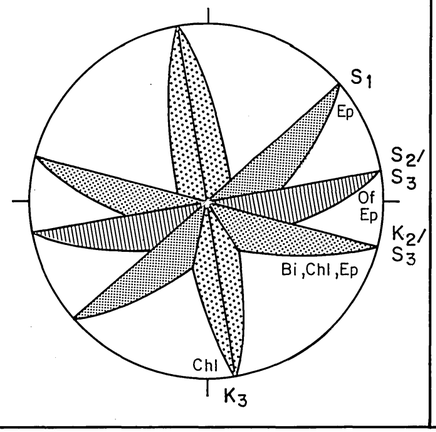

BOSB 80003

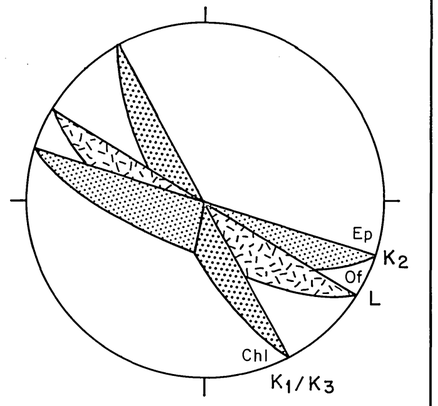

BOSB 80006, 83001, 83008

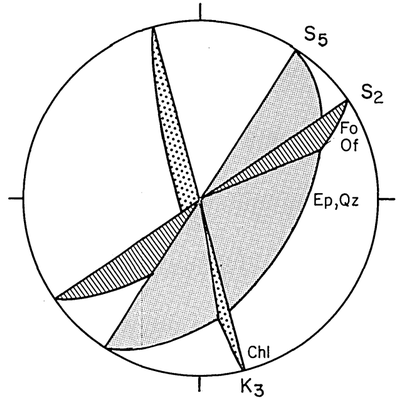

GTS S-ZONE

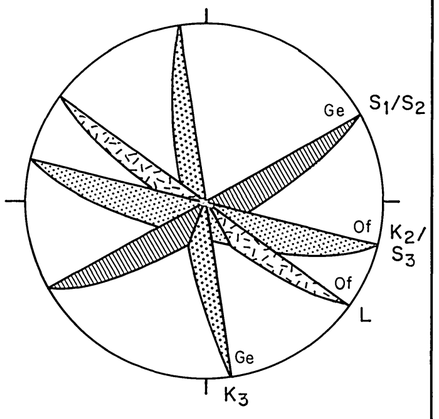

Legend

Bi	only biotite - bearing fractures	Ge	closed fractures
Cc	calcite - bearing fractures	Gli	mica - bearing fractures
Chl	only chlorite - bearing fractures	Of	open fractures
Ep	epidote - bearing fractures	Qz	only quartz - bearing fractures
Fo	foliation		

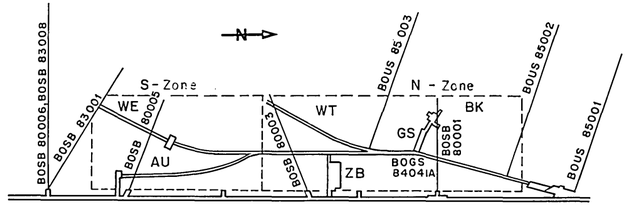

NAGRA **TECHNICAL REPORT NTB 87-14E**

DOMINANT DISCONTINUITY SYSTEMS
IN THE DIFFERENT GTS AREAS

GRIMSEL TEST SITE | DAT.: | **ENCLOSURE 11**

Extent of fracture

25 m

10 m

2.5 m

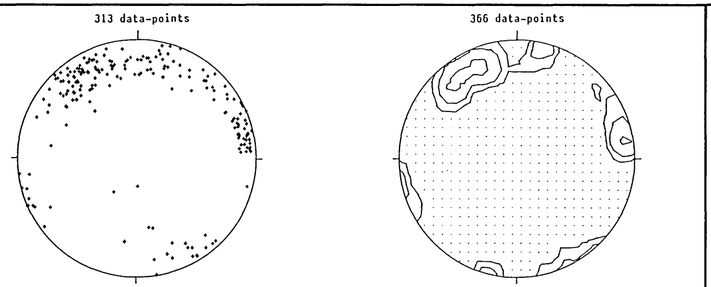

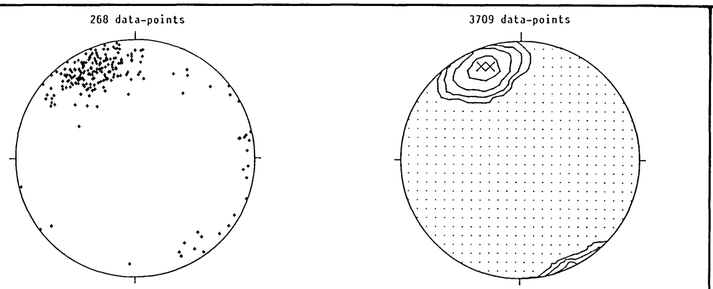

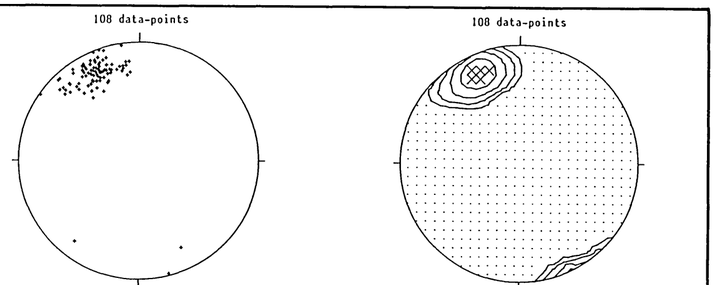

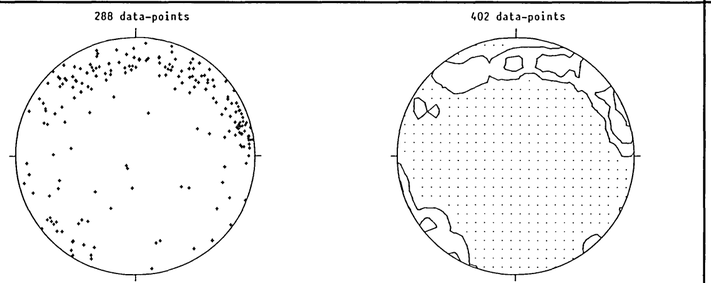

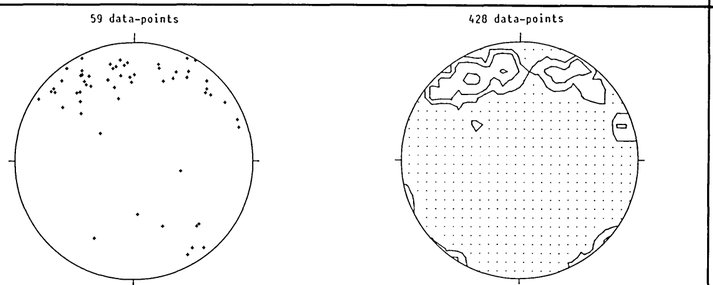

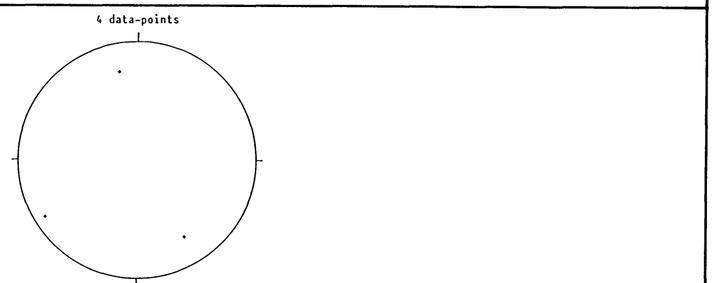

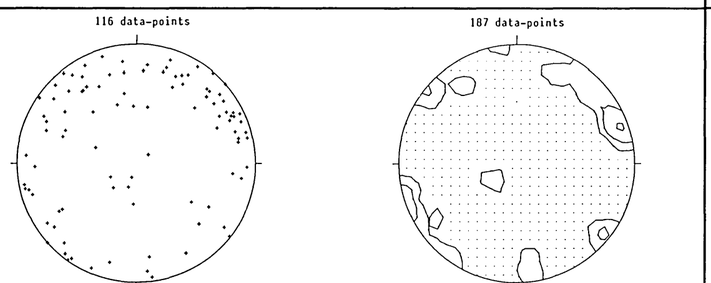

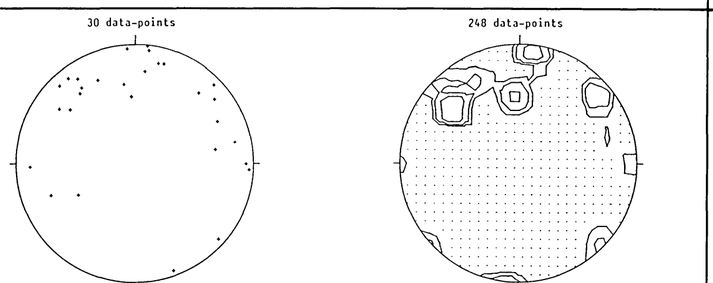

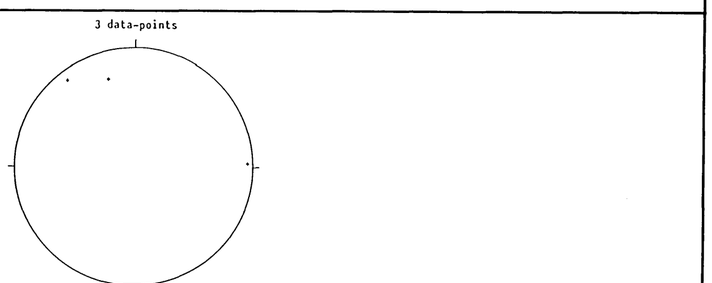

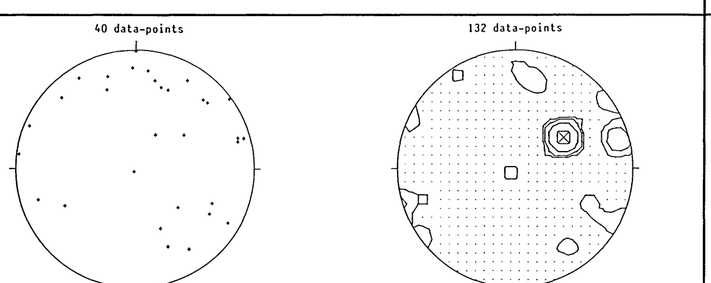

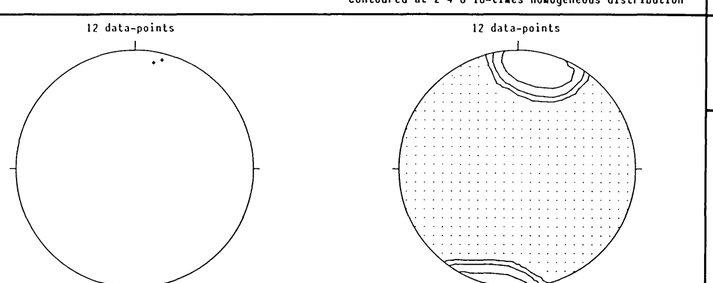

< 0.05 m

Discontinuity spacing > 0·5 m

0.5 – 0.05 m

NAGRA **TECHNICAL REPORT NTB 87-14E**

POLE DIAGRAMS OF SURFACE STRUCTURES DIVIDED ACCORDING TO DISCONTINUITY SPACING AND EXTENT

GRIMSEL TEST SITE | DAT.: | **ENCLOSURE** 12

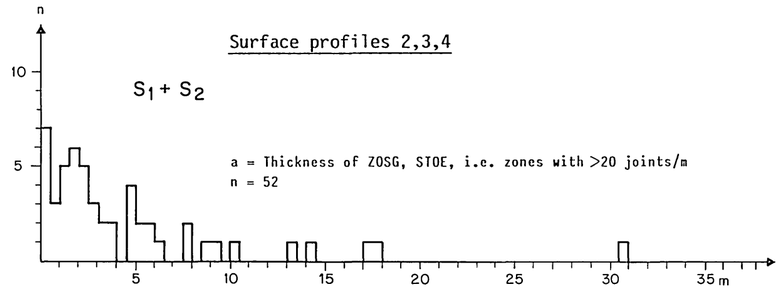

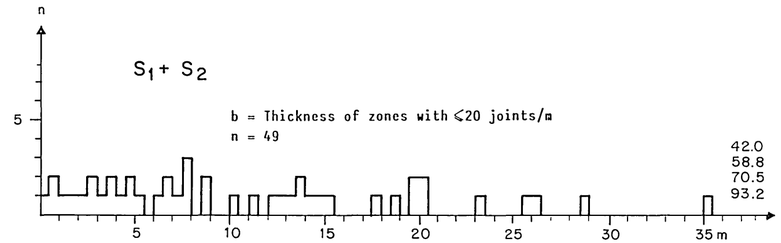

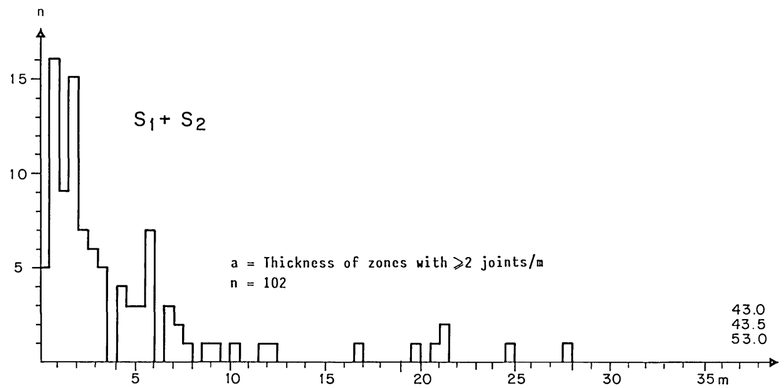

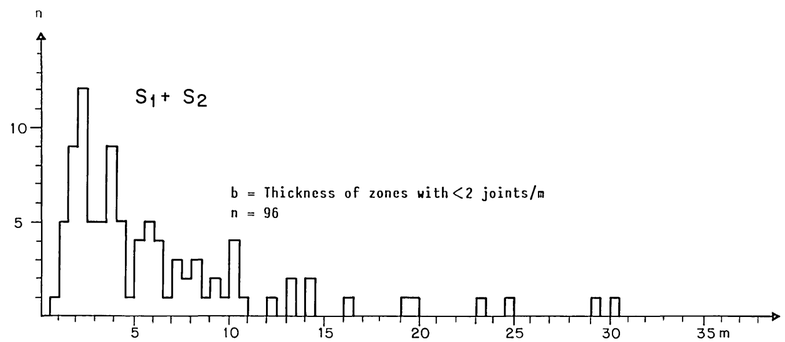

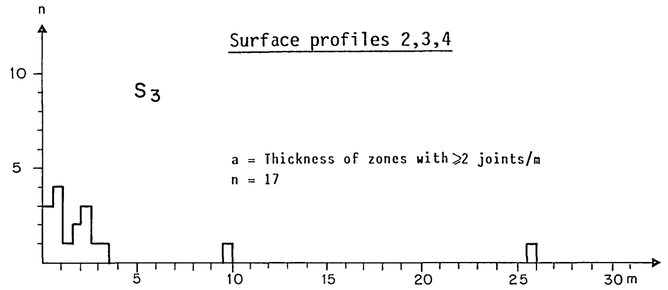

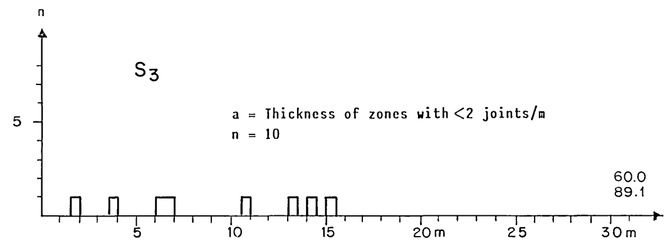

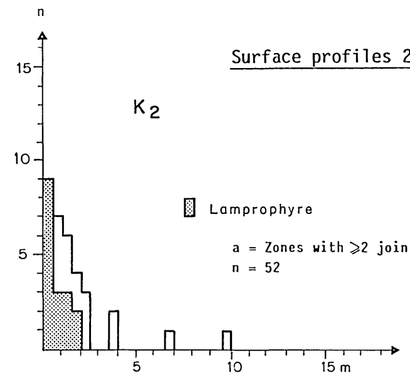

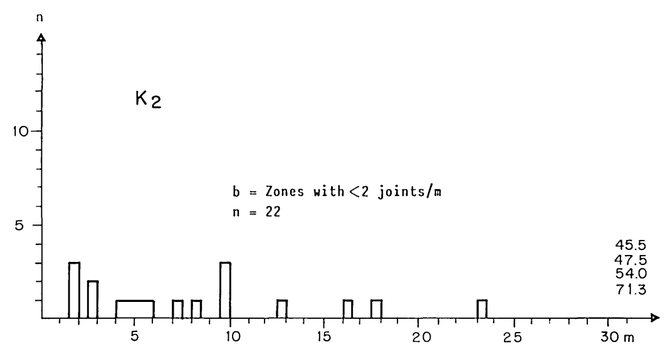

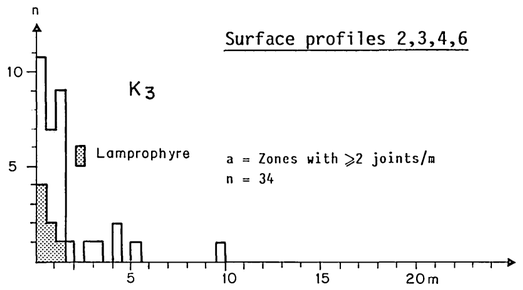

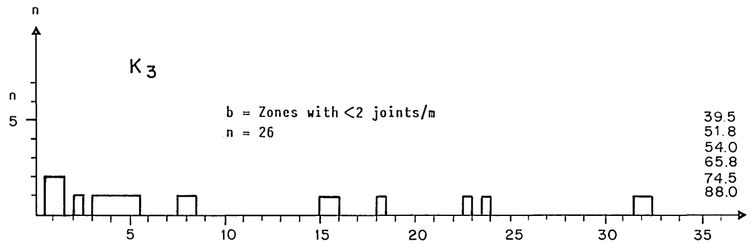

Legend

ZOSG	Strongly jointed zone
STOE	Disturbed zone

NAGRA **TECHNICAL REPORT NTB 87-14 E**

DISCONTINUITY SPACINGS:
HISTOGRAMS OF THE THICKNESSES OF FRACTURED AND UNFRACTURED ZONES

GRIMSEL TEST SITE | DAT.: | **ENCLOSURE 13**

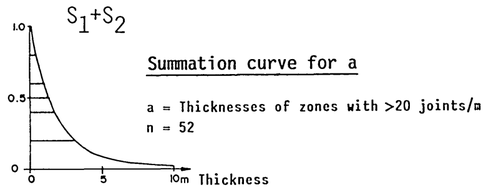

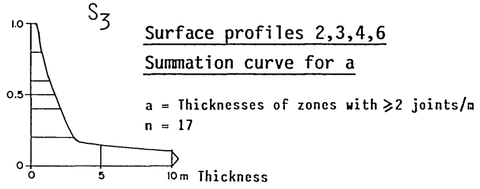

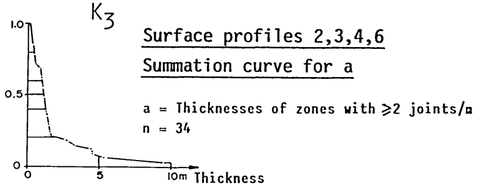

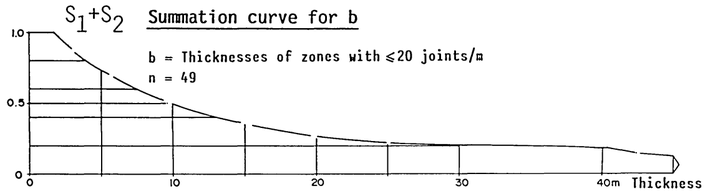

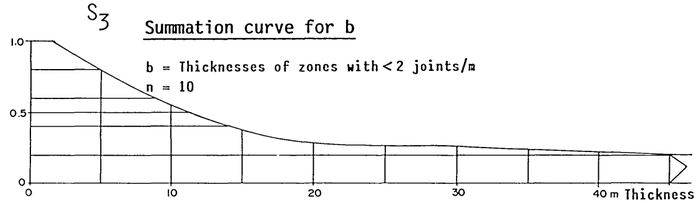

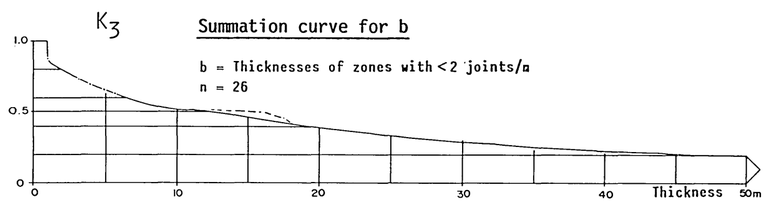

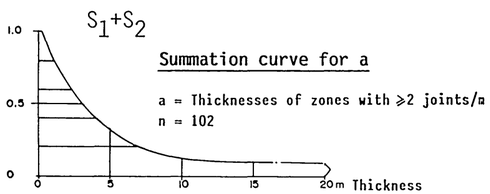

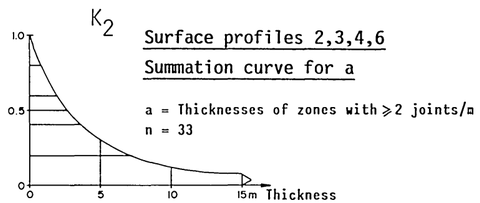

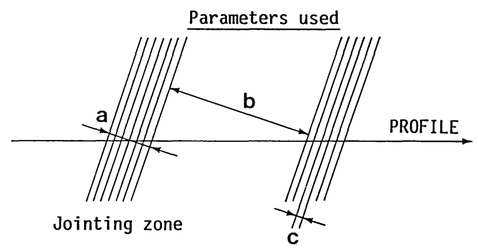

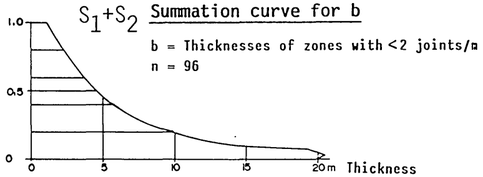

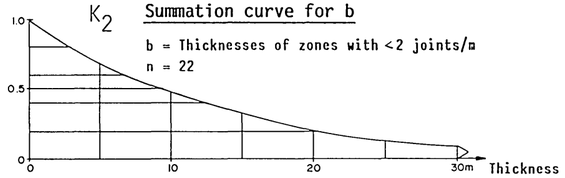

NAGRA	TECHNICAL REPORT NTB 87-14E
DISCONTINUITY SPACINGS: SUMMATION CURVES OF THICKNESSES OF FRACTURED AND UNFRACTURED ZONES	
GRIMSEL TEST SITE	DAT.: ENCLOSURE 14

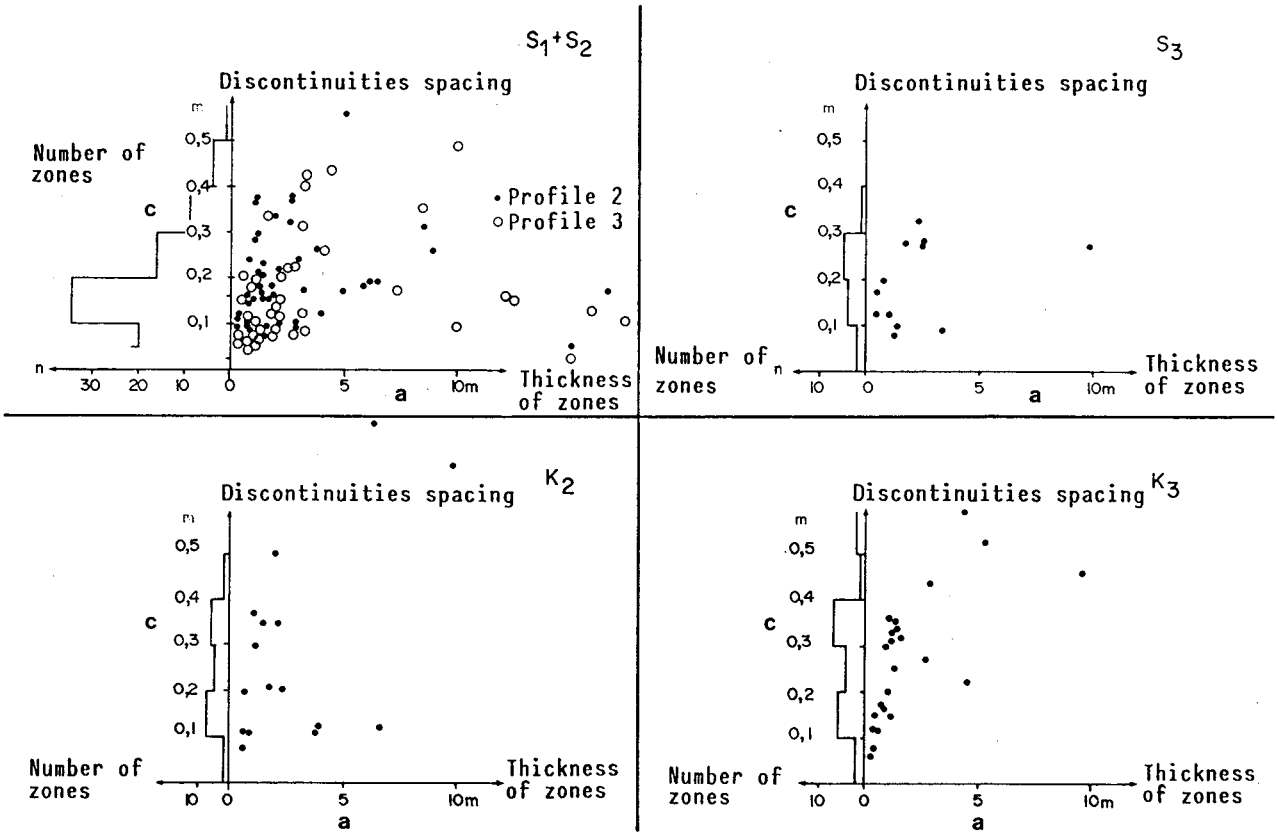

Parameters used

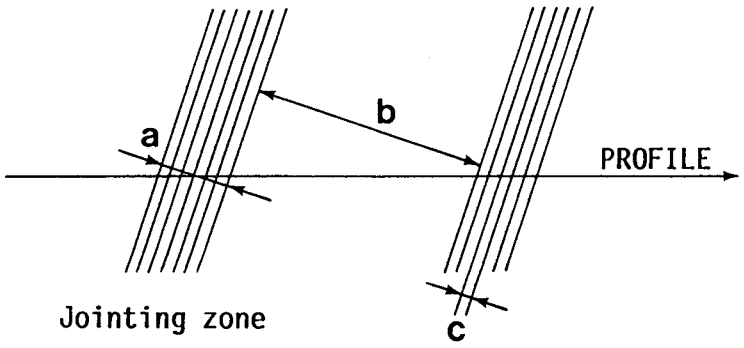

NAGRA	TECHNICAL REPORT NTB 87-14 E
DISCONTINUITY SPACINGS (c) AS A FUNCTION OF THE WIDTH OF FRACTURED ZONES (a)	
GRIMSEL TEST SITE	DAT.: ENCLOSURE 15

Borehole temperatures and air temperatures in the main access tunnel

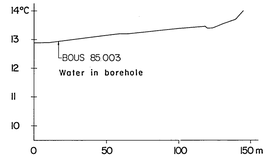

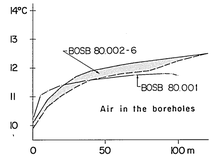

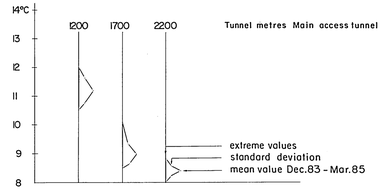

GEOLOGICAL PROFILE

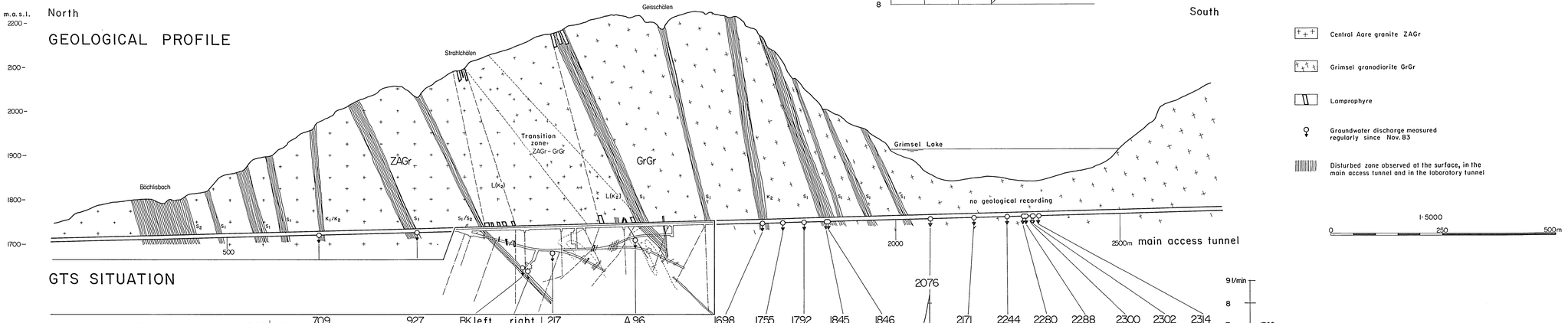

Central Aare granite ZAGr

Grimsel granodiorite GrGr

Lamprophyre

Groundwater discharge measured regularly since Nov. 83

Disturbed zone observed at the surface, in the main access tunnel and in the laboratory tunnel

1:5000
0 250 500m

GTS SITUATION

GROUNDWATER

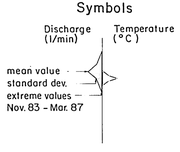

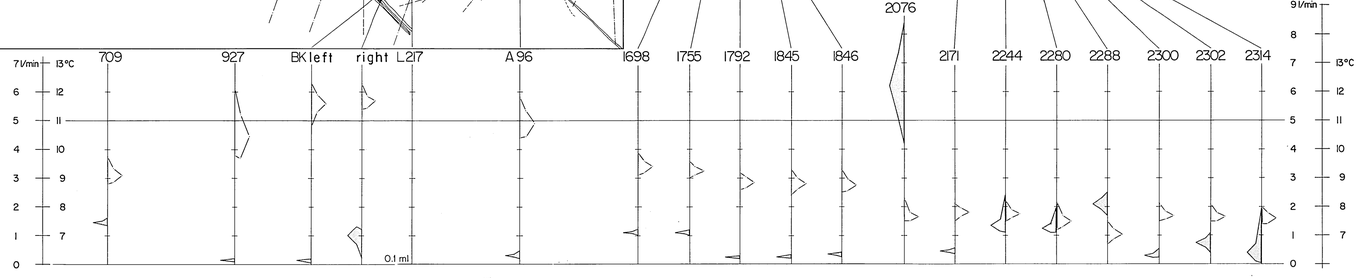

NAGRA	TECHNICAL REPORT NTB 87-14 E
SCHEMATIC GEOLOGICAL PROFILE IN THE GTS AREA WITH WATER INFLOW POINTS AND TEMPERATURES	
GRIMSEL TEST SITE	DAT.: ENCLOSURE 16

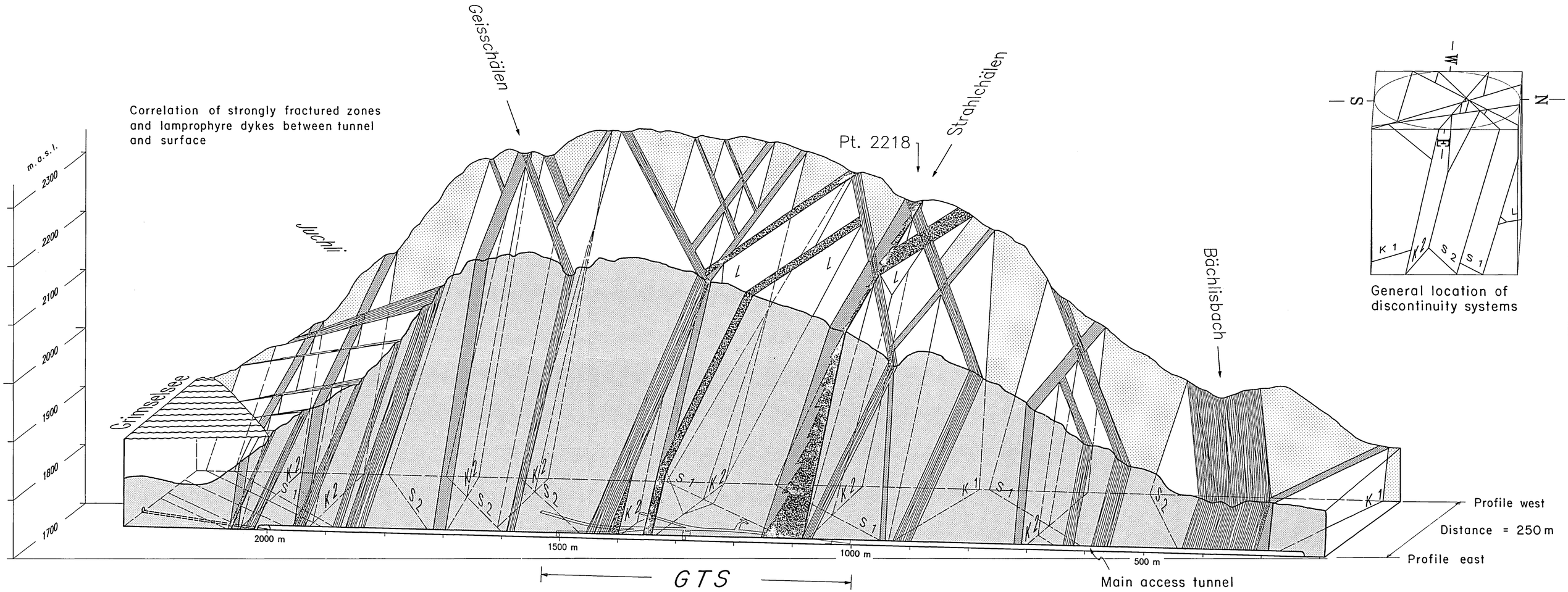

Comment on diagram:
Presentation of the block diagram necessitated a line of sight in a westerly direction towards the east flank of the Juchlistock. This results in a mirror image reversal as compared with other cross - sections

NAGRA	TECHNICAL REPORT NTB 87-14 E	
SCHEMATIC BLOCK DIAGRAM BETWEEN THE GTS AND THE SURFACE		
GRIMSEL TEST SITE	DAT.:	ENCLOSURE 17

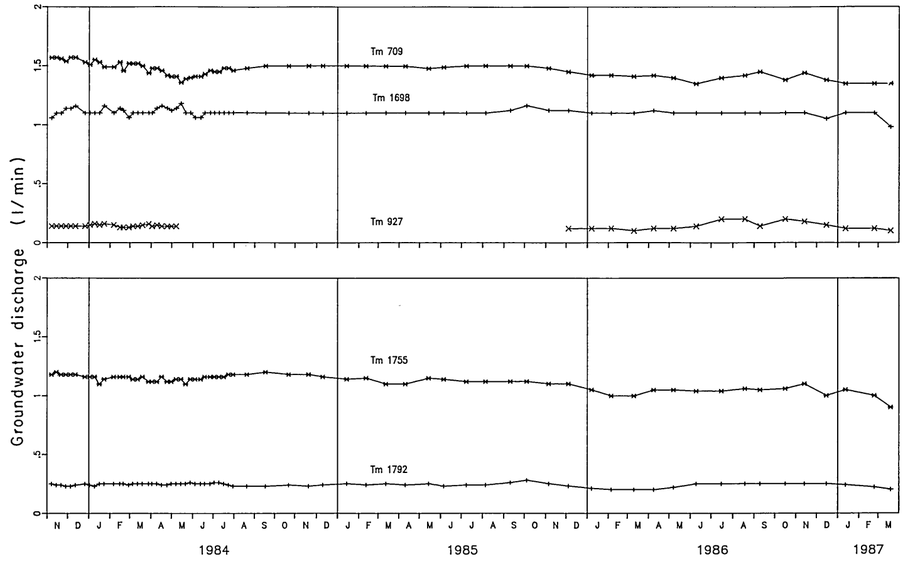

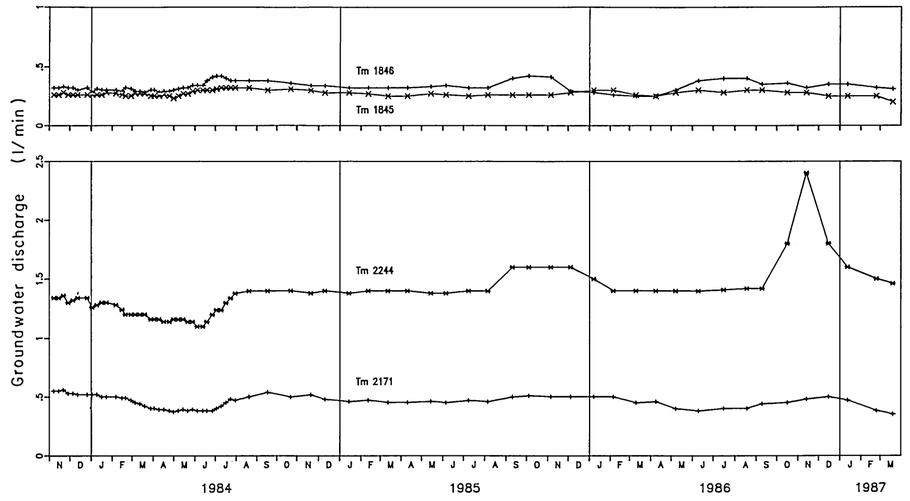

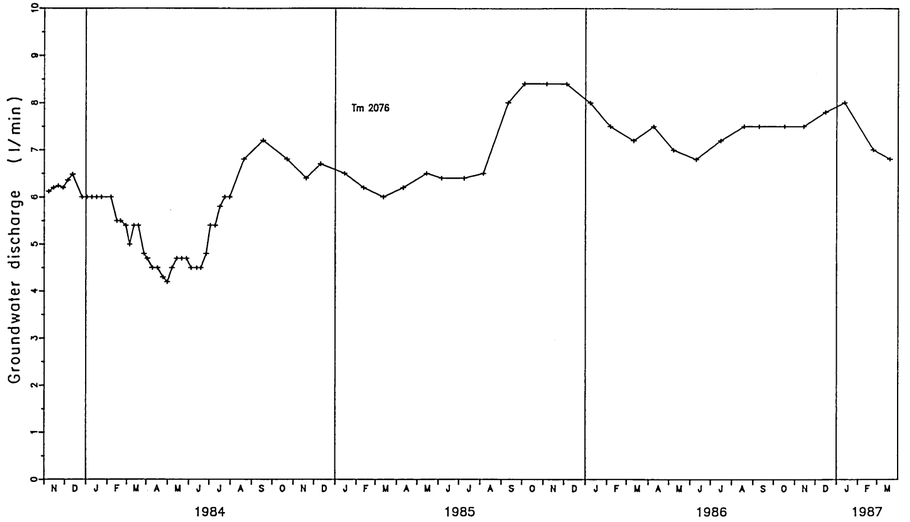

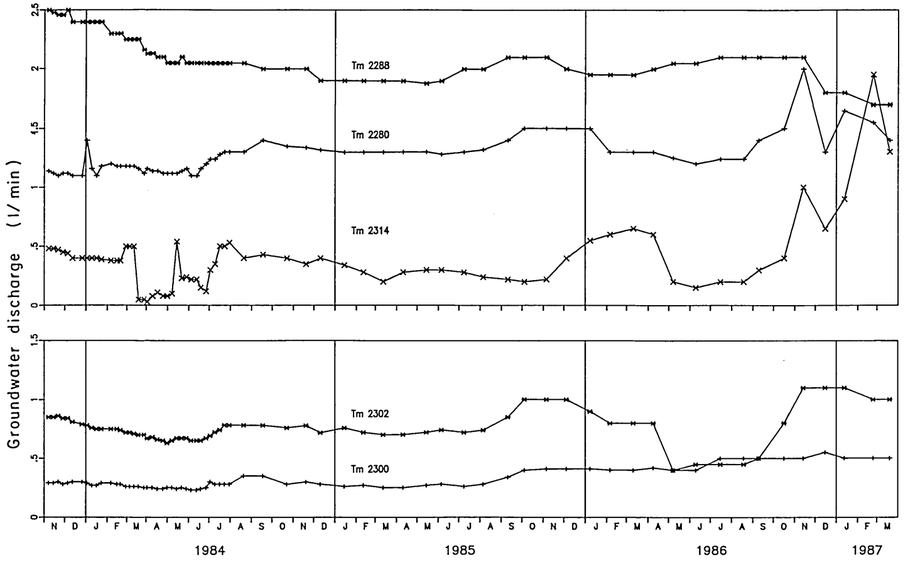

NAGRA	TECHNICAL REPORT NTB 87-14 E
DISCHARGES OF WATER INFLOW POINTS IN THE MAIN ACCESS TUNNEL	
GRIMSEL TEST SITE	DAT.: ENCLOSURE 18

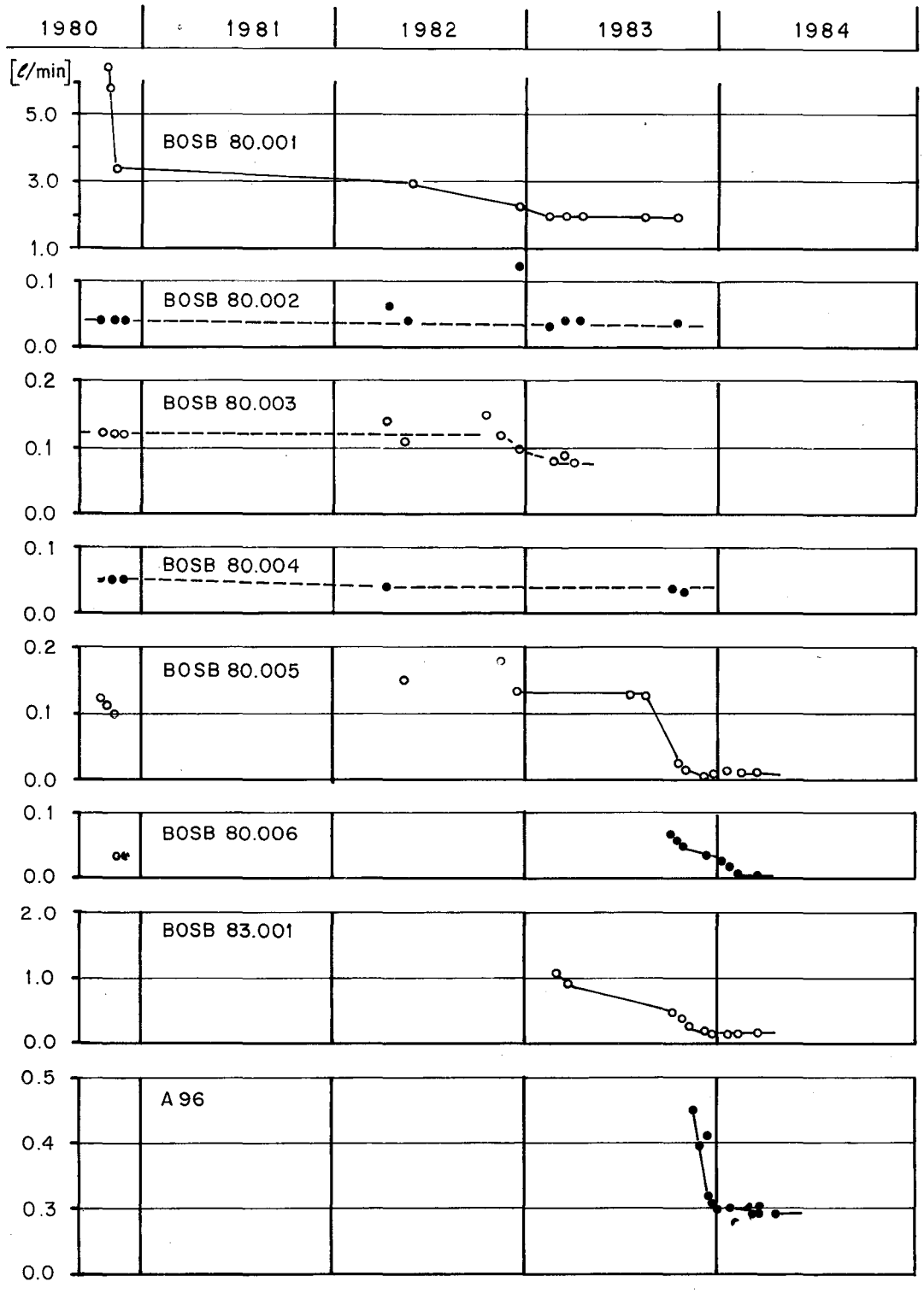

NAGRA	TECHNICAL REPORT NTB 87-14 E
WATER DISCHARGE (1980 – 1984) IN THE BOREHOLES OF THE MAIN ACCESS TUNNEL AND IN A96	
GRIMSEL TEST SITE	DAT.: ENCLOSURE 19